UCRL-19140 c.2

DYNAMICS OF ION-MOLECULE REACTIONS: N^+ AND O_2^+ WITH HYDROGEN ISOTOPES

Chi-wing Tsao
(Ph.D. Thesis)

January 1970

AEC Contract No. W-7405-eng-48

LAWRENCE RADIATION LABORATORY
UNIVERSITY of CALIFORNIA BERKELEY

UCRL-19140

DISCLAIMER

CONTENTS

DYNAMICS OF ION-MOLECULE REACTIONS: N^+ AND O_2^+ WITH HYDROGEN ISOTOPES

Chi-wing Tsao

Inorganic Materials Research Division, Lawrence Radiation Laboratory
and Department of Chemistry
University of California, Berkeley, California

ABSTRACT

A search for complex formations in ion-molecule reactions is made in this thesis research. An ion-beam scattering-cell technique is employed in these studies.

The reaction N+(H2,H)NH+ is exothermic by 0.6 eV. Between an energy range of 2.5 eV to 8.2 eV no evidence of a complex is observed; direct reaction mechanism dominate instead. Reaction maps and velocity spectra are made for the product NH^+. The kinematic data can easily be interpreted in terms of a reaction energy level diagram. The formation of some of the electronic states as well as the ground state of NH^+ can be deduced from the experimental results. The back-scattered products have a most probable velocity close to that predicted by the knockout model. A detailed study of the translational to electronic energy transfer is made between N^+ and He. Transitions like $N^+(^3P) \rightarrow N^+(^3D)$ and $N^+(^5S) \rightarrow N^+(^3D)$ are observed. The scattering data of the former transition can be explained in terms of a curve crossing model.

The reaction $O_2^+ + H_2$ is studied in the energy range 1.47 eV to 12 eV. Four reaction channels are observed leading to the products O_2H^+, OH^+, H_2O^+ and O^+. These reactions are endothermic. Intensity contour maps and velocity spectra are prepared for all the products. At low energy,

all of these reactions except the formation of O^+ proceed via a complex mechanism. A gradual transition from the complex formation to a direct mechanism is observed for the product O_2H^+. H_2O^+ forms only via the complex path. A two step model involving a unimolecular decay of O_2D^+ is proposed to explain the results of both the non-reactive scattering of $O_2^+ + D_2$ and the formation of OD^+ at high energies. It is shown that the majority of O^+ comes from a collision induced dissociation of O_2^+. Isotopic studies with HD reveals that O_2D^+ and O_2H^+ react by different mechanisms. The lifetime of the complex $H_2O_2^+$ is calculated and compared to the experimental data. Intensity data from the reaction are compared to mass spectra of $H_2O_2^+$; no resemblance between these two sets of data are found.

I. INTRODUCTION

The majority of chemical reactions are completed within a few hundred degrees of room temperature. One does not have to go far to find such examples and these chemical reactions have changed the history of mankind. However, chemistry over a few thousand degrees has not received quite as much attention and is a field almost untouched by the chemist. By the acceleration of ions, chemists have a tool to investigate chemical reactions at a few thousand degrees and beyond. Thus ion-molecule reactions and hot atom chemistry fill in the gap of the energy range left out by the ordinary bench top experiments. Studies in ion molecule reactions demonstrated that chemical reactions do occur at high temperature and in some experiments with a rate comparable to those at room temperature.

A. Survey of the Experimental Methods

The field of ion-molecule reactions at room temperature has been reviewed by Lampe, Franklin, and Field,[1] while the latest techniques were the subject of review of Friedman.[2] Dynamics of ion-molecule reactions can best be studied under single collision conditions, that is, when the final fate of an ion is examined after its first encounter with another molecule. Such a problem can be attacked along several lines. Cross-beam methods were first employed by Turner et al.[3] and later followed by Wolfgang et al.[4] These techniques were most suited to study ion-molecule reactions at low energies (below 25 eV) since cross-beam experiments eliminated the problem of random target motion at room temperature. They have the drawback of low product intensity

due to the low neutral beam intensity, and in a reaction where the reactants and products are not easily condensable lead to serious background problems. However, in these experiments both angular and velocity distributions of the products can be made. Differential cross-sections rather than the total cross-section are made with these machines.

Tandem mass spectrometers formed the second class of ion-molecule reaction machines. These machines are best used to determine the total cross-section of the reaction. Examples are the spectrometers designed by Giese and Maier.[5] Henglein[6] used a Wien-filter technique and measured the velocity spectrum of several ion-molecule reactions, thus initiating an intensive effort in ion-molecule dynamics. However, none of these apparatus have the capability of measuring the differential cross-section which is of intrinsic interest in chemical dynamics. Nevertheless, tandem mass-spectrometers have given us unambiguous total reaction cross-sections and led to the quantitative investigation of reaction mechanisms.

The last category of ion-molecule reaction machines are the scattering cell method which we employed in these experiments. These machines have the combined versatility of the tandem mass-spectrometers and the cross-beam methods. In this technique, one of the mass-spectrometers rotates around the center of a scattering cell. In principle, differential cross-sections, velocity spectra, and total cross-sections can be made. With a well designed scattering cell the background problem can be kept to a minimum. The neutral molecule density is considerably higher than that in a cross-beam machine giving more product signal. The only drawback in such an arrangement is that the target

motion is no longer negligible and its effective range of operation is confined to reactions above 15 eV. Typical designs are those of Aberth and Lorents,[7] Bailey et al.[8], and Mahan et al.[9]

B. Survey of the Reaction Dynamics

Efforts over the last few years have mainly concentrated on three reactions: $N_2^+ + H_2$,[3,4,6,8,9] $Ar^+ + H_2$,[4,6,10] and $N_2^+ + CH_4$.[11,12] Already, these techniques have yielded a wealth of data on the dynamics of these reactions unmatched in ion-molecule reactions. Two interesting consequences came out of these studies. Early work with high pressure mass spectrometers and together with the consideration of the ion-induced dipole potential had led some investigators to suggest that the reactions $N_2^+ + H_2$ and $Ar^+ + H_2$ proceeded by a long lived intermediate complex.[13] No evidence was found in support of this speculation in the later investigations of the reaction dynamics. Second, two distinct mechanisms exist for reactions at moderately high energies, depending on the impact distance between the ion and the molecule. Other important features of these reactions were also revealed.

The existence of an intermediate complex in chemical reactions is central to many theories in chemical kinetics, notably the Transition State Theory.[14] Thus, since the beginning of chemical dynamic studies by cross-molecular beams, such a postulate was tested for in every reaction studied. The phenomena of a sticky collision complex was first observed by the Harvard group[15] and many other reaction complexes were subsequently discovered. Efforts in this area repeatedly failed in the investigations of ion-molecule reactions. Experiments in ion-molecule dynamics have taught us that even though two reacting molecules are

known to be able to come to a stable molecular configuration, there will not necessarily be any evidence of long-lived complex formation in the reaction dynamics. For example, the molecular ion H_2CO^+ is stable and can be postulated as the intermediate complex in the reaction $CO^+ + H_2$. Yet no evidence for such a complex was found.[6] We cannot rely completely on such arguments as a guide to the search of a complex reaction.

C. Motives for the Thesis Investigations

The motives for the investigations described in this thesis is a continuation of such a search for a reaction complex in ion-molecule reactions. The molecule NH^+ is of considerable interest in astronomy.[16] The spectra of CH and CH^+ have been observed in outer space.[17] Likewise the existence of NH in the interstellar space has definitely been shown. But unlike CH and CH^+, the existence of NH^+ in the outer space has never been detected, partly because not enough laboratory data was known about this molecule. The objective of this experiment is twofold. First, it should be instructive to study the mechanism by which NH^+ is formed from N^+ and H_2. Again, NH_2^+ is a stable molecule and the reaction

$$N^+ + H_2 \rightarrow [NH_2^+] \rightarrow NH^+ + H \qquad (1)$$

is nearly thermo-neutral. Thus we expect that a long-lived collision complex might occur in this reaction. No definite conclusion about the complex was reached in the experiments performed in this thesis. At the laboratory energies investigated (20 to 70 eV), the reaction goes via a direct mechanism. Second, unlike many of the ion-molecule reactions previously investigated, some of the electronic states of

NH^+ are known.[16] It would be interesting to know if we could identify the states in which NH^+ is formed from the kinematic data. Our data gave ample evidence that, except for the ground electronic state, an unambiguous identification of the electronic states of a product is not possible even for simple molecules like NH^+. In addition to the above mentioned results, interesting data on the conversion of translational energy to electronic excitations were also obtained.

From the start the reaction

$$O_2^+ + H_2 \rightarrow [H_2O_2^+] \rightarrow O_2H^+ + H \qquad (2)$$

looked more promising. $H_2O_2^+$ represents a deep well, about 2.6 eV, on the potential surface, and the reaction is endothermic by 1.8 eV. Here, we have a system completely different from all the other ion-molecule reactions studied before. This reaction cannot be studied by the ordinary room temperature mass-spectrometer method, since the reaction takes at least 1.8 eV to surmount the reaction barrier. There is much chemistry of this type which can only be studied in the high energy regions. As suspected, this reaction reacts via a complex mechanism. Endothermic reactions might give us a new guide in the search for ion-molecule reaction complexes. As expected from a complex, products like OH^+, H_2O^+, and O^+ were also detected. Isotope effects gave new insights into the reaction mechanisms not known before. Definite correlations between the reactive and non-reactive scattering were also observed.

D. Plan of the Thesis

Due to the overlaps in the theoretical interpretations and the experimental procedures in these experiments, the theoretical reaction models will be described briefly and summarized in Section II. Section III concerns the experimental techniques and deals with the differences in the instrumentation in the N^+ and the O_2^+ experiments. The results of the N^+ reactions will be discussed in detail in Section IV, while those of O_2^+ will be presented in Section V. Section VI recapitulates on the experiments. Some future experiments are proposed to complete the study of these reactions.

II. REACTION DYNAMICS

A. Direct Mechanism

Most of the reaction models discussed below have been used extensively in Nuclear Reactions.[18] The discussions will be limited to two dimensional scattering and serve to be a glossary of the nomenclature used throughout this thesis. It has been the tradition of molecular scattering experiments to discuss the results in terms of a Newton diagram[19]; it relates all the interesting kinematic quantities in both the center of mass (CM) and the laboratory (lab) systems. Such a diagram is shown in Fig. 1 for the elastic scattering of two particles with arbitrary masses m_1 and m_2, where m_1 is stationary in the lab system. The kinematics of a two-particle system has been treated in detail in many standard classical mechanics texts[20] and will not be repeated here. We should, however, note that inelastic signals are expected to be found inside the elastic circle.

1. The Pick-up or Stripping Model

In this model, the projectile (m_1+m_2) interacts with (and picks up) one particle (m_3) of the target (m_3+m_4), while leaving the other particle (m_4) alone, as if m_4 were not there. By the conservation of momentum

$$(m_1+m_2)v_0 = (m_1+m_2+m_3)v \tag{3}$$

or

$$v/v_0 = (m_1+m_2)/(m_1+m_2+m_3) \tag{4}$$

Thus the ideal stripping model[6,8,9] predicts that the ratio of the initial velocity (v_0) of the ion to the final velocity (v) of the

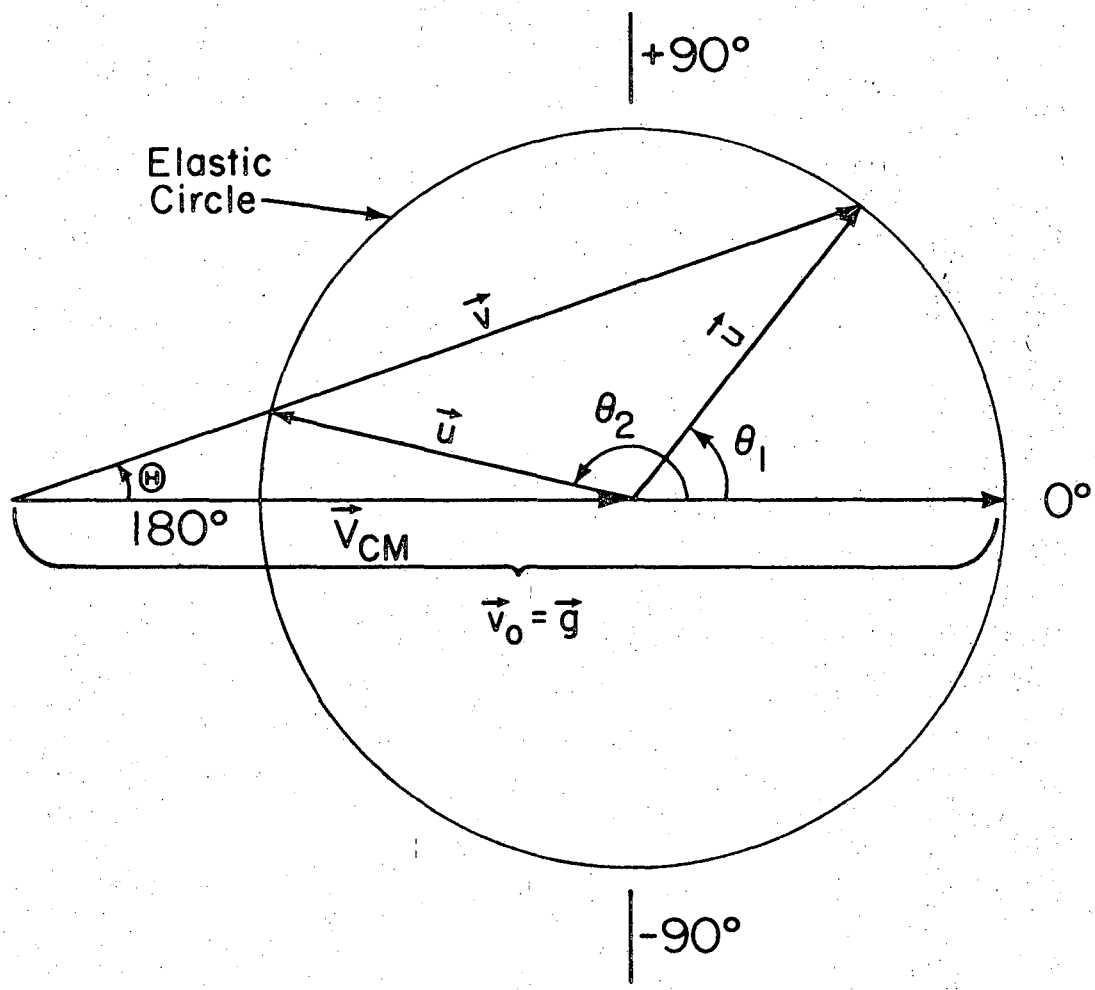

Fig. 1. Newton diagram for an elastic collision between a stationary target and a fast moving projectile.

product ion is a simple ratio of the masses. In the language of nuclear reactions, the above process is known as the pick-up process.[18] However, in chemical dynamics, we are accustomed to name the pick-up process as the stripping mechanism. We shall continue to refer the above process as the stripping model and when the occasion arises such that we have to distinguish the pick-up and the stripping processes, we shall describe the process in some detail to render easy distinction.

2. The Stripping Model

This model is the exact reverse of the pick-up model. The target (m_3+m_4) interacts with only one particle m_1 of the projectile and completely ignores the other one (m_2). If m_1 is incorporated into the target, by the conservation of momentum

$$m_1 v_0 = (m_1+m_3+m_4)v \tag{5}$$

Once again, v/v_0 is reduced to a simple mass ratio. Of course the charge may remain on m_2 too, in this case m_2 will move with the same initial velocity, v_0.

3. The Knockout Model

The projectile collides elastically with one atom (m_3) of the target, ejects it and reacts with the remaining atom (m_4). The kinematics of the ideal knockout process[9] lead to the prediction that for 180° scattering, the velocity ratio is

$$\frac{v}{v_0} = \frac{(m_1+m_2)(m_1+m_2-m_3)}{(m_1+m_2+m_3)(m_1+m_2+m_4)} \tag{6}$$

4. The Rebound Model

The other possibility for a knockout type of reaction is to have the projectile to collide completely inelastically with m_3 and the

resulting molecule $(m_1+m_2+m_3)$ collides elastically with m_4. For an ideal rebound process

$$\frac{v}{v_0} = \frac{(m_1+m_2+m_3-m_4)(m_1+m_2)}{(m_1+m_2+m_3+m_4)(m_1+m_2+m_3)} \tag{7}$$

B. Complex Reactions

1. Velocity Distribution

The projectile collides completely inelastically with the target and the resulting molecule rotates in space for a number of rotational periods. If the products move away from each other with negligible velocity, all the particles will move with the CM velocity.

$$v_{CM} = [(m_1+m_2)/(m_1+m_2+m_3+m_4)]\ v_0 \tag{8}$$

If the products move away from each other with a distinct velocity, then the product velocity distribution will be symmetric with the center of mass of the colliding particles.

2. Angular Distributions

The angular distribution of nuclear fission products have been discussed in detail by Strutinski.[21] Such a model was adopted to a chemical system by Herschbach.[15] With the compound nucleus model, the calculation of the product angular distribution for specified magnitudes of J, M and M' is purely geometrical, where J is the total angular momentum, M is the projection of J on the initial relative velocity vector g, and M' is the projection of J on the final relative velocity vector g'. The form factors for angular distributions and the differential cross-section for various M and M' have been discussed in detail[15] and will not be reproduced here.

In general, the differential cross-section for a statistical complex is expected to peak symmetric to $\pm 90^\circ$ in the CM system.

C. Energy Considerations

For ground state reactions, by the conservation of energy

$$E_s^0 = E_s' + \Delta E_0^0 + U \qquad (9)$$

where E_s^0 is the initial relative energy, E_s' the final relative energy, ΔE_0^0 is the energy change for the reaction and U is the internal excitation of the products. We shall further define Q, the translational exothermicity of the reaction, as

$$Q = E_s' - E_s^0 \qquad (10)$$

$$= \frac{1}{2}\mu' g'^2 - \frac{1}{2}\mu g^2 \qquad (11)$$

where μ and g are the reduced mass and the relative velocity of the reactants respectively and the primed quantities refer to the products. Equation (9) can also be written as

$$Q = -\Delta E_0^0 - U \qquad (12)$$

Hence the range of Q allowed in a given reaction (ground state) is determined by ΔE_0^0 and U, and the limits of Q are restricted by U. If the neutral partner is an atom which does not absorb energy, the lower limit of Q is defined by the restriction that $U \leq D$ (ion), where D(ion) is the dissociation energy of the ionic product. Thus the limits of Q are

$$-\Delta E_0^0 - D(\text{ion}) \leq Q \leq -\Delta E_0^0 \qquad (13)$$

If the neutral fragment is polyatomic, the Q is limited by the sum of the lowest D(ion) and D(neutral). Usually the lower limit of Q can be specified rigorously due to the cancellation of D(ion) in the lower limit.

III. EXPERIMENTAL

A. Brief Description of the Apparatus

The apparatus employed in these experiments has been described in detail in a report by Gentry.[22] The major features of this instrument are shown in the block diagram (Fig. 2). Briefly, ions were formed in a Carlson and Magnuson[23] type of electron bombardment source. The ions were extracted out of the source and shaped into a beam by a double aperture lens and an einzel lens. A quadrupole lens pair then focused the beam into a magnetic mass-spectrometer. After momentum analysis, the ion beam again passed in series through a quadrupole lens pair and an einzel lens which rendered the ions into a parallel beam before colliding with the target gas in the scattering cell. The products together with the primary beam first entered a 90° electrostatic energy analyser* and then separated by a quadrupole mass-spectrometer. The product ions were accelerated to 25 keV and impinged on an aluminum electrode which emitted secondary electrons. The electron pulses were registered on a counter.

B. Data Acquisition and Analysis

During each counting period, current outputs from both the energy analyser and the capacitance manometer were displayed on digital voltmeters and simultaneously converted to BCD code to be stored in the scanner. At the end of each counting, the TIME, COUNT, ENERGY ANALYSER VOLTAGE, and PRESSURE (of the scattering gas) were automatically recorded by the teletype writer. The resulting data were then

*The full width at half maximum resolution (lab) of the energy analyser was 3% and the angular resolution (lab) of the apparatus was about 2°.

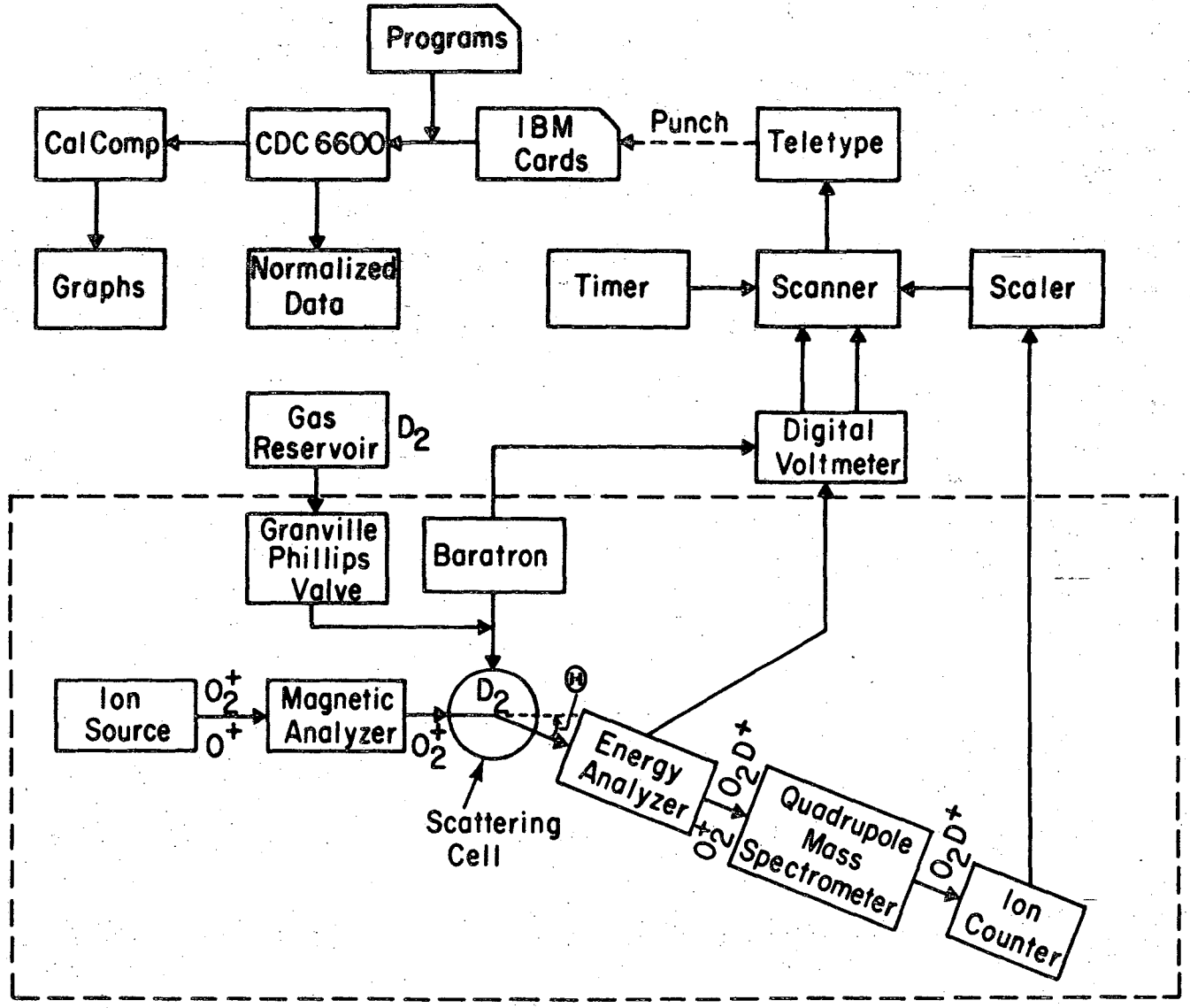
Programs
CalComp
CDC 6600
IBM Cards
Punch
Teletype
Graphs
Normalized Data
Timer
Scanner
Scaler
Gas Reservoir
D_2
Digital Voltmeter
Granville Phillips Valve
Baratron
Ion Source
O_2^+
O^+
Magnetic Analyzer
O_2^+
D_2
H
Energy Analyzer
$+D_2O$
$+O_2$
Quadrupole Mass Spectrometer
$+D_2O$
Ion Counter
Scattering Cell

Fig. 2

Fig. 2. A block diagram of the apparatus used to study the dynamics of ion-molecule reactions. The composition of the ion current for a typical experiment $O_2^+ + D_2$ at various stages is indicated. Solid arrows indicate the direct flow of information. Dotted arrow means indirect flow of information.

normalized with respect to the counting time, scattering gas pressure, scattering volume, primary beam intensity and the velocity space volume. The relative differential cross-section $I(\theta)$ and the relative total cross-section σ can be calculated from these normalized intensities $I(\theta,\phi,u)$ by the following formulas

$$I(\theta) = \int_0^{\infty} I(\theta,\phi,u)u^2 du \tag{14}$$

and

$$\sigma = \int_0^{\pi} I(\theta)\sin\theta d\theta \tag{15}$$

where (θ,ϕ) and u are the scattering angles and the velocity in the center of mass system.

In the experiments both velocity spectra and intensity contour maps were made. A velocity spectrum is conveniently made by sweeping the electrostatic energy analyser over the desired energy range. Normally a spectrum was scanned with the detection train set at 0° laboratory angle. To generate contour maps of scattered ion intensity, angular scans were made at a number of fixed analyser energies. From these scans graphs of normalized intensity versus angle at fixed energy, and likewise intensity versus velocity at fixed angles were prepared. The contours were formed by picking points at the same intensity on these curves. The points thus chosen had two coordinates: angle and velocity; they were again plotted on a graph and formed one intensity contour. Together these contours form an intensity map. To lessen the amount of labor, all the graphs were plotted by a Calcomp.

C. Modifications

1. Capacitance Manometer

In place of the ionization gauge previously used in the N2+(H2,H)N2H+ and N2+(CH4,CH3)N2H+ * experiments, a BARATRON† capacitance manometer was installed to monitor the scattering gas pressure. The BARATRON has a definite advantage over the ionization gauge. It is an absolute measurement of the pressure. The ionization gauge has some further disadvantages; it decomposes some of the molecules of which the pressure is being monitored. This leads to isotope mixing in HD for example, causing erroneous results in the scattering data. It was also found that the collector plate (platinum) of the ionization gauge was attacked by C_2D_2. Thus the ionization gauge interacts chemically with some compounds, and physically excites a portion of the gas into higher vibrational states. The BARATRON used was factory calibrated. No further calibration was made since absolute total cross-sections were not measured in these experiments.

---

*This short hand notation is suggested for ion-molecule reactions, with the ease in computer storage in mind. The order of the terms

N2+(CH4,CH3)N2H+

have the following significance. Outside the brackets, the projectile (N_2^+) is written to the left and the ionic product (N_2H^+) to the right, while the target (CH_4) and the neutral product (CH_3) are written to the left and right respectively inside the brackets.

†Supplied by the MKS Instruments, Inc., Burlington, Mass.

2. Microwave Discharge Source

Due to the rapid oxidation of the tungsten filament in a pure oxygen atmosphere of an electron bombardment source a microwave discharge source was constructed to produce O_2^+ ions. A Broida type cavity[24] designed to operate at 3000 Mc was powered by a QK-61 magnetron and sustained a discharge in a 1 centimeter quartz tube. The basic construction of the microwave discharge source is shown on Fig. 3. The pressure inside the source (typically 10-50 microns) is maintained constantly through a Granville-Phillips valve. A full account of the design characteristics and the operation will be discussed in some other reports.[25]

D. Composition of the Ion Beams

1. N^+ Beam

Most of the experiments of N^+ (300 series) were performed with the electron bombardment source. To facilitate comparison some experiments (500 series) were done with the microwave discharge source. In the production of N^+ by the electron bombardment of N_2 invariably some N_2^{++} were produced. Since N_2^{++} has the same mass to charge ratio as N^+, it (N_2^{++}) will pass successively through both the momentum analyser and the electrostatic energy analyser and be registered as a "mass 14". It is impossible to distinguish N^+ and N_2^{++} in our experimental set up. McGowan and Kerwin[26] investigated the N_2^{++} content in an ion beam coming from a typical electron impact source, using $N_2(29)$ as the parent gas. At a bombarding electron energy of about 100 eV, they found 2% N_2^{++} mixing in the N^+ beam.

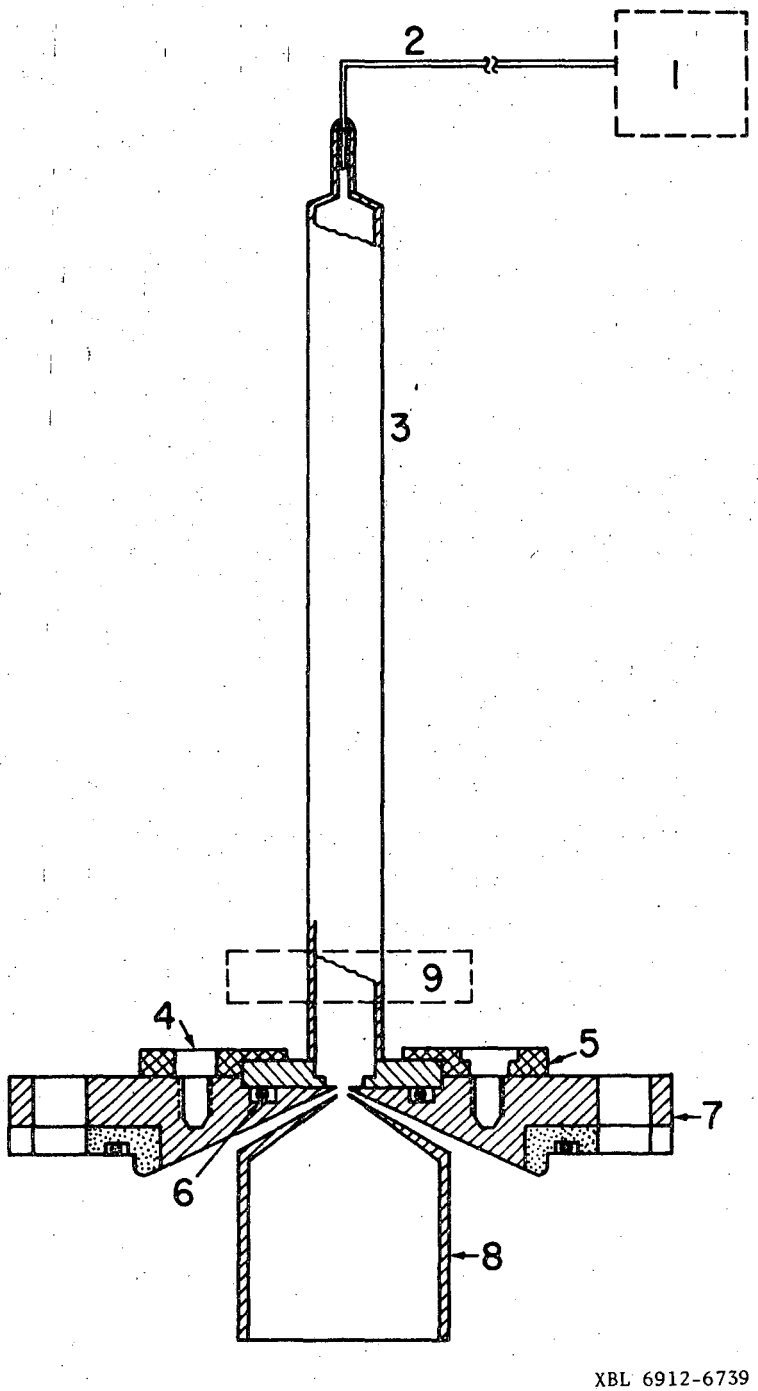

XBL 6912-6739

Fig. 3. Microwave discharge ion source. (1) Gianville-Phillips valve (2) Stainless steel tubing (3) 1 cm quartz tube (4) Screw (5) Flange (6) Viton rubber O-ring (7) Anode (8) Extractor (9) Broida cavity

If N_2H^{++} were formed in the reaction, it would not affect the NH^+ signal. The mass to charge ratio of N_2H^{++} is 14.5 and should be filtered out by the quadrupole mass-spectrometer. The effect of the N_2^{++} on the non-reactive collisions is rather uncertain. Two processes can happen when N_2^{++} collides with He. First N_2^{++} could charge exchange with He, forming N_2^+ and He^+. In such a case, N_2^{++} would have no effect on the N^+ signal because N_2^+ could be separated by the mass-spectrometer. The second possibility is that N_2^{++} could dissociate on collision with He forming N^+ and N^+. Such N^+ ions would have an energy centered around the peak energy of the N^+ beam (see Section V below) and would contribute significantly to the small angle signal. Therefore, signal close to the beam peak (from an electron bombardment source) does not have any unique interpretation.

The use of a microwave discharge source solved the above problem very nicely. Since the discharge source is operated at low electron energy,[27] it is unlikely that any N_2^{++} can be formed—the threshold energy for the formation of N_2^{++} from N_2^+ is 43.5 eV.[28] Even if N_2^{++} is formed, due to the high pressure inside the source, it will charge exchange rapidly with the parent gas. Thus no N_2^{++} is expected from the microwave discharge source. Comparison between the data from the two ion sources will remove any ambiguity in the data where N_2^{++} might have a part in it.

The electronic composition of the N^+ beam from these two sources will be discussed in Section IV.

2. O_2^+ Beam

The combination of low electron energy and high pressure in the microwave discharge source produced O_2^+ exclusively in the ground electronic state ($^2\Pi_u$). Most of the O_2^+ beam extracted had only the first few vibrational states populated. The vibrational excitation of the O_2^+ in these experiments was estimated to be about 0.6 eV to 0.7 eV. Beam attenuation experiments of the type described by Turner et al.[29] showed that the O_2^+ beam contained less than 3% excited metastable ions.

IV. N^+ EXPERIMENTS

A. Introduction

Recently Fehsenfeld et al.[30] studied the reaction

$$N^+ + H_2 \rightarrow NH^+ + H \qquad (16)$$

in an afterglow discharge apparatus. They only measured the rate constant of the reaction (at 300°K) and found it to be about three times less than that of N2+(H2,H)N2H+. The small cross-section coupled with the difficulties in obtaining a high intensity N^+ beam may account for the fact that there have been no other beam or homogeneous kinetic studies of this reaction. In fact, no other literature was found on this reaction. We have studied N+(H2,H)NH+ from 20 eV to 75 eV in the laboratory system. Although no absolute total cross-section was obtained in the experiments, the product signal observed was considerably less than those in N2+(H2,H)N2H+ [9] previously studied by us. As indicated in Section III, most of these experiments were studied with the electron bombardment ion source, while experiments in the 500 series were performed with the microwave discharge source.

B. Bond Energy and Electronic States of NH^+

Our experiments indicated that this reaction proceeds via a direct mechanism. Like other stripping reactions that have been studied,[9,10,11] N+(H2,H)NH+ is thermo-neutral or slight exothermic. The exact value of the energetics of this reaction cannot be assessed readily, due to the uncertainty in the bond energy of NH^+ with respect to the products $N + H^+$. Gaydon[31] gave a value of 3.7±0.4 eV as the bond

dissociation energy of NH^+. This value was calculated from the known ionization potentials of H^+ and NH^+ together with the dissociation energy of NH (see Table I). From a recent tabulation of the heats of formation of gaseous positive ions,[34] a bond energy of 4.13 eV was obtained, which is within the limits of the values given by Gaydon. Since these were the most up to data tabulations, we believe that 4.13 eV is a more reliable value. With this bond energy, reaction (16) is exothermic by 0.6 eV. Colin and Douglas[16] have determined some of the electronic states of NH^+ spectroscopically. Figure 4 shows a schematic of the electronic states of NH^+. The assignment of the excited molecular electronic states to the atomic states is not certain, but their assignments can be rationalized by the following arguments. The $^2\Sigma^-$ state can arise from atomic states (2) and (3). Colin and Douglas gave this state to be 2.67 eV above the ground state. From a Birge-Sponer type of extrapolation of dissociation limits, the bond energy of $NH^+(^2\Sigma^-)$ = 1.48 eV. If $NH^+(^2\Sigma^-)$ dissociates into $N(^2D) + H^+(^1S)$, it would have a bond energy of 3.8 eV which is much larger than 1.48 eV. Therefore, $NH^+(^2\Sigma^-)$ was arbitrarily assigned to the atomic state (2). The assignment of $^2\Delta$ state is also arbitrary, and the $^2\Sigma^+$ has to come from the atomic state (4).

C. Reaction Energy Level Diagram

Using the data available in Table I, a reaction energy level diagram (Fig. 5) can now be constructed. The diagram is drawn analogous to the Grotrian Diagram in atomic spectroscopy or the molecular energy level diagram in molecular spectroscopy. The reaction energy level diagram serves to interrelate all the bond energies and the

Table I

Thermochemical and spectroscopic data for the molecules N, H_2, NH and H and their ions.

I(N) = 14.545 eV[32]	I(H) = 13.595 eV[32]
I(NH) = 13.1±0.2 eV[31]	D (NH) = 3.2±0.16 eV[31]
D (NH^+) = 4.13 eV[34]	D (H_2) = 4.476 eV[17]

Electronic states of NH^+ [16,33]

State	T (eV)	D_0^0 (eV)	r_0 (Å)
$C\ ^2\Sigma^+$	4.284	(1.08)	1.1801
$B\ ^2\Delta$	2.846		1.1519
$A\ ^2\Sigma^-$	2.673	(1.485)	1.2704
$a\ ^4\Sigma^-$	0.004	(4.13)	1.105
$x\ ^2\Pi$	0		1.081

( ) data uncertain

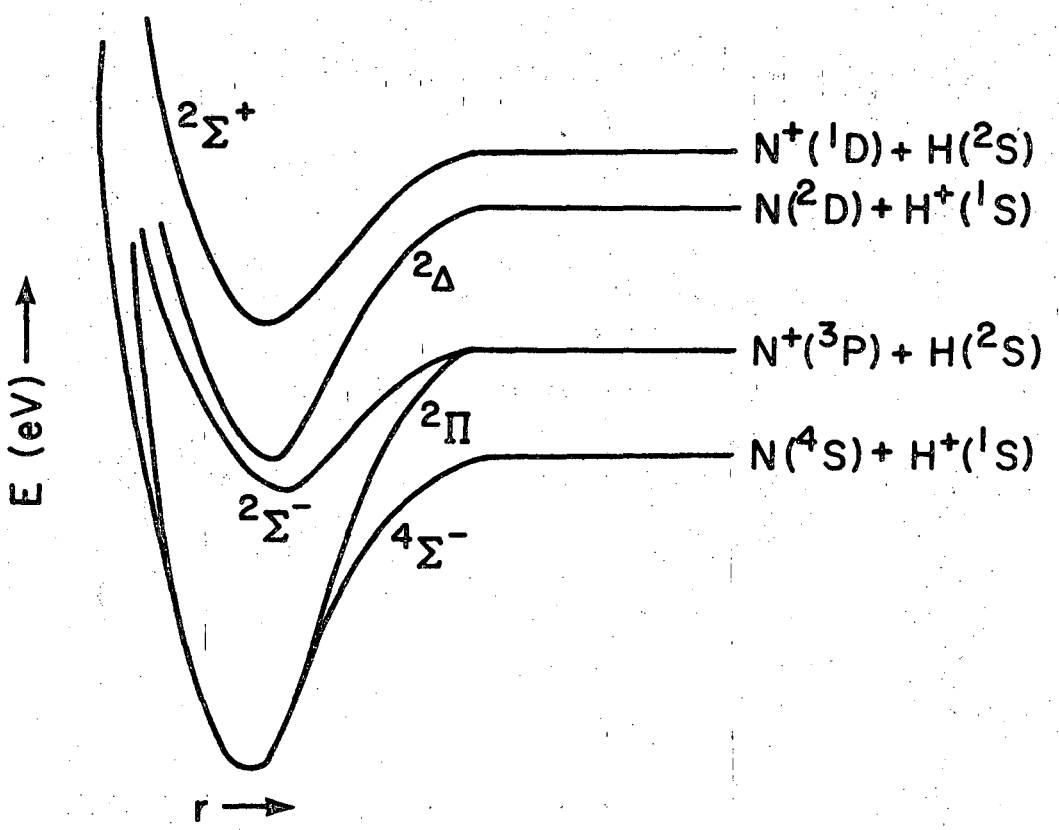

Atomic States		Molecular States
(1)	$N(^4Su) + H^+(^1Sg)$	$\rightarrow NH^+(^4\Sigma^-)$
(2)	$N^+(^3Pg) + H(^2Sg)$	$\rightarrow NH^+(^2\Pi, ^2\Sigma^-)$ and $(^4\Sigma^-, ^4\Pi)$
(3)	$N(^2Du) + H^+(^1Sg)$	$\rightarrow NH^+(^2\Delta, ^2\Sigma^-, ^2\Pi)$
(4)	$N^+(^1Dg) + H(^2Sg)$	$\rightarrow NH^+(^2\Sigma^+, ^2\Delta, ^2\Pi)$

XBL 6912-6737

Fig. 4. Schematics of some of the electronic states of NH^+.

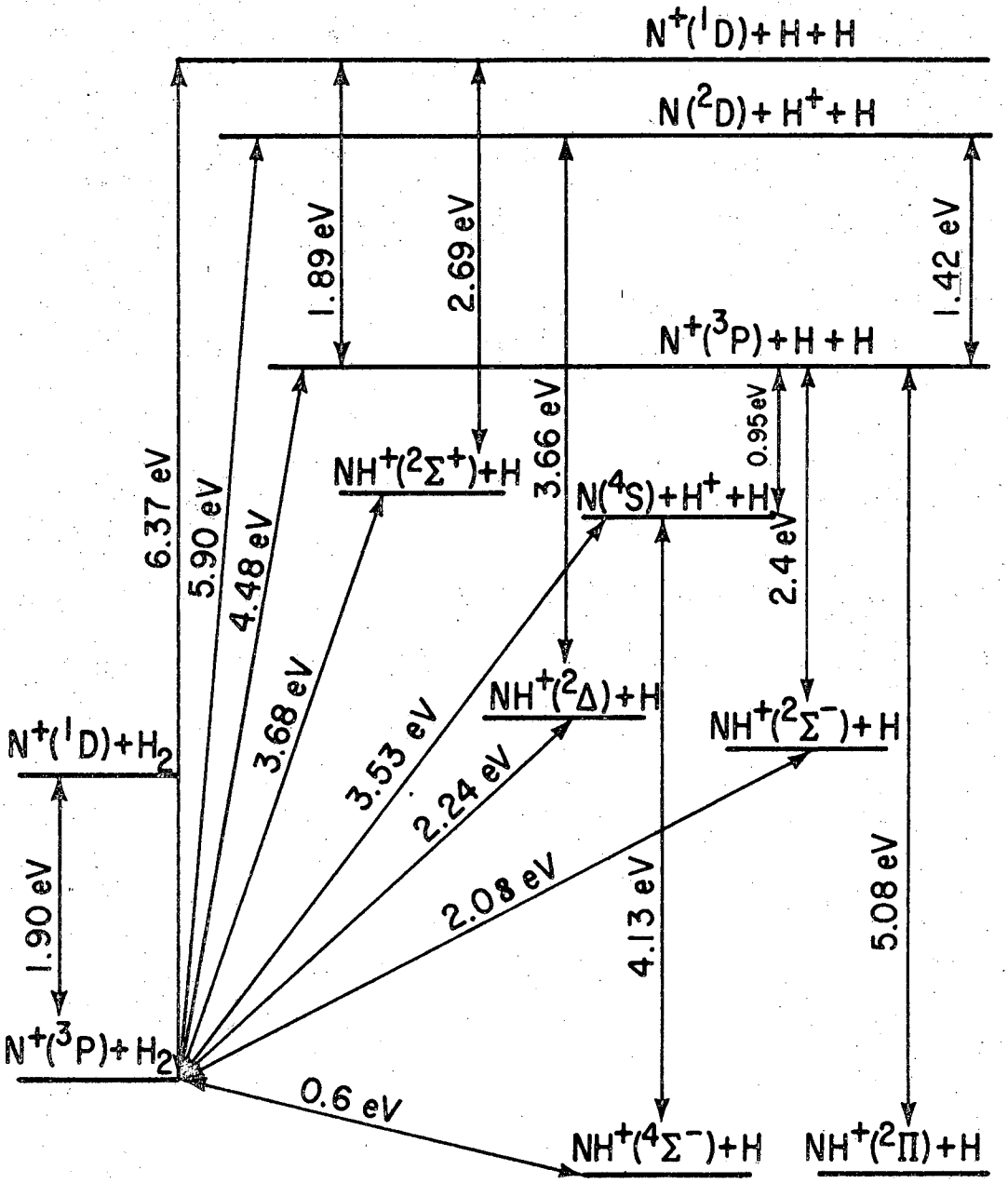

Fig. 5. Energy level diagram for the reaction $N^+(^3P)+H_2$.

ionization potentials involved in this reaction. We shall first indicate the method of construction of such a diagram and then the usage of the diagram in reaction energetics will briefly be discussed.

The reference reaction channel was taken to be $N^+(^3P) + H_2$, with no translational motion. An energy reference zero was assigned to this channel. With reference to $N^+(^3P) + H_2$, the energy necessary to form the products $N(^4S) + H^+ + H$ was indicated on the diagram. Now the $^4\Sigma^-$ state of NH^+ dissociates into $N(^4S) + H^+$, and with the values from Table I the position of $NH^+(^4\Sigma^-)$ was located. Since $NH^+(^2\Pi)$ has almost the same energy as $NH^+(^4\Sigma^-)$, the position of $NH^+(^2\Pi)$ was drawn accordingly. With the ground state thus established all the other electronic states of the product could be located. The dissociation products of these electronic states of NH^+ were drawn in with respect to $N^+(^3P) + H_2$. Since all the electronic levels were known with respect to the ground state the exact energy requirement for the formation of $NH^+(^2\Pi)$ from $N^+ + H$ is critical. Unfortunately, the bond energy of $NH^+(^2\Pi)$ is not known very accurately. The assignment of the exact position (level) of the excited products will have the same error as with the $NH^+(^2\Pi)$, although their relative values are still accurate.

The Q values involved in a certain channel of reaction can easily be calculated. For example, it takes 2.08 eV for $N^+(^3P) + H_2$ to reach $N^+H(^2\Sigma^-) + H$ and that it takes 2.4 eV to dissociate $N^+H(^2\Sigma^-)$. Therefore this reaction is endothermic by 2.08 eV. In our regular terminology, the range of Q allowed in this reaction is

$$-4.48 \text{ eV} \leq Q \leq -2.08 \text{ eV} \quad .$$

The Q values of any other reaction channels can be read off from the diagram in like manners. Moreover, if the relative energy of collision were to be set at 2.2 eV, it can readily be seen from the reaction energy level diagram that only the $^4\Sigma^-$, $^2\Pi$, and $^2\Sigma^-$ states of NH^+ could be formed. Table II is a summary of all the energetic data of N+(H2,H)NH+.

D. Experimental Observations and Discussions

1. Reaction Map

With these ranges of Q in mind, we can examine in detail the data obtained in the experiments. Figure 6 shows a contour map of the reaction at 5.01 eV. The circles drawn at Q = -3.5 eV and Q = +0.6 eV indicate the region of the velocity space where NH^+ is expected to be stable in the $^4\Sigma^-$ state. It can be seen that most of the products formed are inside these circles. However, from Table II, the range of E_0 for $NH^+(^2\Pi)$ formation overlaps that of $^4\Sigma^-$, so the products observed in this experiment can either be $^4\Sigma^-$ or $^2\Pi$. There is no way that one can distinguish between these two species. Of course it is not surprising to find products inside the Q = -3.5 eV circle. At the center of mass the internal excitation of the product is only 5.01 eV. There are other reaction channels which can lead to stable products, and it should be recognized that the resolution of our apparatus is finite. The Q = + 0.6 eV circle indicates the upper limit of Q for the reaction; no reaction products are expected outside this circle. All the products formed at the negative angles are within this circle.

Table II

Energetics of $N^+(H_2,H)NH^+$

Electronic States		Q_{lower}	Q_{upper}	Range of E_0
N^+	NH^+	(eV)	(eV)	(eV)
^3P	$^4\Sigma^-$	-3.5	+0.6	0.0 → 52
	$^2\Pi$	-4.48	+0.6	0.0 → 67
	$^2\Sigma^-$	-4.48	-2.07	31 → 67
	$^2\Delta$	-5.91	-2.24	34 → 88
	$^2\Sigma^+$	-6.37	-3.68	55 → 96
^1D	$^2\Sigma^+$	-4.48	-1.78	27 → 67

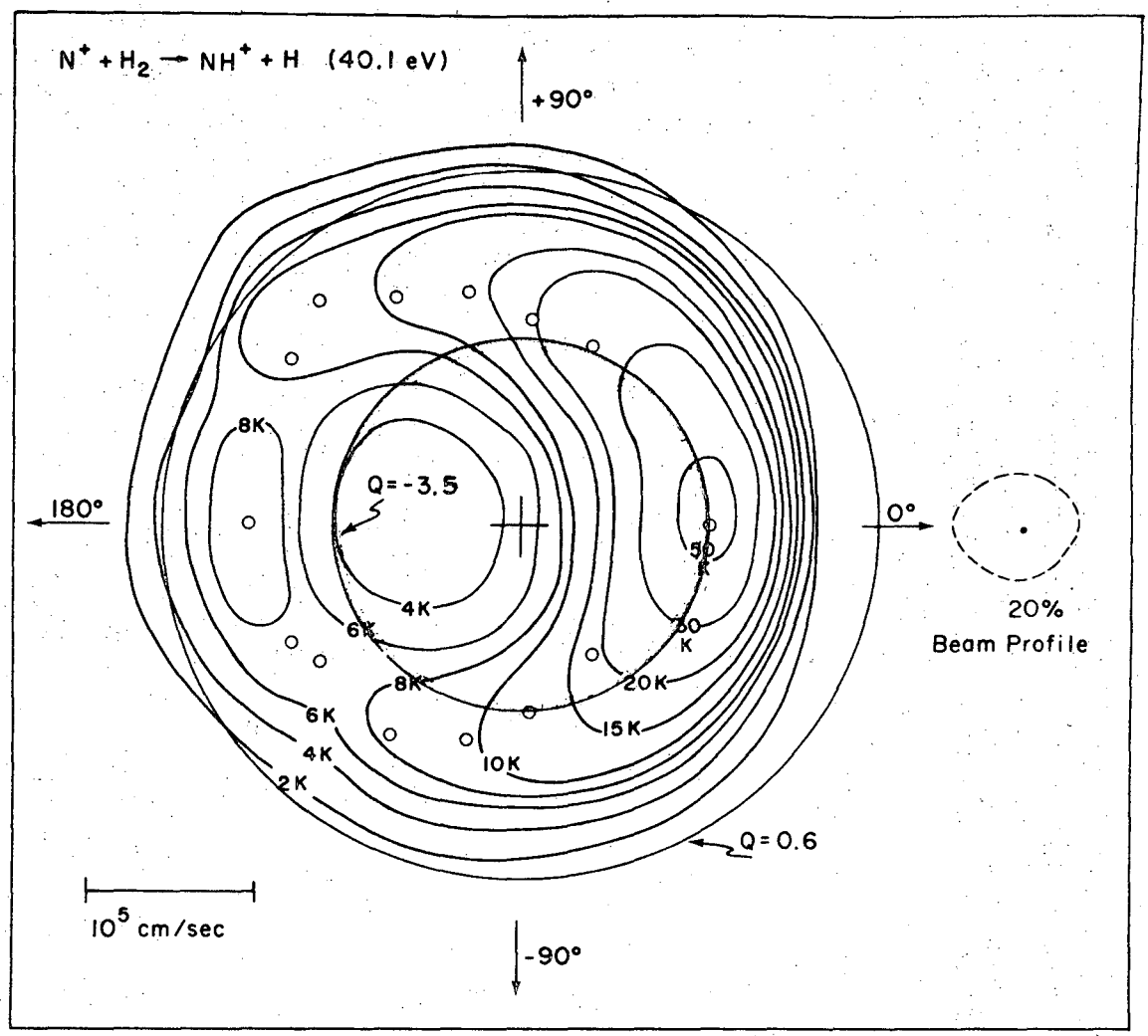

XBL 6912-6703

Fig. 6. An intensity contour map of NH^+ at 5.01 eV. The small circles locate the intensity maxima in the scattering. The cross is the position of the center of mass of the system.

We need to digress a little on the intensity between + 90° and 180°. On examination of the beam angular profile, a secondary peak with intensity 1/10 of that of the main peak was found. If a velocity vector diagram is drawn for this secondary peak using the scattering information from the main peak, it can be seen that 90% of the intensity from the secondary peak will fall on the positive angle side of the map and so the intensity outside the 0.6 eV circle. For the examination of the reaction dynamics, the intensity on the positive side of the map should be ignored. Actually, it is not important to have a 360° distribution of the product. The scattering is axially symmetric and 0° to 180° information is sufficient. Recalling the calculated Q = +0.6 eV, it can be inferred that the exothermicity of $N^+(H_2,H)NH^+$ is less than 0.6 eV. Since the exothermicity of this reaction depends on $D(NH^+)$, this also implies that the bond energy of NH^+ is probably overestimated.

2. Velocity Spectra

Table III listed the experimental results of this reaction. There are two features which caught our attention; these are best shown on Figs. 7 and 8. Figure 7 gives the velocity ratio (v/v_0) of the product and primary ions. For the ideal stripping process this ratio is 0.933. Two distinct regions can be discerned in the figure: Below 45 eV, v/v_0 is 0.925, a little bit slower than that predicted by the stripping mechanism. Above 45 eV, the velocity ratio is about 0.932 which is almost exactly the ratio calculated by the stripping model.

Figure 8 is more revealing. Again two distinct regions appear, those below 45 eV and those above 45 eV. Between 20 eV and 45 eV all

Table III

Scattering data for the reaction $N^+(H_2H)NH^+$

Exp. No.	E_0 (eV)	V_0[a] $\times 10^{-5}$ cm/sec	E_S^0 (eV)	Forward peak V[a] 10^{-5} cm/sec	Forward peak V/V_0	Forward peak Q (eV)	Backward peak V $\times 10^{-5}$ cm/sec	Backward peak V/V_0	Backward peak Q (eV)
313	20.14	16.67	2.52	(15.38)[b]	(0.923)	(-1.70)	-	-	-
302	30.09	20.378	3.76	18.80	0.923	-2.59	(16.82)	(0.825)	(-2.50)
305	31.84	20.963	3.98	19.43	0.927	-2.50	17.18	0.820	-2.38
530	35.36	22.09	4.42	20.46	0.926	-2.83	-	-	-
301	40.09	23.522	5.01	21.70	0.923	-3.43	18.95	0.806	-1.73
319	45.05	24.933	5.63	23.05	0.924	-3.70	20.13	0.807	-2.10
320	49.80	26.215	6.22	24.35	0.929	-3.70	-	-	-
300	50.09	26.292	6.26	24.50	0.932	-3.50	21.17	0.805	-2.29
322	53.39	27.140	6.67	25.28	0.931	-3.76	21.97	0.809	-2.77
323	56.61	27.952	7.08	26.05	0.932	-4.04	(22.57)	(0.807)	-2.65
324	60.16	28.814	7.52	26.82	0.931	-4.31	23.25	0.807	-2.73
535	65.41	30.04	8.176	28.06	0.934	-4.27	-	-	-

[a] V is the velocity of the product peak at zero laboratory degree and V_0 is the initial ion beam velocity. For ideal stripping $V/V_0 = 0.933$ and for ideal knockout $V/V_0 = 0.809$.

[b] ( ) results very uncertain.

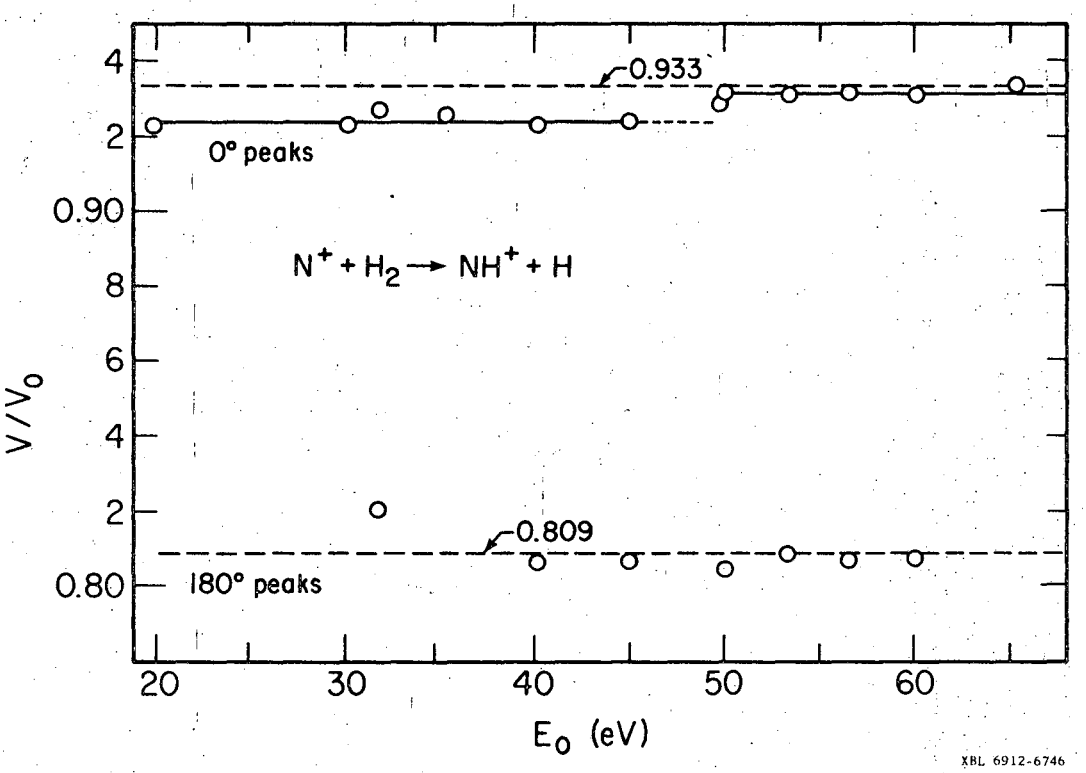

Fig. 7. Product ion velocity as a function of the initial energy of the primary ion. For ideal stripping $V/V_0 = 0.933$ and for ideal knockout $V/V_0 = 0.809$.

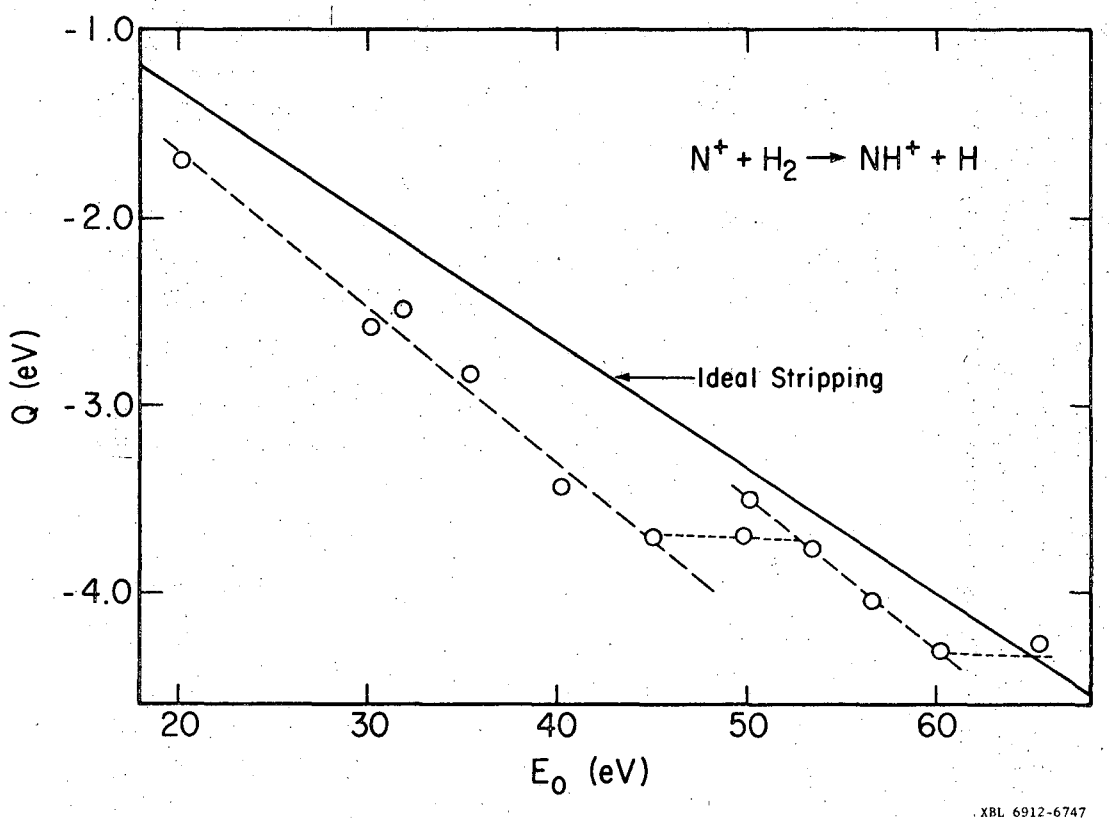

Fig. 8. Variations in the translational exothermicity as a function of the initial energy of the primary ion.

points roughly fall on the same straight line; so do the points between 50 eV and 60 eV. From the calculated limits of Q (see Table II), below 35 eV (N^+) only $NH^+(^4\Sigma^-$ or $^2\Pi)$ are expected to be stable. Above 35 eV $^4\Sigma^-$, $^2\Pi$, $^2\Delta$, and $^2\Sigma^-$ can be stable. Why does such an abrupt change occur at 45 eV? One possible explanation is that above 45 eV only $NH^+(^2\Sigma^-)$ or $^2\Delta$ is formed. If $NH^+(^4\Sigma^-$ or $^2\Pi)$ were also present above 50 eV, we would expect a rather broad NH^+ product peak which spans over 0.925v and 0.932v, but the experimental peaks were as sharp as the primary beam. Using the same arguments, it can be seen that only the $^4\Sigma^-$ and $^2\Pi$ states of NH^+ were formed below 45 eV.

If the above statement is correct, we may further speculate into the reason why the $NH^+(^2\Pi)$ velocity is much slower than the ideal stripping reaction while $NH^+(^2\Sigma^-)$ is close to it. Let us try to follow the reaction pictorially. At the instant of reaction $N^+ + H_2$ probably has a configuration like $(N^+H\cdots H)$ although it may not be linear—we shall refer to $(N^+H\cdots H)$ as the transient state. As N^+H leaves the reaction site, it may rotate so that the transient state looks more and more like HNH^+. Since the bond energy of $HN\text{-}H^+$ is about 6 eV,[35] the "spectator" H atom interacts with NH^+ and slows it down (see Fig. 9). If such an argument is correct, other reactions, in which the transient state has a known, stable, strong bonding configuration, would behave in such a manner also. CO+(H2,H)COH+ is such a reaction.[6,12] The transient molecule H_2CO^+ is stable and the $HCO\text{-}H^+$ bond is quite strong. Indeed, the velocity of HCO^+ occurred below the stripping velocity in the primary ion (CO^+) range 15 eV to 40 eV. No other known example was found in the literature.

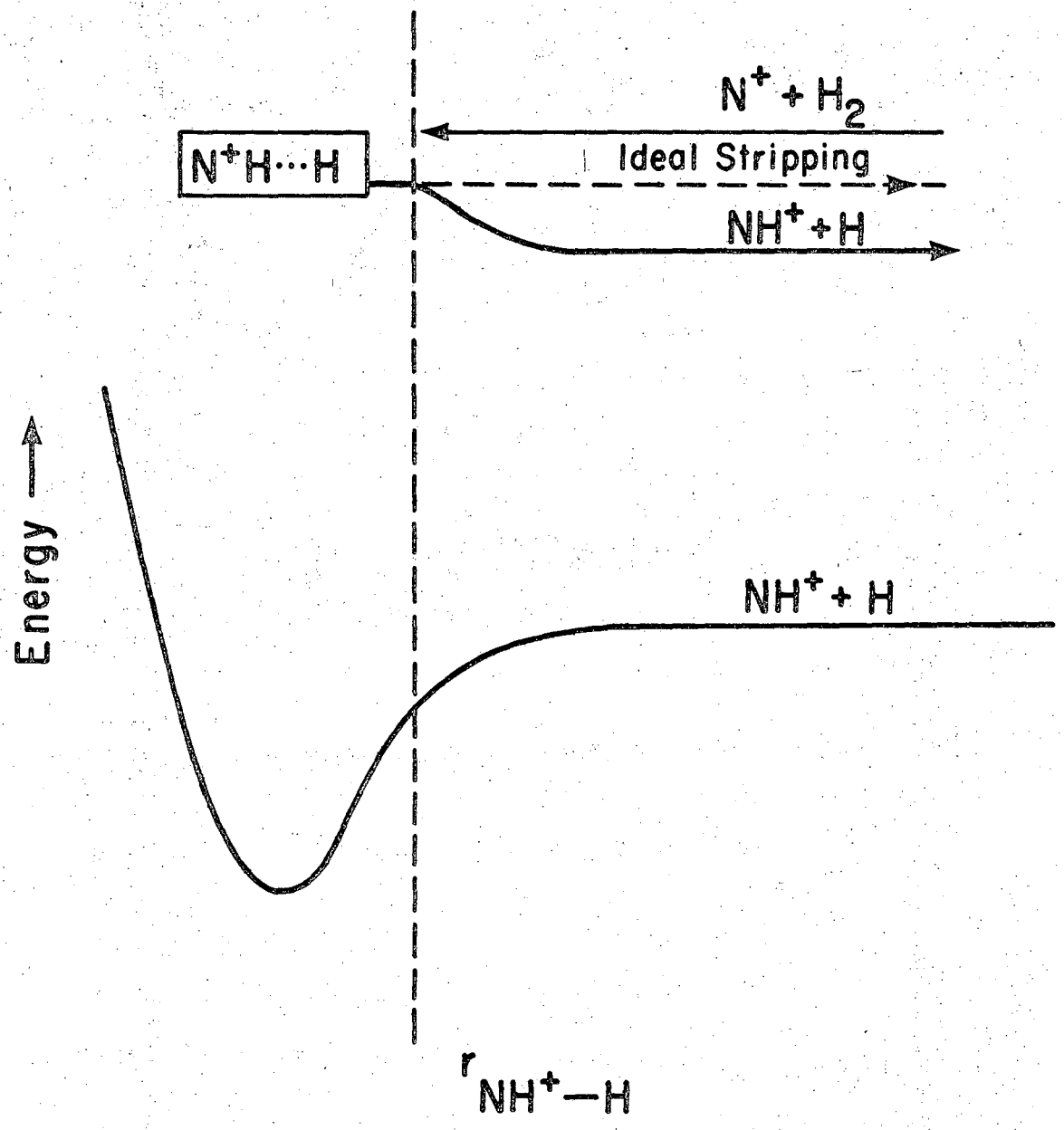

XBL 6912-6738

Fig. 9. Schematics of a reaction path (one dimensional) of $N^+ + H_2 \rightarrow NH^+ + H$.

Other possible examples are O+(N_2,N)NO+ and C+(H_2,H)CH+. Their transient states N_2O^{+} and CH_2^{+} are stable molecules and have strong bonds.

A better analysis can be given to the transient state leading to the product $NH^{+}(^2\Sigma^{-})$. There seems to be no spectroscopic data available on NH_2^{+} and the arguments below are based on what little we know about CH_2, which is isoelectronic with NH_2^{+}. $NH^{+}(^2\Sigma^{-})$ + $H(^2S_g)$ give the $^3\Sigma_g^{-}$ state (linear) and $^3B_1$ state (bent) of NH_2^{+}. The H atom is strongly bonded to NH^{+} in the $^3\Sigma_g^{-}$ state, $D(HN\text{-}H^{+}) \geq 4.0$ eV.[36] The dissociation energy of the $^3B_1$ state is not known. Probably $D(HNH^{+})$ in the $^3B_1$ state is smaller than the $^3\Sigma_g^{-}$ by 1 eV to 2 eV.[37] Due to the geometry of the reaction, we would not expect the transient molecule, NH_2^{+}, to interact like the linear $^3\Sigma_g^{-}$ state; instead the $^3B_1$ state could be a close approximation to the actual configuration. No information is available on the $^3B_1$ state of CH_2. However, after reaction, N^{+} will either be dragging the picked up H atom behind or the newly formed NH^{+} will be tumbling in space with the "spectator" H atom a short distance behind. In either case, the $H\cdots NH^{+}$ bond will be very strained and in such case the interaction is quite weak. Hence NH^{+} does not feel much dragging force from the spectator and we expect to have the NH^{+} velocity close to but never faster than the stripping velocity. This is exactly what was observed in the experiments done between primary energies 50 eV to 60 eV. The product $NH^{+}(^2\Sigma^{-})$ velocity is just below the ideal stripping velocity, indicating that the $NH^{+}(^2\Sigma^{-})$ and H interaction is very weak. To carry one step further, v/v_0 can be greater than 0.933 only if the interaction between NH^{+} and H is repulsive. No such analysis can be extended to the formation of

$NH^+(^4\Sigma^-)$ and $NH^+(^2\Pi)$; our knowledge of CH_2 is limited to the few states close to the ground state. If the above argument is correct, the attraction between $NH^+(^4\Sigma^-$ or $^2\Pi)$ and H is probably stronger than those in $NH^+(^2\Sigma^-)$ + H.

As the reaction energy is increased, products in the $^2\Sigma^+$ and $^2\Delta$ states will be formed. However, at a relative energy of 9.5 eV or 76 eV (lab), the energy is high enough to dissociate the H_2 molecule. Above 76 eV (lab) the reaction channel N^+ + H + H will compete statistically with other channels of reaction. The NH^+ signal at 65 eV is quite low already, and we might not see any NH^+ with the dissociation channel competing in the reaction. One more point to be noted is that in $N_2^+ + D_2$ experiments,[9] collision induced dissociation of H_2 has a threshold of 6.0 eV, so this channel of reaction may start to compete with other channels around 50 eV.

The reaction of $N^+(^1D) + H_2$ is not important. As shown in Section E-5 below, it is not likely to find $N^+(^1D)$ in the primary ion beam from the electron bombardment source.

3. Differential Cross Sections

Figure 10 shows the differential cross sections at energies 3.98 eV and 5.01 eV respectively. The cross sections at 100° and 120° of the reaction at 5.01 eV are probably in error. If the argument in Section E-1 is followed, these points should be lowered to the indicated position. The angular distribution becomes broader as we go from 3.98 eV to 5.01 eV. This apparently is due to a more intimate collision at higher energies as was observed in the $N_2^+ + CH_4$ reaction.[11] Because of the poorer angular resolution of this system, the

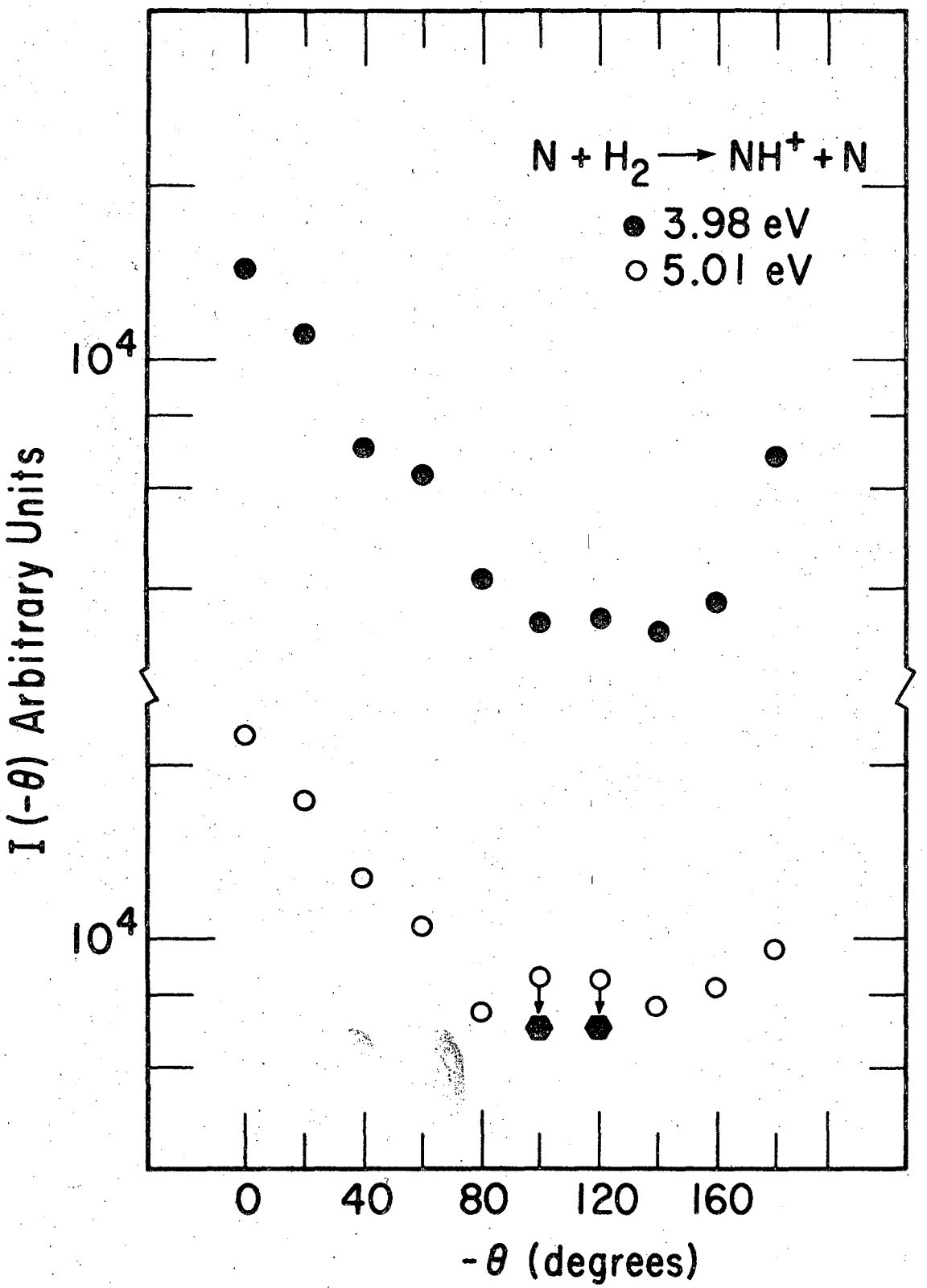

Fig. 10. Differential cross-sections for the reaction $N^+ + H_2$. The two points at 100° and 120° of the 5.01 eV reaction are probably in error and should be lowered to the indicated position.

differential cross-section is not as sharp as that of the $N_2^+ + CH_4$ reaction. Figure 11 gives the CM angular resolution of the elastic collisions of $N_2^+ + CH_4$ and of $N^+ + H_2$. Angle AOB is the laboratory resolution. As shown in the drawing, the CM angular resolution in $N^+ + H_2$ is 17° whereas it is only 6° in $N_2^+ + CH_4$. For reactive scattering the resolution is worse than this. The maximum laboratory scattering angle of N+(H_2,H)NH+ is 3.6°, compared to 8.25° in the elastic scattering case. The CM resolution in the reactive system of $N^+ + H_2$ is about 40°! Thus for the same laboratory resolution, we have a very different CM resolution in different systems. The angular resolution affects the differential cross-section greatly. Recently, Aberth and Lorents[38] showed that an improvement of angular resolution from slit dimensions 0.5×0.05 cm^2 to 0.1×0.05 cm^2 increased the small angle differential cross section of $Li^+ + He$ by more than 100%! Until the angular resolution of $N^+ + H_2$ is reduced to 5° or better, no meaningful comparison can be made between these systems.

4. Back-Scattered Product

Like the reactions N2+(D2,D)N2D+ and Ar+(D2,D)ArD+, intensity maxima were observed behind the center of mass in N+(H2,H)NH+. The results are tabulated in Table III and in Fig. 7. In general, these intensity maxima are braoder than the (forward) stripping peak, indicating many different processes lead to this back maximum. However, all the intensity peaks observed centered around the so-called knock-out peak[9] position as can be seen in Table III. The Q values observed in these intimate collisions are well below the dissociation limits of NH^+ and their intensities remain relatively constant over the range of energies studied.

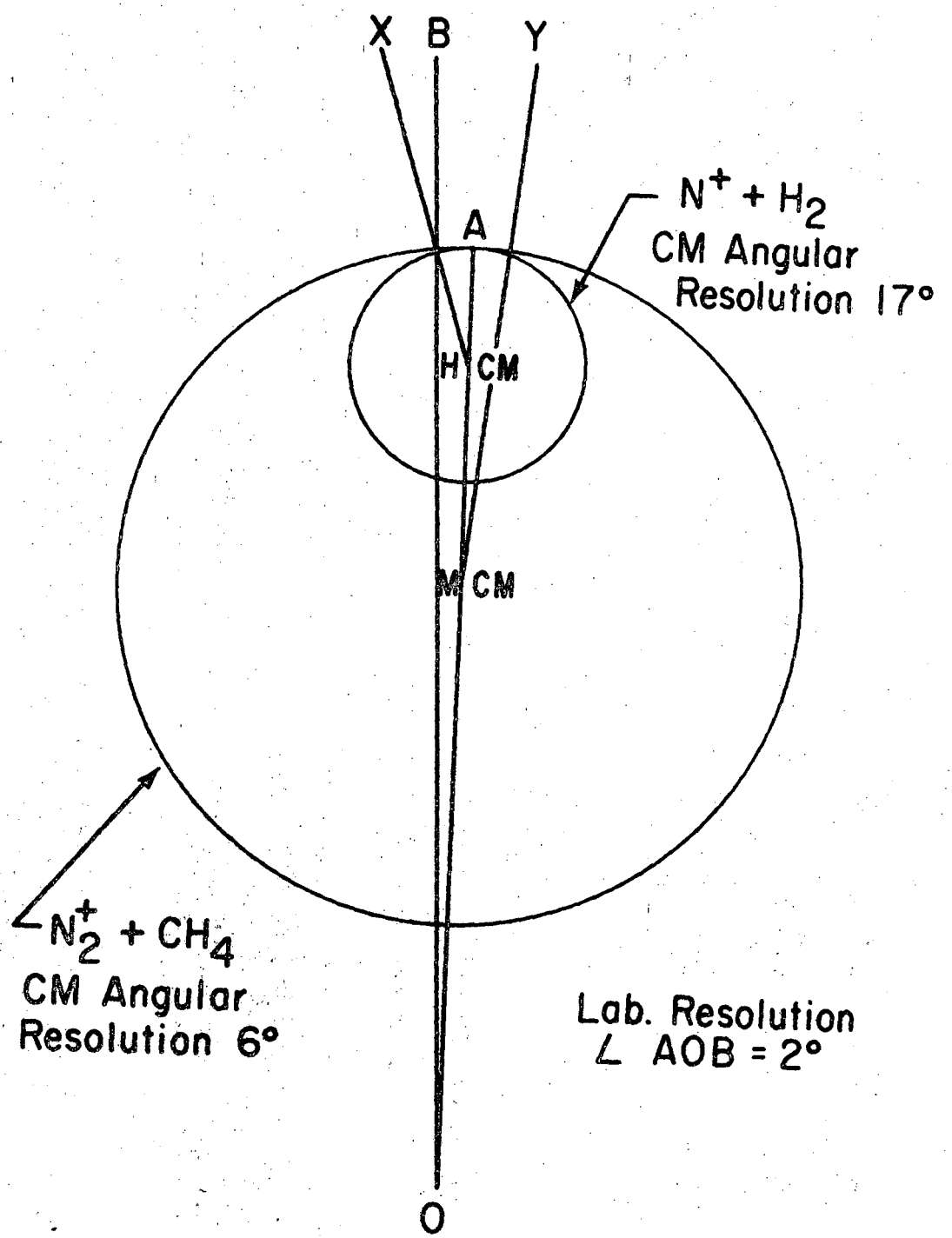

Fig. 11. Vector diagram of elastic scattering showing the angular resolutions of the collisions $N_2^+ + CH_4$ and $N^+ + H_2$ in both the CM and Lab systems.

5. Conversion of Translational Energy to Internal Excitation

Concurrent with the reactive studies, nonreactive collisions of N^+ with He were also carried out. The only possible internal excitation for this system is an electronic excitation of N^+. The range of energy used was too low to excite He electronically. Indeed, electronic excitations of N^+ were observed. Figure 12 shows an intensity map for the following scattering

$$N^+(^3P) + He \rightarrow N^+(^3D) + He \qquad (17)$$

The energy required for the transition is 11.4 eV and is indicated on the map by the 11.4 eV circle. The scattering signal appearing at large angles is due to elastic collision on He.

The interesting feature on the map is the 11.4 eV intensity peak. Normally, it is expected that close or head-on collisions are necessary to transfer large amounts of energy. As a result, inelastically scattered N^+ would be expected to appear near 180° and perhaps the backward elastic scattering should be diminished. To the contrary only small angle scattering was seen. If the primary beam profile is compared with that of the 11.4 eV intensity peak, the inelastically scattered N^+ will come out almost exactly at 0°. Mahan[39] suggested that in the collision, the potential energy curve of $N^+(^3P)$ + He crossed or came very close to that of $N^+(^3D)$ + He at some internuclear distance and N^+ exited via the $N^+(^3D)$ + He curve (see Fig. 13). If $N^+(^3D)$ + He is attractive, after-curve crossing N^+ will be attracted toward He; as a result $N^+(^3D)$ will appear to scatter through a small angle.

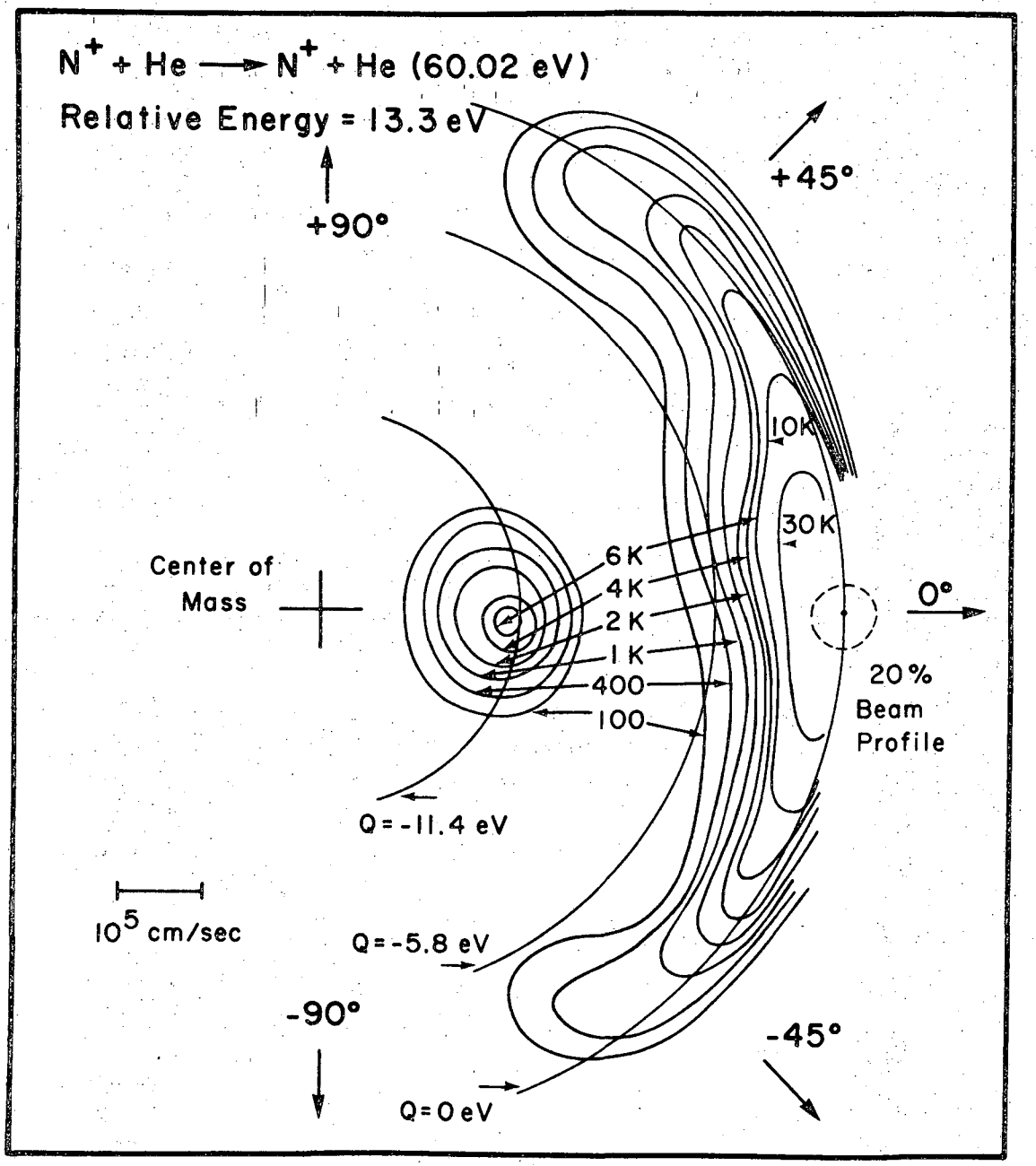

XBL 6912-6701

Fig. 12. A contour map of the relative intensity of N^+ scattered from He. The dashed line gives the profile of the ion beam at 20% of its maximum intensity. The change in the relative translational energy (Q) of the collision partners is indicated on the map.

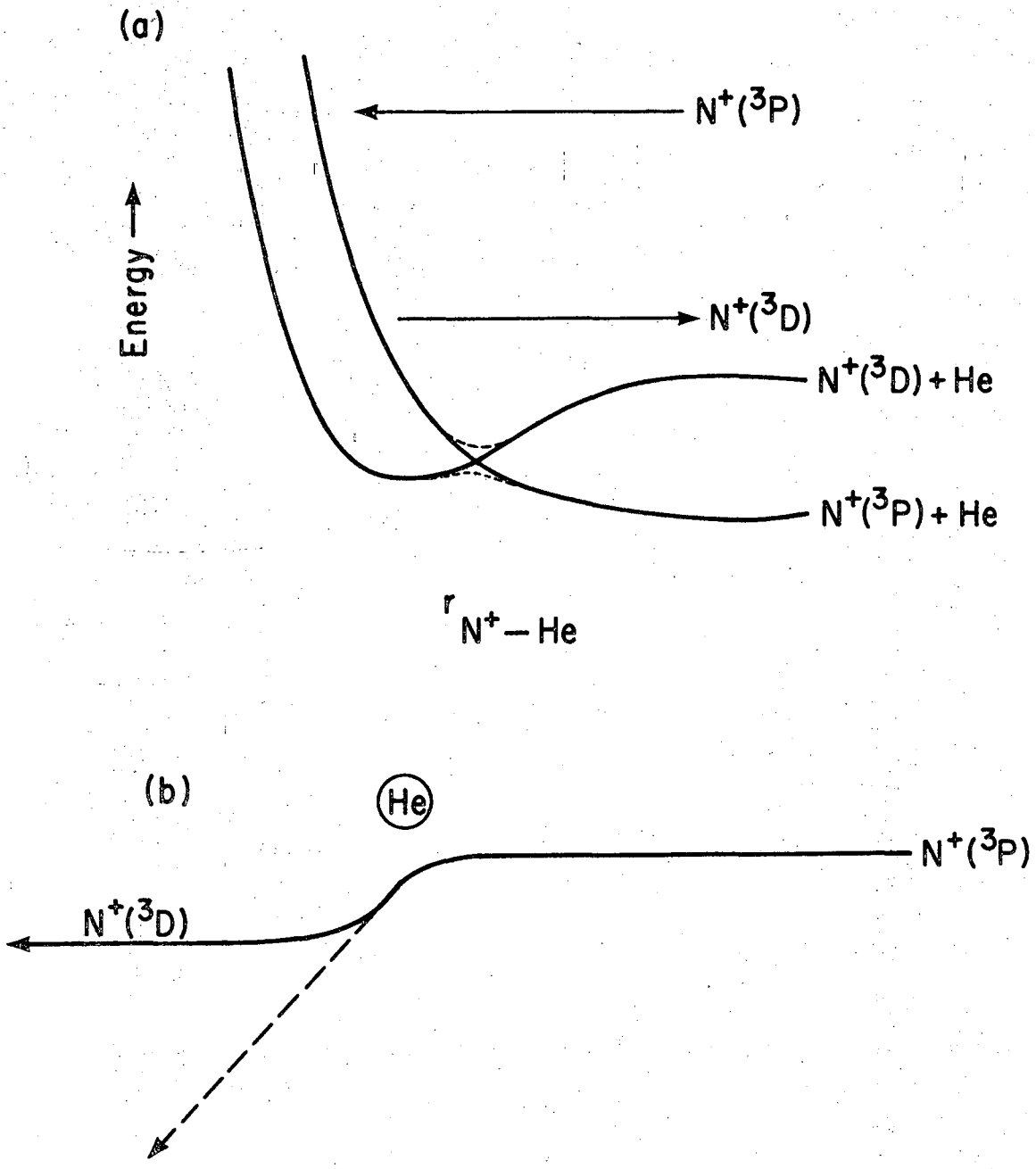

Fig. 13. Schematics of an inelastic process. (a) One dimensional scattering: Curve crossing of $N^+(^3P)$ + He and $N^+(^3D)$ + He. (b) Two dimensional scattering: If there is no attraction between $N^+(^3D)$ and He, $N^+(^3D)$ would proceed via the dotted path.

A series of these experiments were performed with different energies of N^+ and they are summarized in Table IV, together with the assignment of possible transitions. No angular measurements were made with these collisions. Experiments in the 300 series were performed with the electron bombardment source while the 500 series with the microwave source. Figure 14 is a Grotrian diagram of N^+ with energy values taken from Moore.[40] From the data, the transitions of $N^+(^3P) \rightarrow N^+(^3D)$ and $N^+(^5S) \rightarrow N^+(^3D)$ were identified. In general, an assignment was made based on the fact that a transition cannot take place with an energy less than that required for the process. For example, in experiments 309 and 310, the Q values involved were -5.6 eV and -5.7 eV respectively. Now the transition $^3P \rightarrow {}^5S$ takes 5.85 eV while $^5S \rightarrow {}^3D$ requires only 5.6 eV. In these experiments, there was not enough energy for the $^3P \rightarrow {}^5S$ to take place. Furthermore, the ions from the microwave source should not have any $N^+(^5S)$, as evident from the arguments in the text below. The 5.6 eV transition was not observed in all the experiments performed with the microwave source indicating the absence of the $^3P \rightarrow {}^5S$ transition. The assignments were then made to $^5S \rightarrow {}^3D$ unambiguously.

It may be rather surprising not to see the $^3P \rightarrow {}^3P$ transition. The relative energies in some of these experiments were sufficient to cause the excitation. There are two reasons that such a transition was not observed. If the potential curve of $N^+(^3P)$ + He is repulsive the signal would be scattered out to large angles and missed the detector. Since the $^3P \rightarrow {}^3P$ transition is allowed optically, its radiative lifetime is very short and the presence of this transition

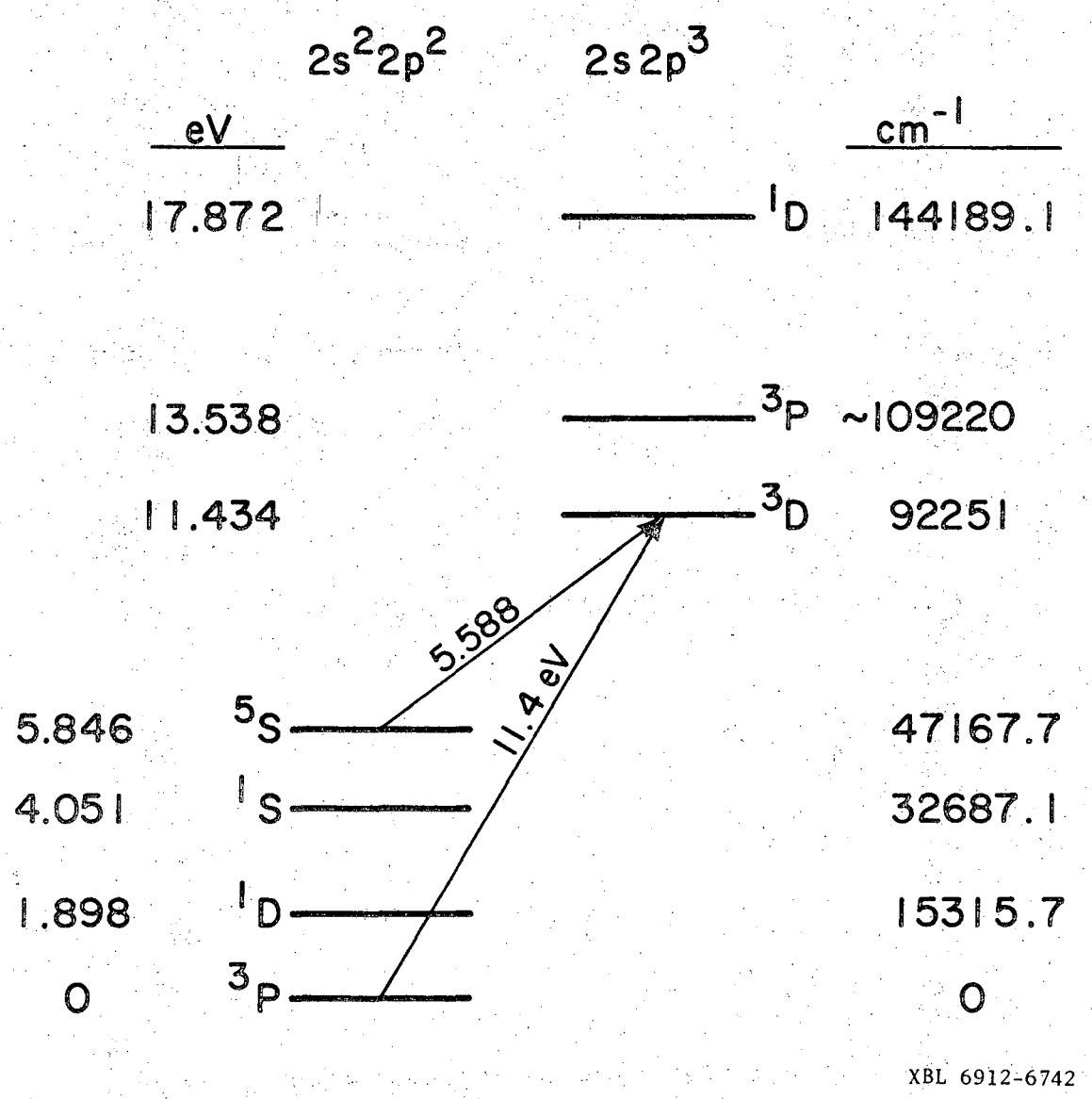

Fig. 14. Electronic energy level diagram for N^+.

is best observed optically. Secondly, if the curve were attractive, the curves might cross at an energy higher than those reached in these experiments. Hence, it should also be pointed out that failure in observation of the other transitions does not necessarily indicate small cross-section.

The inelastic scattering data also reveal the composition of our ion beam. N^+, as produced from the microwave discharge source, should mostly be in the ground electronic state. The source pressure is typically set at 10 to 50 microns, and N^+ will suffer several collisions before being extracted from the source. In this case, almost all N^+ would be de-excited before colliding with He. However, Experiments 506 and 534 show that the beam coming from the microwave source may contain some $N^+(^1D)$. The Q value observed in 506 can only be assigned to $^1D_2 \rightarrow {}^3D$, while the assignment for 534 can either be $^3P \rightarrow {}^3D$ or $^1D \rightarrow {}^3P$. This is expected since the electron energy inside the source (6 eV)[27] is high enough to excite $N^+(^3P)$ to $N^+(^1D)$. The composition of N^+ from the electron bombardment source is more complicated, due to the high electron energy (about 90 eV) in the source. By comparing the velocity spectrum of N^+ from the microwave and from the electron bombardment source at 40 eV (lab) and at 65 eV (lab), the existence of $N^+(^5S)$ in the electron bombardment source can positively be shown. It is not likely to find the first excited state (^1D) from the electron bombardment source since electron impact studies have not been able to demonstrate the formation of this state.[41] Furthermore, according to the Wigner-Witmer rules, $N^+(^1D)$ correlates only with quartet states, but no quartet states of N_2^+ have been observed spectroscopically.

Table IV

Electronic transitions in N^++He

Exp. No.	E_0 (eV)	E_S^0 (eV)	Q(peak) (eV)	Possible Transitions
311	39.93	8.87	-(2.30)	, ($^1D_2 \rightarrow {}^1S_0$)
			-5.4	$^5S_2 \rightarrow {}^3D$
507	40.00	8.88	No signal	
308	50.02	11.12	-(3.5)	
			-6.7	
506	50.18	11.15	-10.8	($^1D_2 \rightarrow {}^3D$)
315	60.02	13.34	-11.6	$^3P \rightarrow {}^3D$
309	65.25	14.50	-5.6	$^5S_2 \rightarrow {}^3D$
			-11.8	$^3P \rightarrow {}^3D$
505	70.91	15.76	-11.8	$^3P \rightarrow {}^3D$
310	75.25	16.72	-5.7	$^5S \rightarrow {}^3D$
			-11.9	$^3P \rightarrow {}^3D$
316	109.45	24.32	-7.6	$^5S \rightarrow {}^3P$
			-12.3	$^5S \rightarrow {}^1D$
534	110.23	24.49	-12.0	$^3P \rightarrow {}^3D_0$ $^1D \rightarrow {}^3P$

( ) Data very uncertain.

E. Summary

In this section, a reaction model was proposed to explain the observed data. In its simplest form, this model utilized the stripping mechanism at the first instance of reaction. After the reaction a "chemical potential" was turned on between NH^+ and H causing the product NH^+ to slow down. Such a model explained the kinematic results qualitatively. Due to a complete lack of knowledge of such chemical potential, no numerical computation was attempted.

In the nonreactive collisions, a curve crossing model was proposed to explain the transition $N^+(^3P) \rightarrow N^+(^3D)$. The assignment of $N^+(^5S) \rightarrow N^+(^3D)$ was deduced from experiments done with ions produced from both the electron bombardment source and the microwave source.

V. O_2^+ EXPERIMENTS

A. Survey of Literature

Previous investigations in ion-molecule reactions by beam techniques[4,6,9] have been limited to thermo-neutral or exothermic reactions. These exothermic reactions have the attractive features that their products are confined to a small forward cone due to favorable mass ratios and that the cross-sections of reaction are quite large. Both of these features enable detection of the products with instruments of relatively low sensitivity. Endothermic ion-molecule reactions have long been investigated by mass-spectrometry.[42,43] These studies revealed two distinct differences between the endothermic and the exothermic reactions. First, the endothermic reaction has a reaction threshold behavior sharply different from that of the exothermic reaction. Second, in general, the reaction cross-section at low energies is much larger for exothermic systems than the endothermic ones. However, these studies did not indicate the mechanism by which the molecules react.

The reaction $O_2^+ + H_2$ has been examined in detail by mass-spectrometry. The formation of O_2H^+ from O_2-H_2 mixtures in a mass-spectrometer ion source was observed by Schissler and Stevenson.[44] They concluded that their O_2H^+ came from the reaction H2+(O2,H)O2H+. Moran and Friedman[45] studied the isotope effects (with HD) and hinted about the intermediate complex $H_2O_2^+$. The energy dependence of the cross-section for the formation of O^+, OH^+ from $O_2^+ + H_2$ was investigated by Rafaey and Chupka.[46] Again no mechanistic studies were made. Fehsenfeld et al.[30] in an afterglow discharge experiment failed to observe any

reaction for thermal $O_2^+(^2\Pi_g) + H_2$. This is expected; the reaction is endothermic. Guided by these previous investigations, a detailed study of the reaction dynamics of $O_2^+ + H_2$ was carried out.

B. Reaction Energy Level Diagram

A casual examination of the $O_2^+ + H_2$ reaction reveals that the following reaction channels are possible.

$$
\begin{aligned}
&(1) \quad O_2^+ + H_2 \rightarrow O_2H^+ + H \qquad \Delta E_0^0 = 1.82 \text{ eV} \qquad (18)\\
&(2) \quad \rightarrow OH^+ + OH \qquad \Delta E_0^0 = 2.14 \text{ eV}\\
&(3) \quad \rightarrow H_2O^+ + O \qquad \Delta E_0^0 = 0.81 \text{ eV}\\
&(4) \quad \rightarrow O^+ + H_2O \qquad \Delta E_0^0 = 1.81 \text{ eV}\\
&(5) \quad \rightarrow H^+ + O_2H \qquad \Delta E_0^0 = 3.88 \text{ eV}\\
&(6) \quad \rightarrow H_2^+ + O_2 \qquad \Delta E_0^0 = 3.227 \text{ eV}
\end{aligned}
$$

The heats of reaction are indicated to the right; they are all endothermic. Reaction channels (5) and (6) were not studied; the H^+ and H_2^+ produced in these reactions have energies too low to be detected in our experimental system. All the other reaction channels were observed.

Table V lists the ionization potentials and the dissociation energies of all the reactants and products involved in the reactions.[17,36,47] From Table V, an energy level diagram for all possible ground state reaction channels can be prepared, as in Fig. 15. Some explanation of the diagram is in order. The energy level diagram is drawn analogous to the ones we so often see in molecular spectroscopy. The heavy horizontal lines give the reaction channels in units of energy above or below the reference channel; here $O_2^+ + H_2$ is taken as the zero energy reference channel. Positive energies indicate

Table V

Thermochemical and spectrocopic data for the reaction $O_2^+ + H_2$

Molecules or ions	I[a] (eV)	D_1[b] (eV)	D_2 (eV)
H_2^+	-	2.648	-
O_2^+	-	6.8	-
O_2H^+	-	* 2.66 (O_2^+-H)	*4.4 (O-OH^+)
OH^+	-	* 4.765 (OH^+)	-
H_2O^+	-	* 5.68 (HO^+-H)	-
$H_2O_2^+$	-	* 4.49 (HO_2^+-H)	*4.40 (HO^+-OH)
H	13.595	-	-
O	13.615	-	-
H_2	15.427	4.476	-
O_2	12.20	5.08	-
O_2H	11.53	1.99 (O_2-H)	2.7 (HO-O)
OH	13.18	4.35	-
H_2O	12.61	5.113	-
H_2O_2	10.92	2.12 (HO-OH)	3.88 (HOO-H)

*Calculated value (Born-Haber cycle).[48]

a. Ionization potential.

b. Bond dissociation energy.

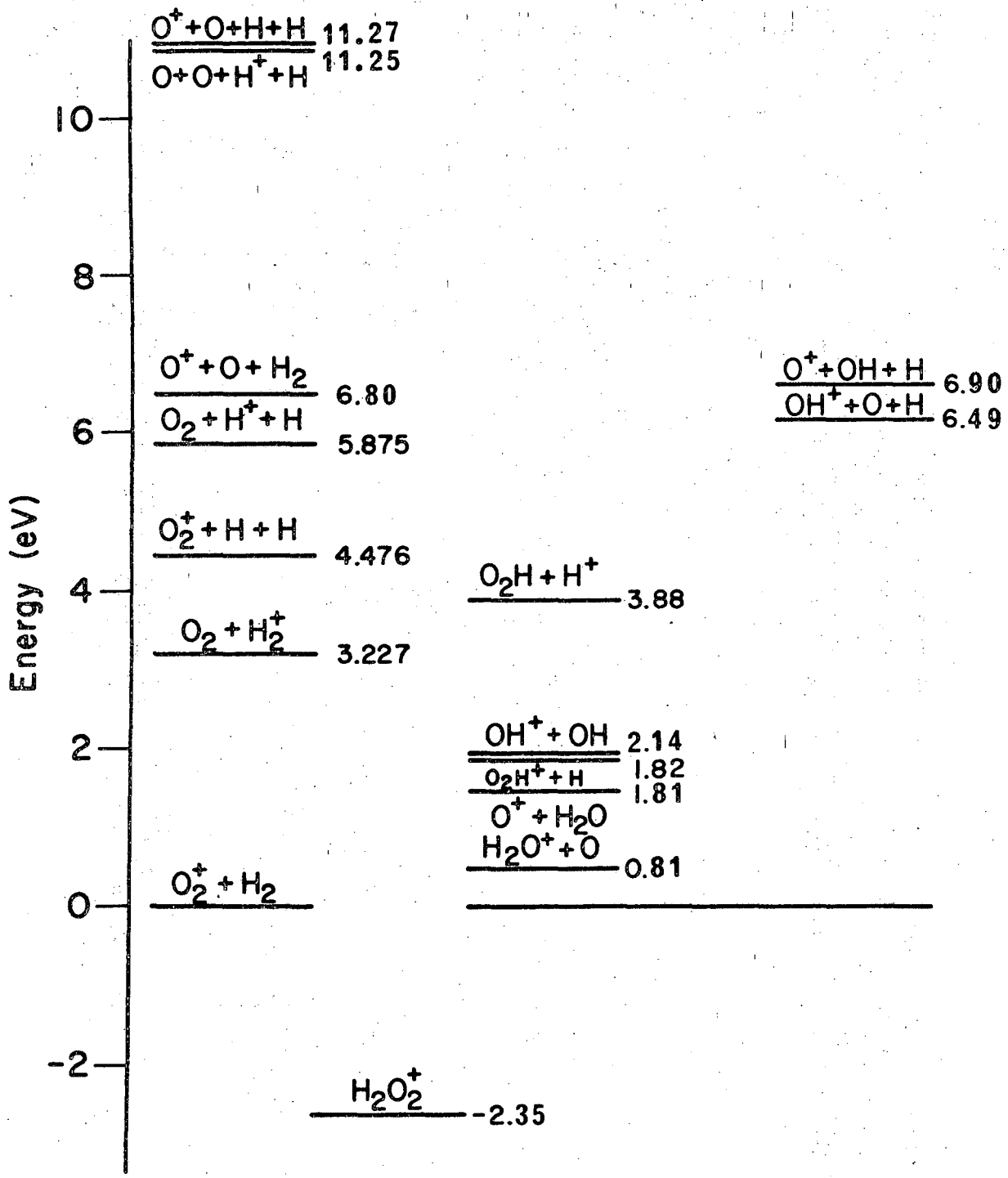

Fig. 15. Reaction Energy level diagram for ground state $O_2^+ + H_2$.

endothermic systems while negative energies give exothermic reactions. For example, to go from $O_2^+ + H_2$ to the products $O_2H^+ + H$, the endothermicity is + 1.8 eV as designated in the diagram, while the formation of $H_2O_2^+$ is exothermic by -2.35 eV. The difference in the endothermicity of levels yields the energy required for a specific process between two different reaction channels.

The reaction channels drawn in the middle of the diagram are the six basic reactions that we referred to earlier. The two channels on the right come from the dissociation of reaction channels from the middle of the diagram. Non-reactive collisions are indicated to the left of the diagram. Although some of these reactions may be the dissociative products of the reactive channels, they are listed with the non-reactives.

C. Configuration of the Complex

With the formation of a complex, we can speculate on the configuration of the transition state. Of course when the collision energy is high enough and when the lifetime of the complex is short any geometry is possible for the complex. Since we are dealing with a four atom system, there are not too many arrangements that one can make. Some of these can be eliminated on the grounds of rotation of the molecule. Figure 16 (a) displays the four possible configurations of this four-atom system at the first instance of reaction.

However, if the complex has a lifetime of more than a few rotations, the molecule will have time to rearrange itself. Thus the configurations with the lowest energies tend to be most probable. Herzberg[49] has discussed some of the stable configurations of H_2O_2 and they are

(a) At high reaction energy

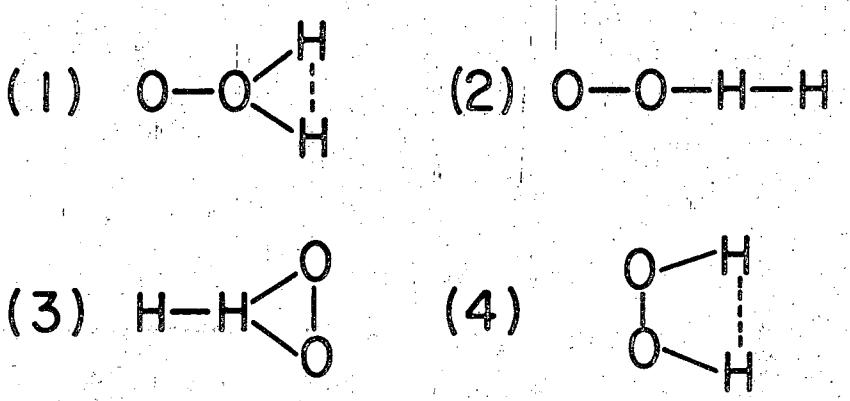

(b) At energies closed to the threshold

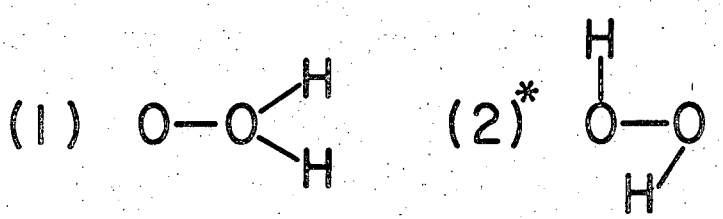

*(b-2) is nonplanar

XBL 6912-6741

Fig. 16. Suggested configurations of $H_2O_2^+$.

in Fig. 16 (b). These are the favored configurations at energies closed to the threshold of the reaction.

D. General Features of the Reaction

The existence of a collision complex in bimolecular reactions has been postulated many years in the Absolute Rate Theory. Such a theory was applied and found good agreement between some experimental and theoretical results.[14] The occurrence of a collision or activated complex is central in the Absolute Rate Theory. Collision complexes in simple bimolecular reactions were searched in earlier efforts in crossed molecular beam studies.[50] However, for the majority of the reactions they examined, no evidence of a collision complex was found. Instead, direct mechanisms predominated in these reactions. Recently, groups in Harvard and in MIT[15,51] found definite evidence for collision complexes in the reactions of alkali atoms and alkali halides. It seems that the concept of an activated complex is verified, although complexes do not exist in every reaction, as would be necessary for the universal applicability of the Activated Complex Theory. It is to be expected that in the future, further examples of both types of reaction mechanisms will be found.

The efforts in the search for a collision complex in ion-molecule reactions parallelled those in neutral-neutral reactions. Indeed, investigators in ion-molecule reactions have more to hope for since all ion-molecule reactions involve the strong ion induced-dipole interaction. Early experiments in the study of $N_2^+ + (H_2, H)N_2H^+$ [4,6,9] and $Ar^+ + (H_2, H)ArH^+$ [9,6,10] failed to find any trace of a complex even when the reaction energy was as low as 0.1 eV. Subsequent investigations

in $H_2^+ + H_2$,[52] $N_2^+ + CH_4$,[11] $N_2^+ + C_2D_2$,[53] and a host of other reactions did not yield any evidence for a complex. A very large domain of ion-molecule reactions is dominated by direct reactions.

Recently, groups in California and Colorado reported evidence of intermediate complex formation in ion-molecule reactions. The Colorado group communicated on the reaction[54]

$$C_2H_4^+ + C_2H_4 \rightarrow [C_4H_8^+] \rightarrow CH_3 + C_3H_5^+ \qquad (19)$$

They observed a product distribution which was symmetric to the ±90° in the center of mass system. Similar evidence was also found in our study of $O_2^+ + H_2$, and the initial results have been published.[55] A more detailed analysis of the reaction is now given in this thesis.

Due to the complexity of this reaction we will concentrate successively on each product in the following order: O_2H^+, H_2O^+, OH^+, and O^+. Contour maps and velocity spectra were made for all the products observed. Because of the problem of mass separation between O_2^+ and O_2H^+ at energies close to the primary beam, D_2 was used in place of H_2 in most experiments. We should emphasize that there is no problem in separating O_2H^+ and O_2D^+.

1. O_2H^+

a. Reactive Maps. Figures 17 through 20 show the intensity contour maps of O_2D^+ in progressing reaction energies. For

$$O_2^+(^2\Pi_g) + D_2 \rightarrow O_2D^+ + D \qquad (20)$$

the values of Q consistent with this reaction are given by

$$-4.55 \text{ eV} \leq Q \leq -1.89 \text{ eV}$$

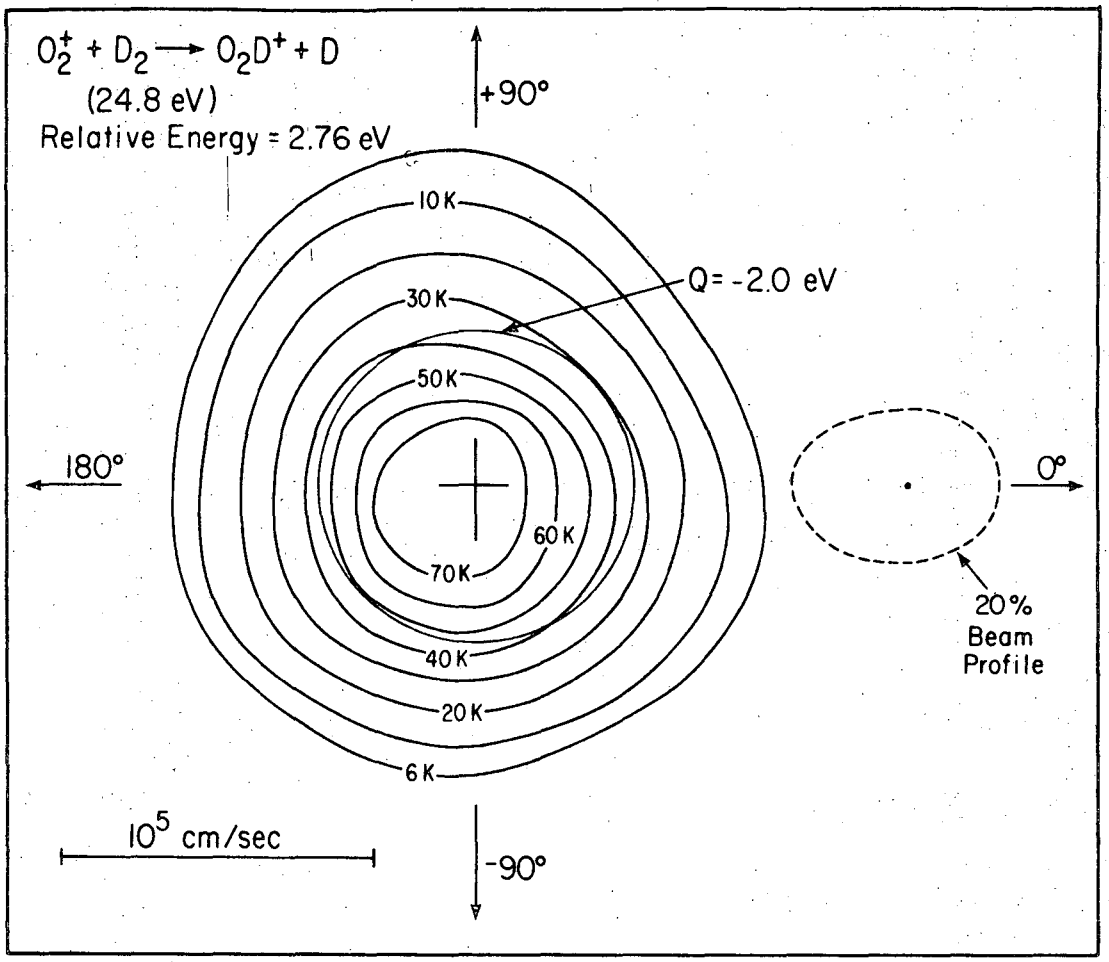

XBL 6912-6698

Fig. 17. An intensity contour map of O_2D^+ in the center of mass coordinate system at 2.76 eV.

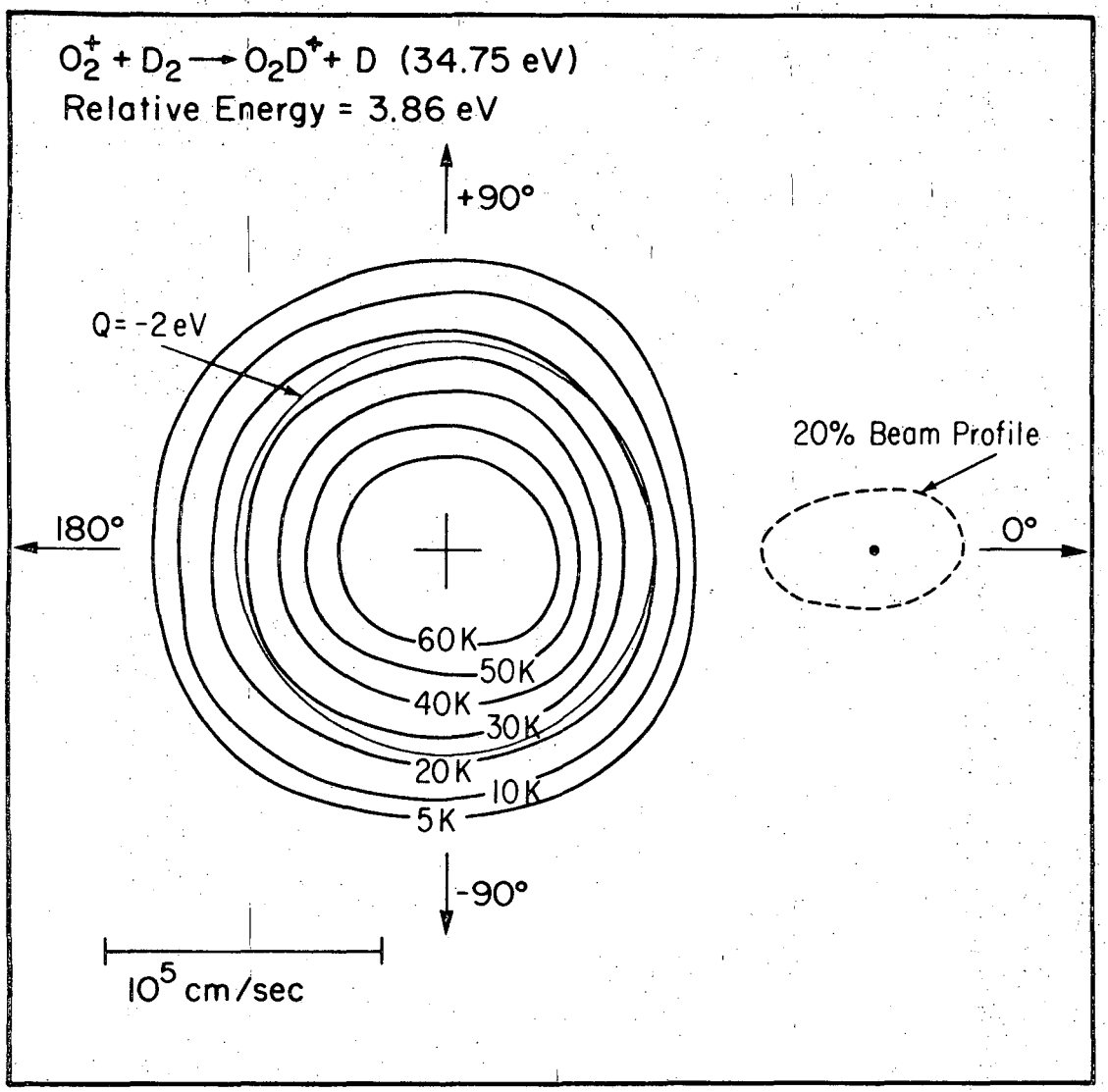

XBL 6912-6699

Fig. 18. An intensity contour map of O_2D^+ in the CM system at 3.86 eV.

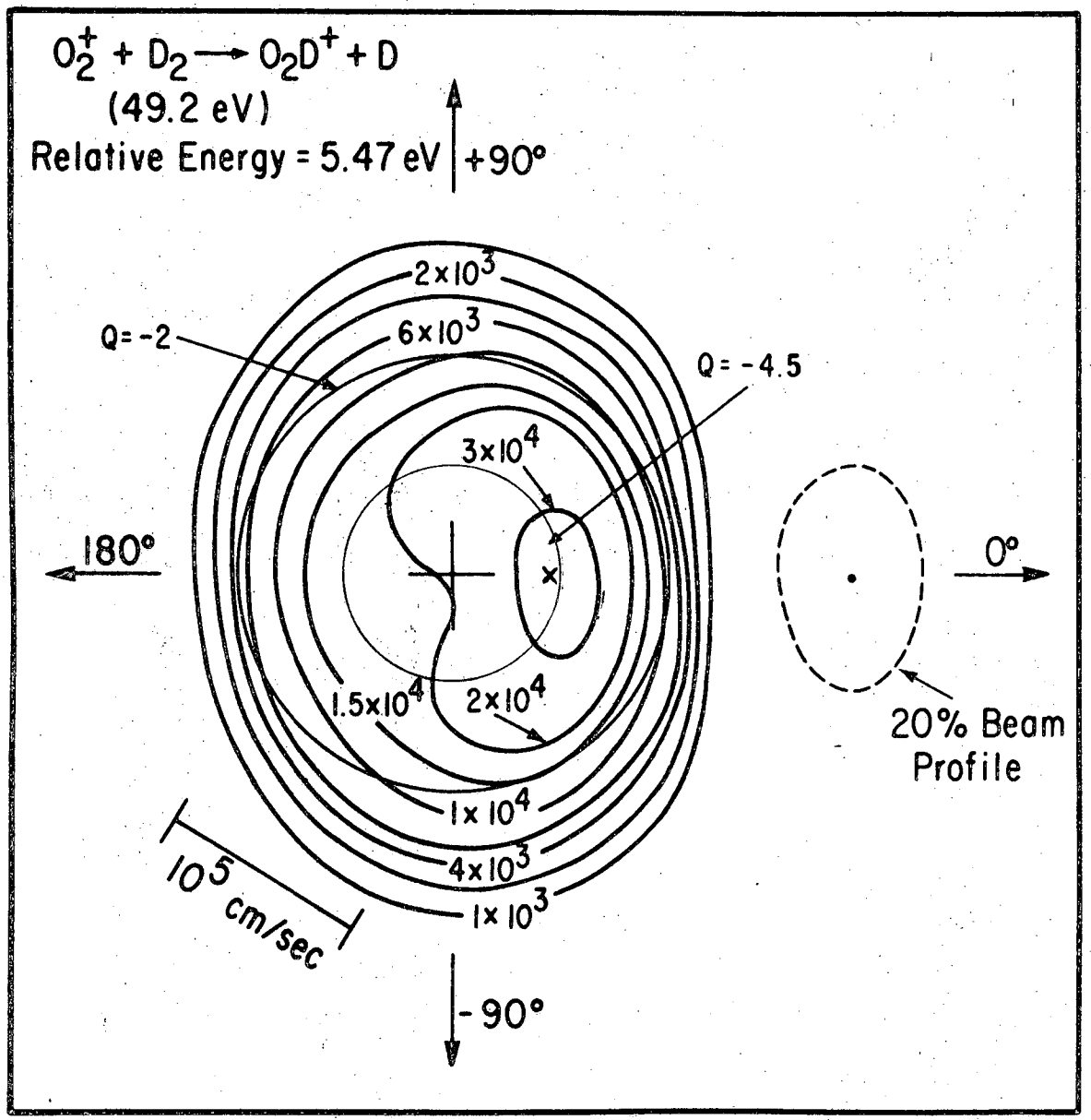

Fig. 19. An intensity contour map of O_2D^+ at 5.47 eV. The cross indicates the position of maximum O_2D^+ intensity.

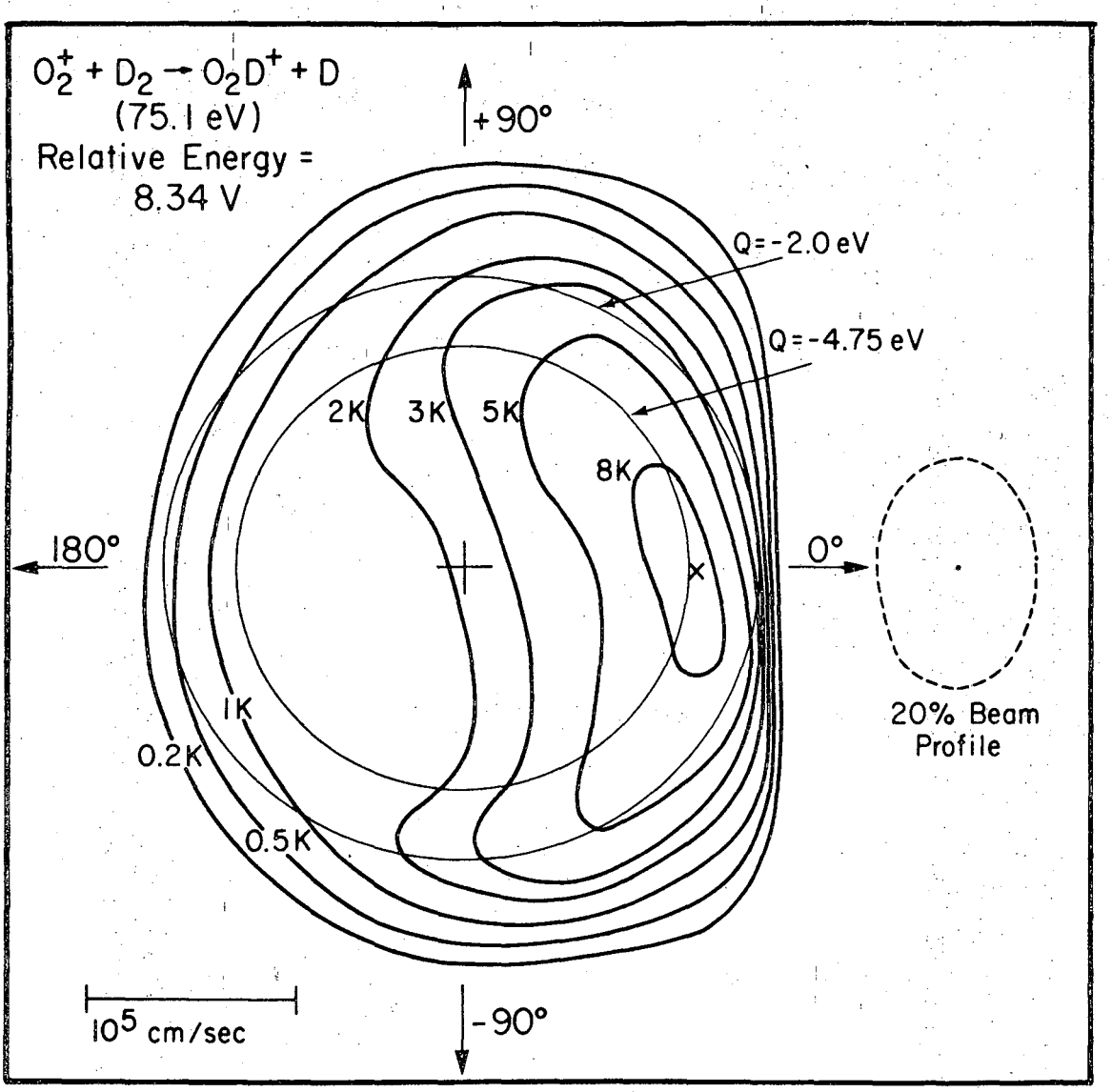

XBL 6912-6695

Fig. 20. An intensity contour map of O_2D^+ at 8.34 eV. The cross near the peak intensity locates the ideal stripping velocity. The asymmetry observed at small scattering angles is due to poor mass resolution.

On the maps, the circle drawn at Q = -2.0 eV marks the upper limit of Q where the product O_2D^+ is expected to be formed. No products are anticipated for Q larger than -1.9 eV since this reaction is endothermic by 1.9 eV. Indeed most of these products were found inside the circle. The product observed outside the cicrle could be attributed to the fact that our apparatus does not have an infinite resolution. If the beam profile is taken into account, it can easily be seen that almost all products are within this circle. For reactions with energies 2.76 eV and 3.86 eV the product distribution is symmetric around the center of mass, with the highest intensity occurring at or very near the center of mass velocity. The peaking at the center of mass and the symmetry of the intensity about the barycentric angles of $\pm 90°$ indicate the occurrence of a collision complex which lasts several rotational periods, a time long enough for the molecule (the complex) to forget the initial directions of the target and the projectile atoms. Figure 21 shows the differential cross-section for O_2H^+ at 1.77 eV, and for OH^+ and H_2O^+ at 2.9 eV. Within experimental error, these differential cross-sections display the same general shape and exhibit the backward-forward symmetry about $\theta = 90°$ as expected from a statistical complex.

For the 3.86 eV reaction, the internal excitation of O_2D^+ is approximately 2 eV—a substantial amount of excitation, but not enough to break the O_2^+—D bond. As the energy of the reaction is increased, the lifetime of the complex decreases (see Section V-G below). At some energy the average lifetime becomes shorter than one rotational period, and the product distribution will be asymmetric with respect

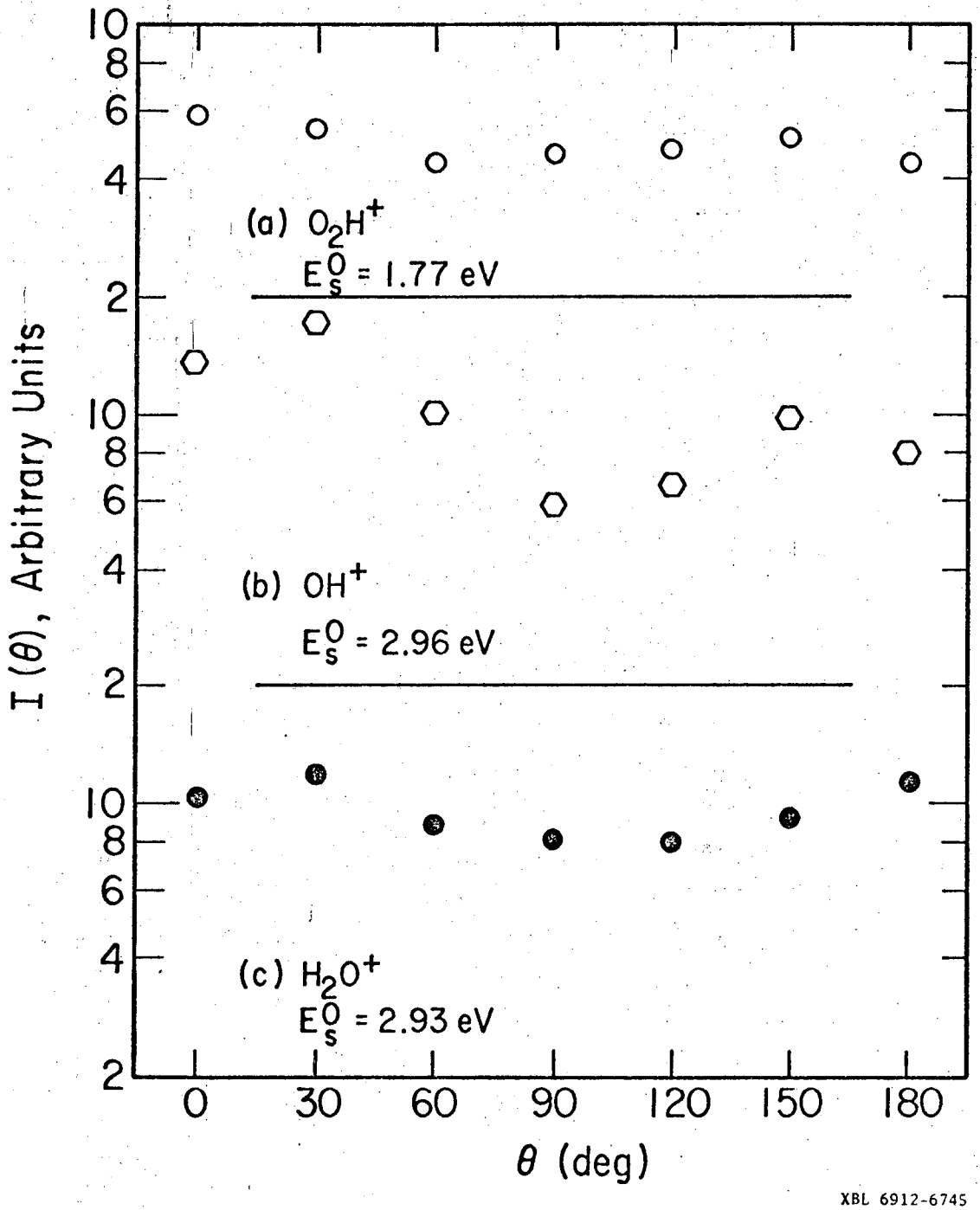

Fig. 21. Differential cross-sections for the products O_2H^+, OH^+, and H_2O^+.

to the center of mass. This observation is displayed in Fig. 19; at a relative energy of 5.47 eV the excitation of O_2D^+ at the center of mass is about 3.6 eV, and O_2D^+, with such velocity, is no longer expected to be stable with respect to the products O_2^+ and D. In order for a stable O_2D^+ to be formed, the product in its ground state must stay outside the 4.5 eV circle. We see that the peak intensity of the 5.47 eV reaction stays just on the brink of this circle. The forward peaking on the reaction implies a more direct type of interaction (like the hydrogen abstraction reaction[9]). If a long-lived complex still existed we would expect a crater like distribution of products with the peak intensity evenly distributed around the -4.5 eV circle. Product intensity inside the -4.5 eV circle will be depleted due to its instability. Figure 20 shows the O_2D^+ distribution at a reaction energy of 8.34 eV. The features are more or less the same as the 5.47 eV reaction, except the product is more forward peaked. In fact the most probable velocity of O_2D^+ has just reached the velocity predicted by the ideal stripping mechanism. The contour map of the 8.34 eV reaction displays the same features as some of the direct reactions studied by us and others, for example: N2+(D2,D)N2D+.[4,6,9]

b. Velocity Spectra. Table VI summarizes the data obtained in velocity spectra studies and gives a more detailed picture of the reaction. The intensity peaks at low energies are quite broad as can be seen in the reaction maps and in Fig. 22, hence the exact location of the peaks cannot be found uniquely. However, no ambiguity will arise if a line is drawn bisecting the half width at full maximum of the peak in the velocity spectrum. The location of the intensity peak is found where

Table VI

Reactive data for the products O_2H^+ and O_2D^+

Exp. No.	E_0	V_0	V	V_{CM}	V/V_0	$V_{180°}$	E_S^0	E'_S	Q	σ [a]
O_2H^+										
439	24.95	12.27	11.64	11.55	0.948	-	1.47	-	-1.42	3.35×10^4
429	30.11	13.48	12.73	12.69	0.944	-	1.77	-	-1.76	5.97×10^4
428	35.18	14.57	13.73	13.72	0.942	-	2.07	-	-2.06	7.21×10^4
387	50.30	17.43	16.39	16.40	0.940	-	2.96	-	-2.96	1.22×10^5
O_2D^+										
436	24.80	12.24	10.90	10.88	0.890	-	2.76	-	-2.75	1.15×10^5
435	30.25	13.51	12.02	12.01	0.889	-	3.36	-	-3.36	1.06×10^5
417	34.75	14.49	12.96	12.88	0.894	-	3.86	0.02	-3.84	1.59×10^5
442	42.13	15.95	14.64	14.18	0.917	-	4.68	0.69	-3.99	-
402	49.2	17.24	15.96	15.32	0.925	13.82	5.47	1.30	-4.17	1.65×10^5
443	61.14	19.21	17.97	17.08	0.935	16.23	6.79	2.51	-4.28	-
561	67.70	20.22	18.90	17.97	0.934	--	7.52	2.77	-4.75	-
552	74.98	21.28	20.07	18.91	0.942	17.85	8.33	4.27	-4.07	-
395	75.07	21.29	20.07	18.92	0.942	-	8.34	4.18	-4.16	-
466	75.20	21.31	20.07	18.94	0.941	17.90	8.36	4.07	-4.29	-
444	90.07	23.32	22.12	20.73	0.948	-	10.01	6.17	-3.84	-
574	99.75	24.54	23.30	21.81	0.949	20.46	11.08	7.26	-3.82	-
570	109.75	25.74	24.48	22.88	0.951	-	12.19	8.12	-4.07	-

All energies have units of eV. All velocities have units of 10^5 cm/sec.

a. Arbitrary units.

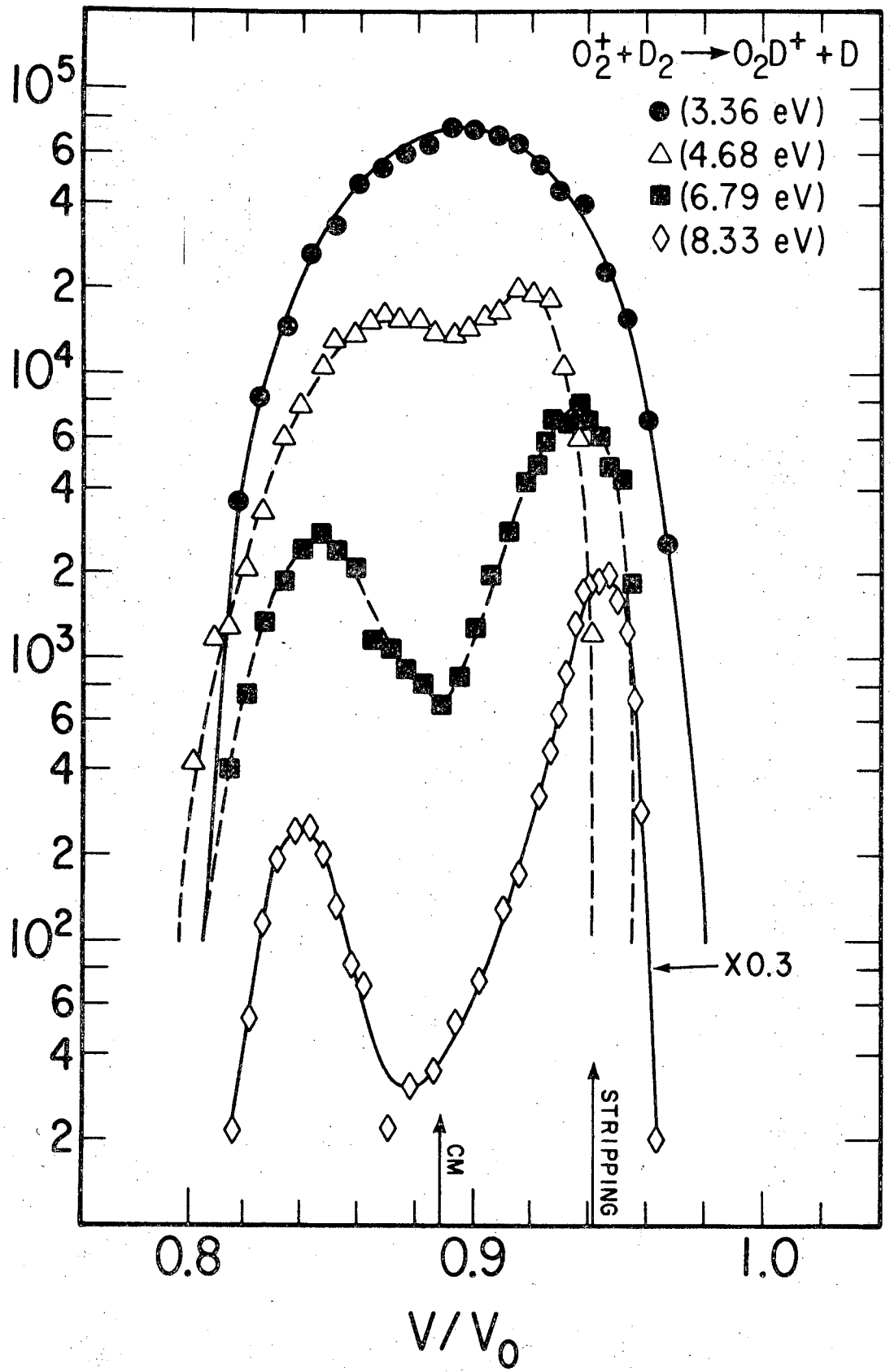

Fig. 22. Velocity spectra of O_2D^+.

this line intersects the velocity scale. This value is intuitively correct, since the primary beam intensity distribution is often symmetric to its peak intensity within experimental errors.

Figure 22 is a graphical display of some of the velocity spectra of O_2D^+ at energies 3.36 eV, 4.68 eV, 6.79 eV, and 8.33 eV. To facilitate comparison of the spectra at different energies, a reduced velocity scale v/v_0 is used where v is the product velocity and v_0 is the velocity of O_2^+. This scale puts experiments at different energies to the same scale. For example, in the O2(D2,D)O2D+ experiments the center of mass velocity would be at 0.884 using this new scale, and the ideal stripping velocity would be at 0.941, no matter what the reaction energy is.

From the velocity spectra, it is clear that the reaction goes from a complex reaction to a direct mechanism as the energy of the reaction is increased, and finally the intensity peak reaches the ideal stripping velocity at 8.33 eV. According to the ideal stripping process, for reactions having an energy of 8.33 eV and beyond the O_2D^+ will have an excitation exceeding 4.5 eV. In order for the product to be stable, the reaction product has to peak forward to the stripping position. This is observed experimentally. In the reactions above 8.33 eV(lab), the D atom must have recoiled away from O_2D^+ and in the process carried away part of the excitation in O_2D^+.

Figure 23 is another way of looking at the reaction data. Within experimental error the final relative energy E_s' is a linear function of the initial relative energy E_s^o up to a certain energy. Three experiments were performed at 8.3 eV and they indicated the magnitude of the

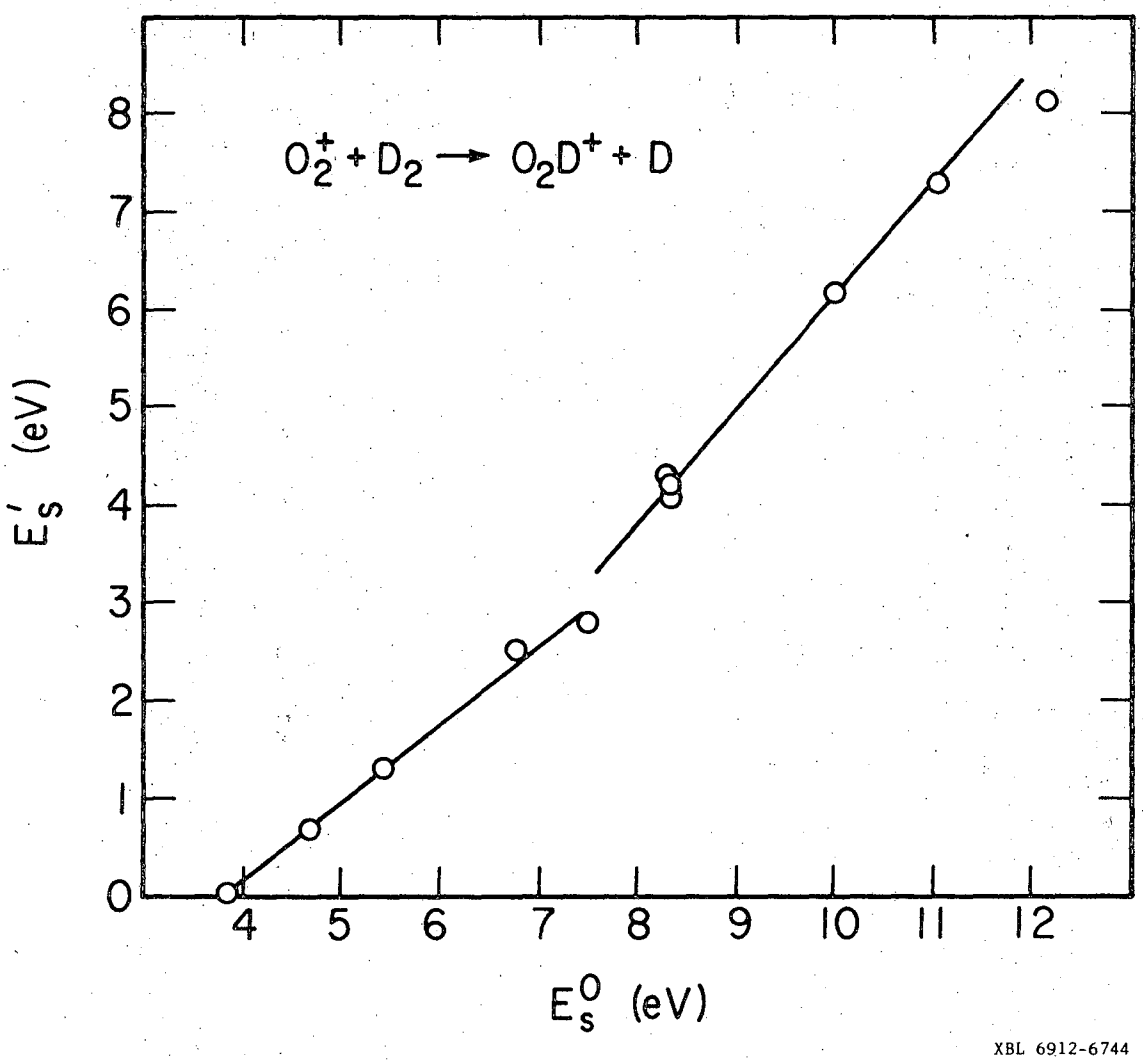

Fig. 23. Final vs. initial relative kinetic energy for 0° scattering.

experimental error. Extrapolation of the lower portion of the curve to $E_s' = 0$ eV gives $E_s^0 \approx 3.8$ eV, which is confirmed by the experiment done at 3.86 eV. The experiments gave us a rather unexpected conclusion that the products can hold an excitation of up to 1.9 eV. Excitation which is more than 1.9 eV will be partitioned between the internal excitation and the translational motion. It is not difficult to understand the mechanism of such energy partition if the internal excitation of O_2^+ is taken into account. The ions formed in the microwave discharge source will have several vibrational states populated. Furthermore O_2H^+ was observed from O2+(H2,H)O2H+ at an energy of 1.47 eV, indicating that most of the O_2^+ ion had a vibrational excitation of at least 0.4 eV. From the extrapolation in Fig. 23, we concluded that the internal excitation of O_2^+ was about 0.6 eV to 0.7 eV.

Two implications came out of these observations. First the products cannot absorb an infinite amount of excitation, that is, there has to be an upper limit where the product can remain stable. The experiments showed that the products "remember" their initial directions above an energy of 3.8 eV. Now if the internal excitation of O_2^+ is added to the 3.8 eV, the total reaction energy would be 4.5 eV which is the upper limit of the stability of O_2D^+ with respect to the products $O_2^+ + D$. Further increase in the reaction energy must result in its partitioning into translational motion if the O_2D^+ is to remain stable. Thus the transition from a complex type of mechanism to a more direct type of mechanism is a direct consequence of the Q of the reaction. It is interesting to note that there is a clear break of the curve at about 7.0 eV. The products above 7.0 eV recoiled away from each other more violently than those below 7.0 eV indicating that the interaction between the products at higher energies could be repulsive.

Second, the maximum reaction cross-section would occur close to E_s^0 = 3.8 eV. At this energy O2+(D2,D)O2D+ competes favorably statistically with other channels of reaction. Beyond 3.8 eV the channel of unimolecular decay of O_2D^+ gains in importance and we gradually lose the O_2D^+ intensity; as a result the reaction corss-section will drop. Unluckily it is rather inefficient for our present apparatus set up to determine total cross-sections. The few total cross-sections that we have measured are not enough for us to examine this point critically.

No threshold behavior was investigated. We could not produce an ion beam at this energy with sufficient intensity to do an experiment. It is interesting to note that Hengelin[56] has done

$$O_2^+(^4\Pi_\mu) + D_2 \rightarrow O_2D^+ + D \qquad (21)$$

which is exothermic by about 2.0 eV. Their results showed that this reaction reacts via a direct mechanism in the reaction energy range 1.7 eV to 80 eV(lab). In contrast, in our ion beam there was only 3% electronically excited O_2^+, and 97% of the beam was in the $^2\Pi_g$ state. Thus we did not have the interference of $O_2^+(^4\Pi_\mu)$ and the reaction is endothermic as expected.

The nature of the 180° peak formed at high energies is not clear from the study of O2+(D2,D)O2D+. Unlike the back scattered products in N2+(D2,D)N2D+ [9] and N+(H2,H)NH+,[57] the O_2D^+ scattered through 180° have a very large internal excitation. We will have more to say about this O_2D^+ when the isotope effects in this reaction are discussed.

2. H_2O^+

Due to the low intensity of H_2O^+ observed, only five experiments were performed and the results are tabulated in Table VII. The energy of H_2O^+ is so far behind the primary beam and their masses are so different that we no longer have the problem of mass separation. The range of Q allowed in

$$O_2^+(^2\Pi_g) + H_2 \rightarrow H_2O^+ + O \qquad (22)$$

are

$$-6.49 \text{ eV} \leq Q \leq -0.81 \text{ eV}.$$

Table VII

Reactive data for the products H_2O^+, D_2O^+, OH^+, OD^+ and O^+

Exp. No.	E_0	V_0	V	V_{CM}	V/V_0	E_S^0	Q	σ [a]
H_2O^+								
412	34.82	14.50	13.71	13.65	0.946	2.05	-2.05	-
392	49.84	17.35	16.33	16.33	0.939	2.93	-2.93	1.08×10^4
D_2O^+								
416	34.82	14.50	-	12.89	-	3.87	-	-
399	49.95	17.37	15.41	15.44	0.887	5.55	-5.55	-
465	75.09		No signal					
OH^+								
413	34.82	14.50	-	13.65	-	2.05	-	-
389	49.75	17.33	16.55	16.31	0.955	2.93	-2.92	-
391	50.32	17.43	16.30	16.40	0.935	2.96	-2.96	1.11×10^4
OD^+								
397	50.20	17.41	15.62	15.48	0.897	5.58	-5.57	-
562	67.7	20.22	18.5	17.97	0.915	7.52	-7.51	-
463	75.45	21.34	19.38	18.97	0.908	8.38	-8.35	5.4×10^4
467	100.09	24.58	22.90	21.85	0.931	11.12	-10.92	2.0×10^5
O^+ from $O_2^+ + D_2$								
405	50 eV		No signal			5.55		
460	76.4	21.48	21.02	19.09	0.978	8.49	--	-
459	100.59	24.64	24.52	21.91	0.995	11.18	---	1.49×10^4
O^+ from $O_2^+ + He$								
472	64.79	19.78	19.60	17.58	0.990	7.20	--	-
462	74.82	21.25	21.15	18.89	0.995	8.31	--	1.4×10^3
456	100.11	24.59	24.50	21.85	0.996	11.12	--	-
470	148.75	29.97	29.90	26.64	0.997	16.53	--	-

All energies have units of eV. All velocities have units of 10^5 cm/sec.
a. Arbitrary units.

Figure 24 shows a contour map of this reaction at 2.93 eV. The circle drawn at -2.0 eV was put in to indicate the Q values involved in this reaction. Again, the products have a distribution symmetric to the center of mass, indicating an intermediate complex was involved in the reaction. The fact that very little signal was observed at 2.05 eV may indicate that the reaction

$$O_2^+(^2\Pi_g) + H_2 \rightarrow H_2O_2^+ \qquad (23)$$

has a substantial activation barrier, perhaps close to 2.0 eV. In order for the reaction to occur, O_2^+ has to have sufficient energy to pass over this barrier. A threshold experiment is crucial to the understanding of the formation of H_2O^+. However, due to the low beam intensity and the small cross-section involved, we are not certain about the interpretation of the 2.05 eV experiment. Threshold measurements are best done with the type of apparatus designed by Giese.[5]

3. OH^+

The reaction O2+(H2,OH)OH+ has been studied by Refaey and Chupka[46] who determined the total cross-sections from 20 eV to 350 eV(lab). The total reaction cross-section is very small, with a maximum of 0.55 $Å^2$ at 60 eV(lab). But these measured total cross-sections are very uncertain, due to the large amounts of $O_2^+(^4\Pi_\mu)$ in their ion beam.

There are two reactions operating at different energy ranges that lead to the formation of OH^+:

$$O_2^+ + H_2 \rightarrow OH^+ + OH \qquad (24)$$

with

$$-6.90 \text{ eV} \leq Q \leq -2.14 \text{ eV}$$

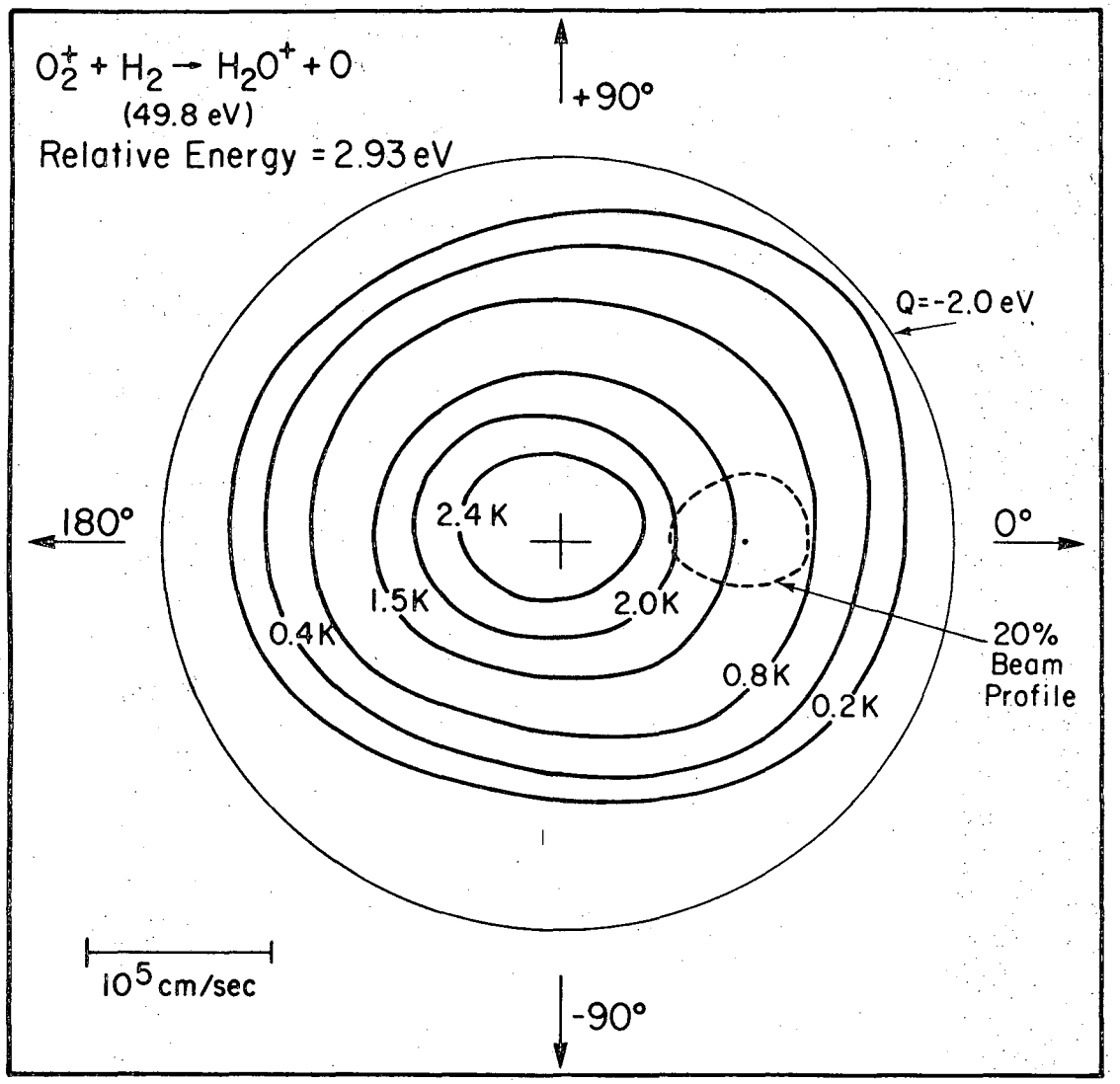

Fig. 24. An intensity contour map of H_2O^+ at 2.93 eV.

and

$$O_2^+ + H_2 \rightarrow OH^+ + O + H \qquad (25)$$

with

$$-11.25 \text{ eV} \leq Q \leq -6.49 \text{ eV}$$

The energetics of these reactions are listed in Table VII.

A contour map of this reaction is shown in Fig. 25. The circle drawn at Q = -1.90 eV roughly indicates the upper limit of Q in this reaction. This reaction is similar to O2+(H2,O)H2O+ in every respect, except the intensity of OH^+ is a little bit higher than H_2O^+. Again the OH^+ distribution is roughly symmetric with respect to the center of mass.

Figure 26 and 27 are contour maps of OD^+ at higher energies. The circles drawn in these maps have the following significance: (1) Q = -6.9 eV indicates the upper limit of OD^+ stability if all the excitation goes into OD^+. Reaction (25) is also energetically possible inside this circle. (2) Some $OD^+(^3\Pi)$ is expected to be found inside the circle Q = -11.25 eV. From the maps it is clear that in the reactions at 8.33 eV and 11.12 eV the OD^+ product is peaking slightly forward. As in the O_2H^+ reaction, the reaction energy is partitioned into the internal excitation and the translational motion of the products. Thus a more direct type of interaction is taking place at these energies. There are two possible mechanisms which explain such observations.

One of these models utilizes the direct mechanism, and the sequence of reaction is indicated as follows:

$$O_2^+ + D_2 \xrightarrow[\text{interaction}]{\text{direct}} O_2D^+ \xrightarrow[\text{decay}]{\text{unimolecular}} OD^+ + O \qquad (26)$$

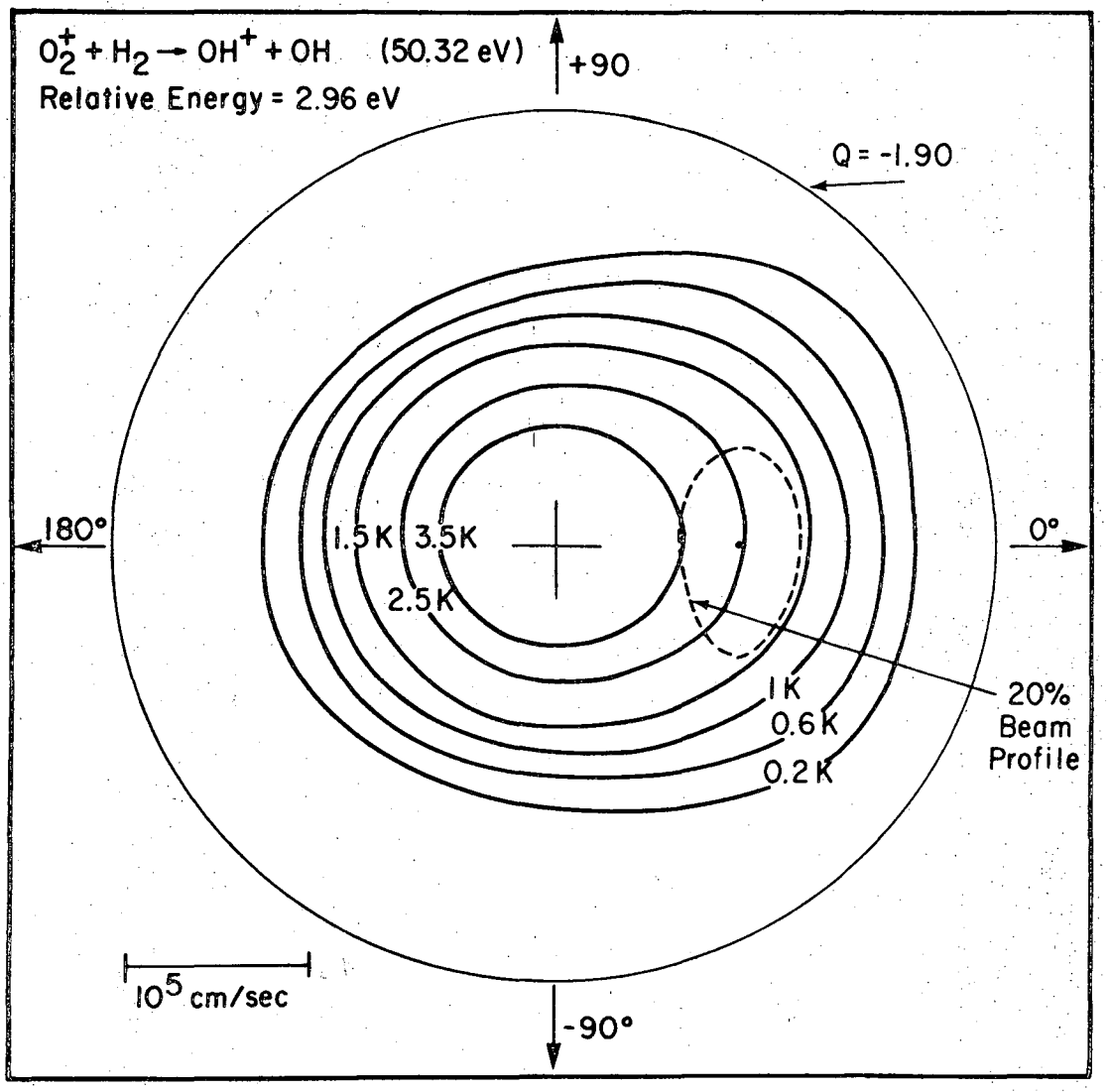

Fig. 25. An intensity contour map of OH^+ at 2.96 eV.

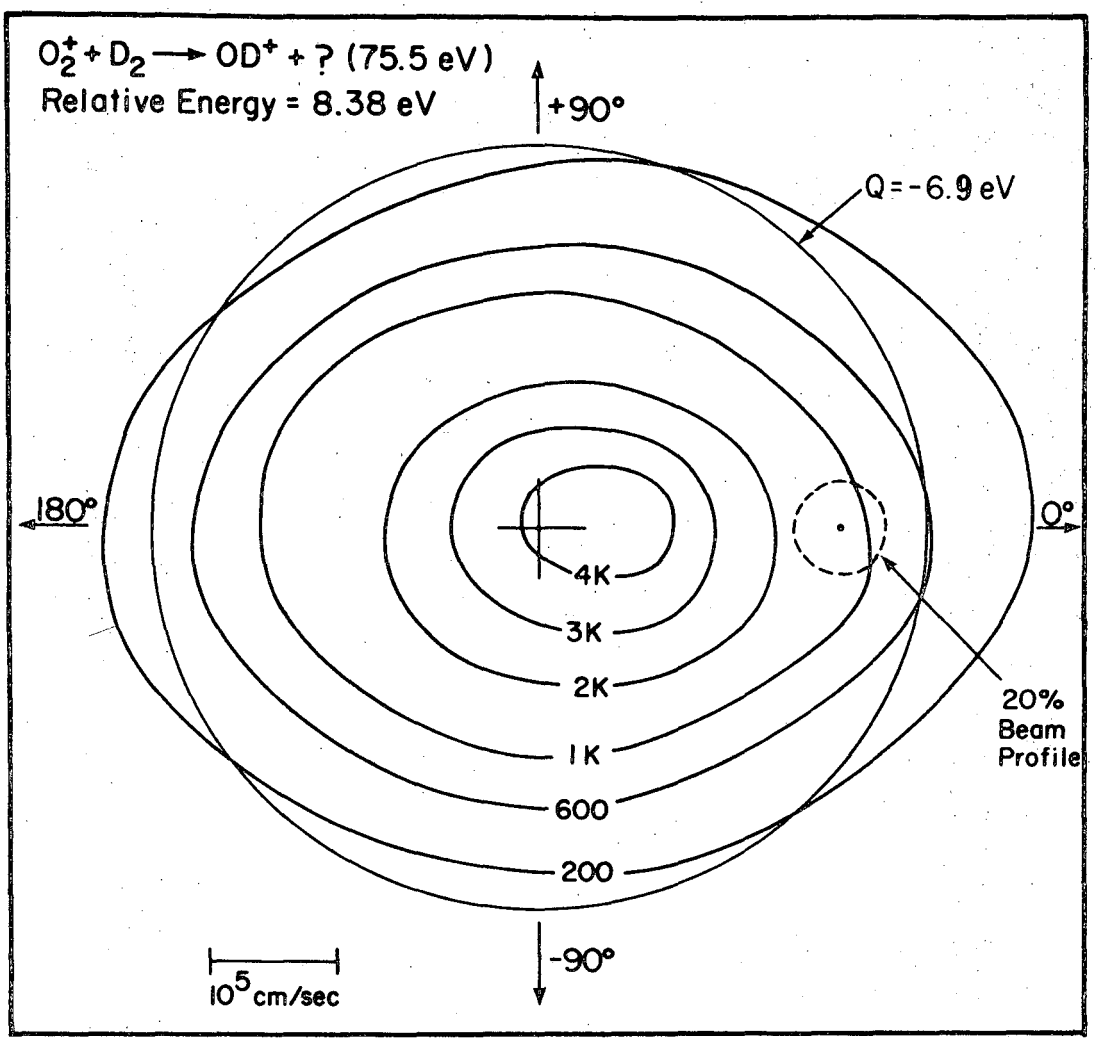

XBL 6912-6735

Fig. 26. An intensity contour map of OD^+ at 8.38 eV.

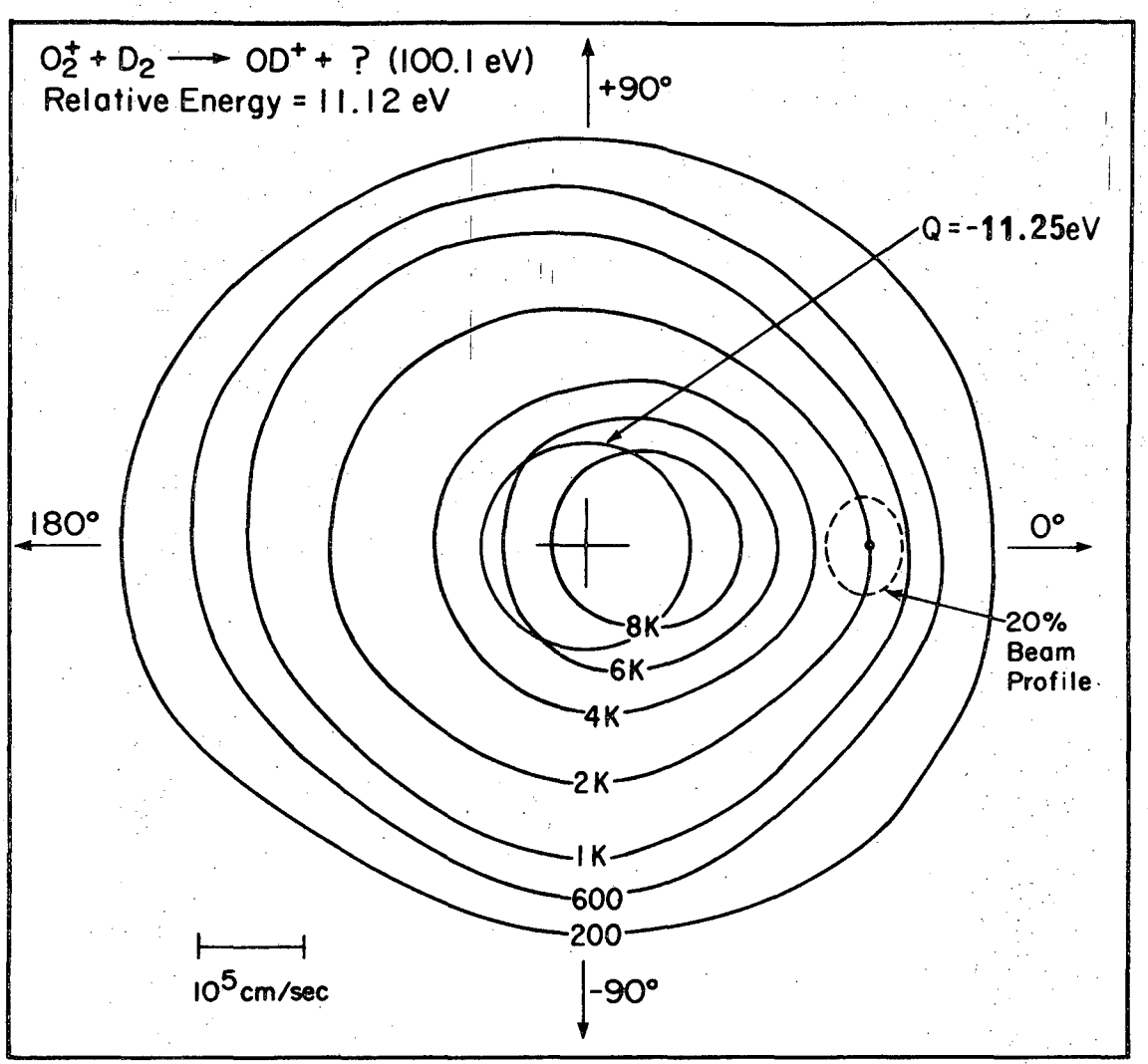

XBL 6912-6734

Fig. 27. An intensity contour map of OD^+ at 11.12 eV.

For an ideal stripping process the reaction is energetically possible only if the energy is above 11 eV. But we do not have an ideal stripping process in these reactions. Comparison between the data of O_2D^+ and OD^+ reveals that this reaction is allowed experimentally at an energy as low as 7 eV. OD^+ was found at a velocity slower than that of O_2D^+. Furthermore the dissociation

$$O_2D^+ \rightarrow O_2^+ + D \qquad \Delta H = 2.6 \text{ eV} \qquad (27)$$

should greatly predominate over

$$O_2D^+ \rightarrow OD^+ + O \qquad \Delta H = 4.4 \text{ eV} \qquad (28)$$

This partially explains the low intensity observed in these experiments.

Another possible reaction path is

$$O_2^+ + D_2 \xrightarrow[\text{direct}]{\text{complex or}} D_2O^+ \xrightarrow[\text{decay}]{\text{unimolecular}} OD^+ + D \qquad (29)$$

This reaction scheme has the attractive feature that all the reaction energy is available for the internal excitation of D_2O^+. The thermodynamic threshold for reaction (29) is 6.5 eV, or 59 eV(lab). Energetically this reaction is more favorable than reaction (26), but it does not predict the velocity of OD^+ as explicitly as reaction (26). More evidence in support of these models will be given in the non-reactive collision section below.

4. O^+

The reaction

$$O_2^+ + D_2 \rightarrow O^+ + D_2O(?) \qquad (30)$$

has a Q value of anything up to -1.8 eV. Unlike the other products (O_2D^+, OD^+, and D_2O^+) of $O_2^+ + D_2$, this reaction seems to proceed via a completely different mechanism. Figure 28 shows a reaction map at 11.18 eV. The product distribution is peaked asymmetrically forward of the center of mass, indicating a direct reaction. It should be both

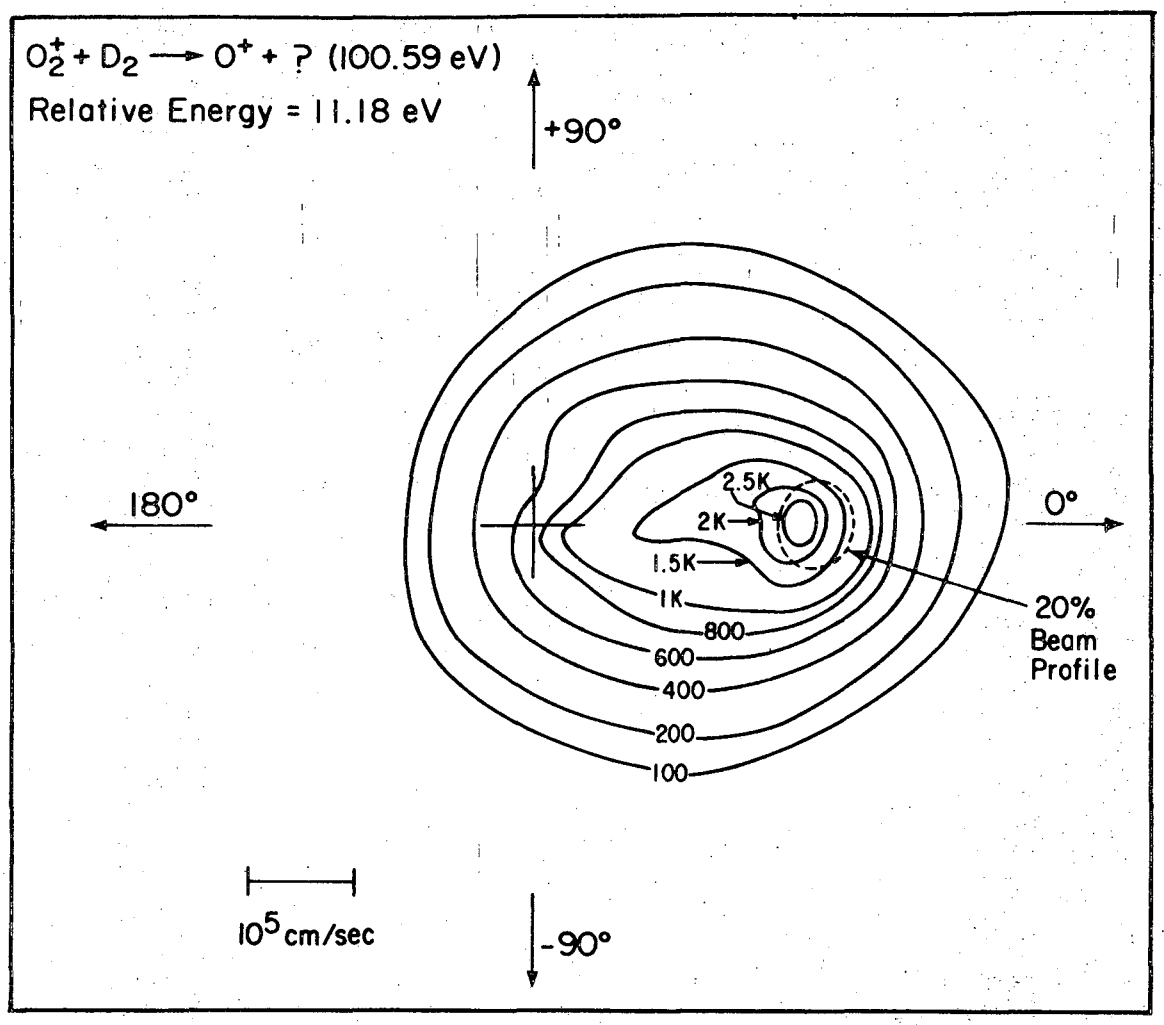

XBL 6912-6693

Fig. 28. An intensity map of O^+ from $O_2^+ + D_2$ at 11.18 eV.

interesting and informative if we can compare the reaction with

$$O_2^+ + He \rightarrow O^+ + O + He \qquad (31)$$

Helium has the same mass as D_2, and at high energies both D_2 and He are expected to interact with O_2^+ in similar manners. Figure 29 shows a contour map of Reaction (31) at a comparable energy. It is obvious that the two maps have the same general features with a strong peak in front of the center of mass. Furthermore, if the velocity spectra are compared, the intensity peaks almost have the same velocity. This immediately leads to the conclusion that these two reactions go by the same mechanism. Reaction (31) has been studied in detail in the collision induced dissociation investigations.[58,59] Threshold studies disclosed that no signal was observed for both Reactions (30) and (31) at 5.5 eV. The threshold for O_2^+ dissociation is 6.8 eV or 61 eV(lab). Unlike O^+, OH^+, O_2D^+, and H_2O^+ were detected at 50 eV, and these products were shown to come from a complex. All these lead to the conclusion that O^+ does not come from the complex $H_2O_2^+$, rather the signal we saw was from a collision induced dissociation of O_2^+!

In at least one reaction

$$O_2^+ + D_2 \rightarrow D_2O^+ + O \qquad (32)$$

$$\rightarrow D_2O + O^+ \qquad (33)$$

we may find O^+ from the complex. However, the ionization potential of O is 1 eV above that of D_2O. Therefore in the dissociation of $D_2O_2^+$, the charge is more likely to end up in D_2O than in O. There may still be some O^+ coming from $D_2O_2^+$; the signal may be so weak that it escaped detection in our apparatus, or be completely masked by the signal coming from the collision dissociation of O_2^+.

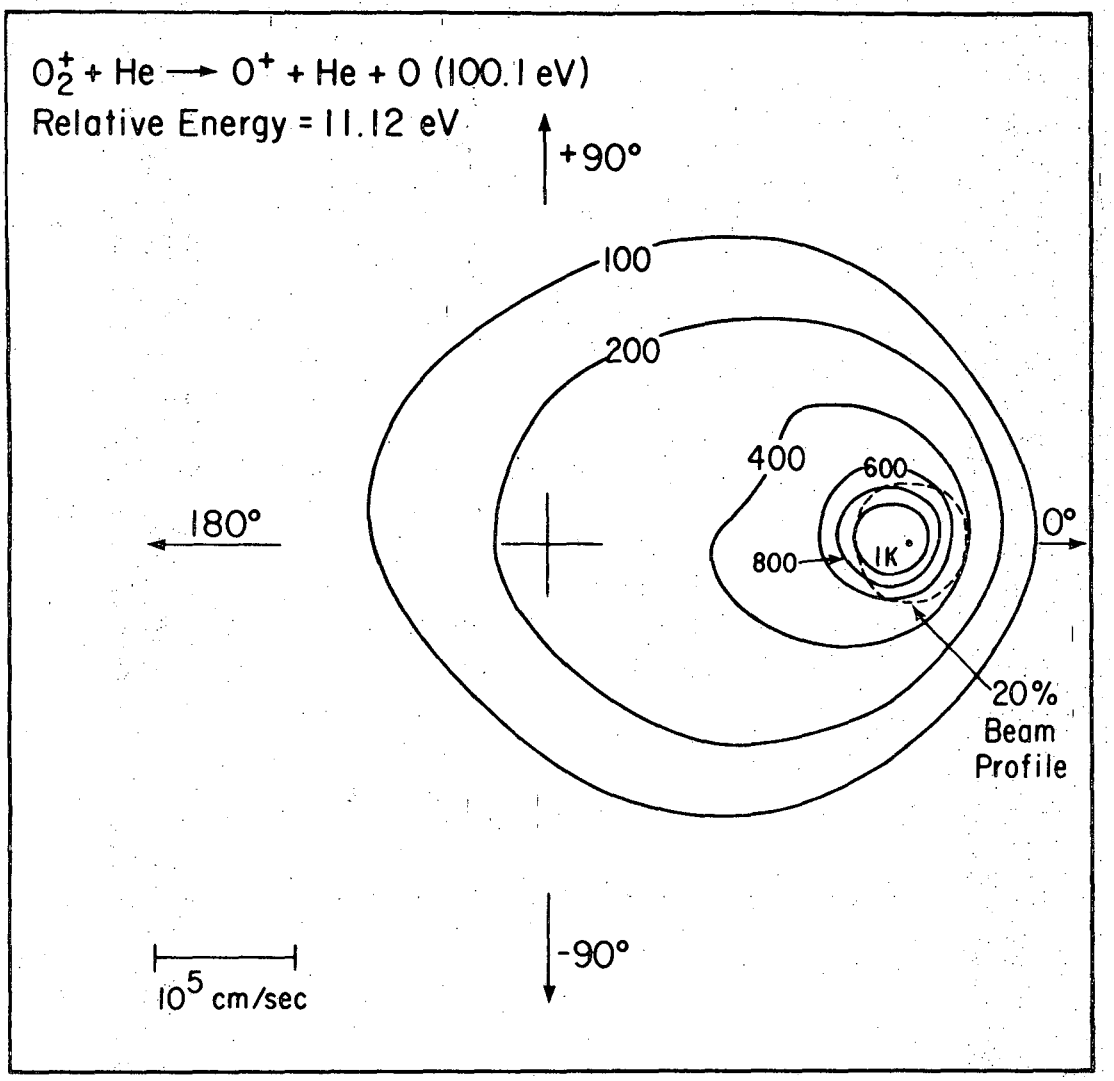

XBL 6912-6702

Fig. 29. An intensity contour map of O^+ from O_2^+ + He at 11.12 eV.

The mechanism of collision induced dissociation was discussed in detail in another report.[59] The version of the stripping model best describes the formation of O^+ in these reactions. In this model, one atom of the molecular ion interacts with the target molecule, while the other half of the ion proceeds as a spectator and is subjected to little or no force. Thus in this mode of reaction, the spectator ion will appear close to the velocity of the parent ion. Such predictions were observed in the O^+ experiments as can be seen from the data listed in Table VII.

E. Non-Reactive Collisions with D_2 and He

The basic purpose of a non-reactive collision study in a chemically reactive system is to find information which may supplement that obtained in the reactive studies. Kinsey[51] inferred complex formation in the non-reactive collision of alkali metal atoms with CO_2 and SO_2, although no reaction took place in these reactions. "Sticky" collision bumps were also observed in the non-reactive collisions of alkali atoms with alkali halides by Herschbach, et al.[15] In these cases chemical reactions took place.

We have studied non-reactive scattering together with reactive collisions in the reactions $N_2^+ + D_2$,[9] $N_2^+ + CH_4$,[11] and $Ar^+ + D_2$[10]; definite correlations could be made. For example the non-reactive experiments in $Ar^+ + D_2$ and He enabled us to estimate the reaction probability of the reaction.

Figures 30, 32, and 34 show the angular distributions of the non-reactively scattered O_2^+. The Q circles have the following meaning: 4.55 eV is the dissociation limit of the D_2 molecule; 6.80 eV is the

threshold for the dissociation of O_2^+, and 9.9 eV is the vertical transition (Franck-Condon type) of $D_2(^1\Sigma_g)$ to $D_2(^3\Sigma_\mu)$. For comparison the contour maps of O2+(He,He)O2+ are shown in Figs. 31, 33, and 35 at comparable energies.

Let us first compare Figs. 30 and 31. Three striking features appear. (1) There is no intensity inside the Q = -6.48 eV circle for O_2^+ + He while lots of signal is found inside the circle for O_2^+ + D_2. (2) There is some O_2^+ scattered very inelastically to 180° in the reactive system. (3) Elastic scattering of O_2^+ from D_2 was observed to ±50° in the CM system, while 180° elastic or slightly inelastic scattering of O_2^+ in He was observed. Apparently the presence of a reactive molecule D_2 caused all these differences. The interpretation of feature (1) is quite straightforward. For the O_2^+ + He case, the oxygen molecule could not take up more than 6.80 eV of excitation and there was no signal inside the 6.48 eV circle. For the O_2^+ + D_2 case, part of the excitation can be transferred to D_2 and O_2^+ was found scattered into this circle. Features (2) and (3) imply that close collisions between O_2^+ and D_2 have a reaction probability near unity. Similar features were also observed in N2+(D2,2D)N2+.[9] The intensity of O_2^+ close to the Q = -6.48 eV circle is more interesting. This also leads to the question of why the O_2^+ was preferentially scattered forward. If the signal came from the unimolecular decay of $D_2O_2^+$, an isotropic distribution around the center of mass would be expected. It was suggested earlier in the OH^+ section that the OD^+ might come from a unimolecular decay of O_2D^+. It was also indicated that more O_2^+ would be coming from the unimolecular decay of O_2D^+ since the O–O bond is stronger than the OD bond in O_2D^+.

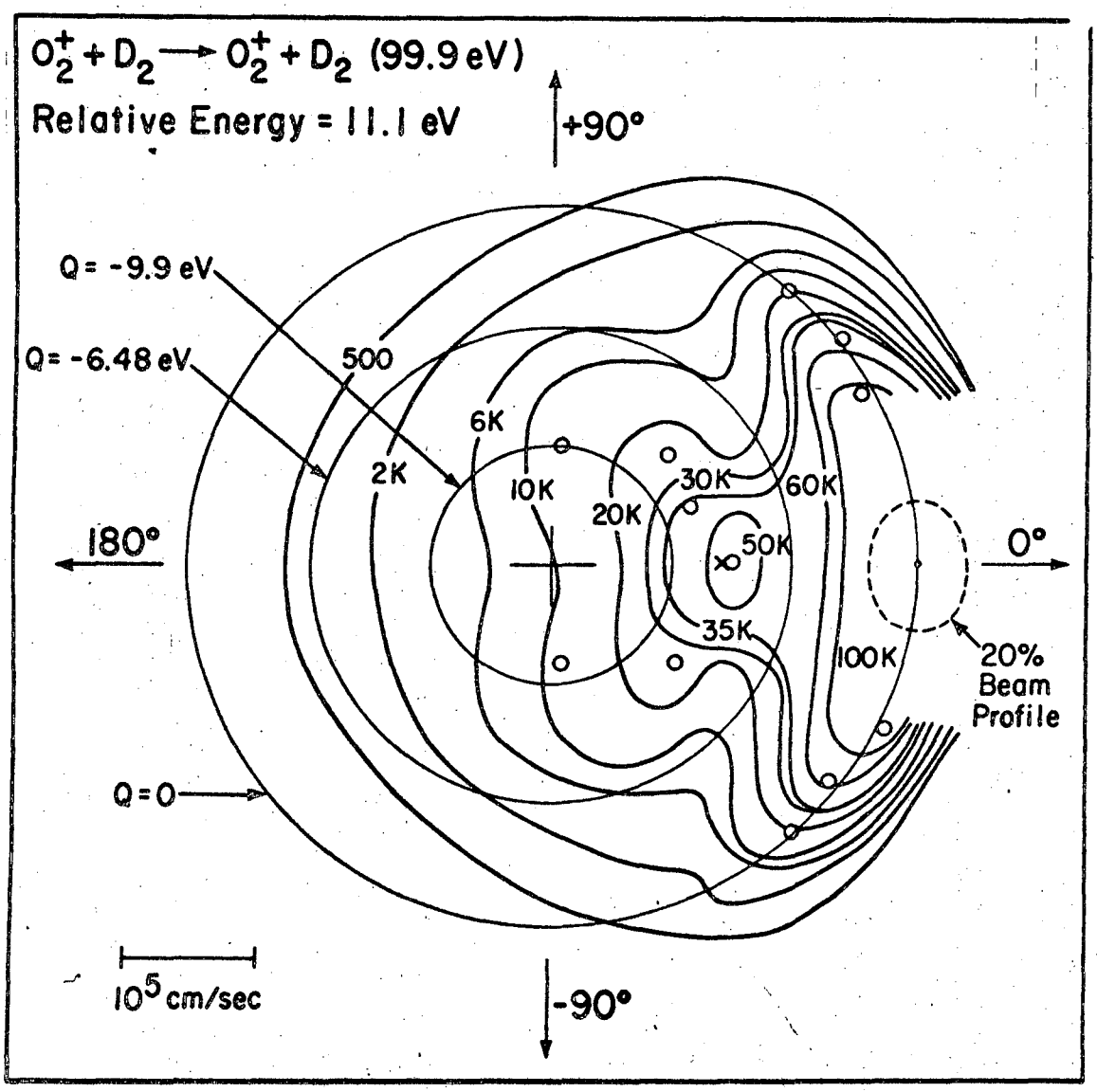

Fig. 30. An intensity contour map of O_2^+ from $O_2^+ + D_2$ at 11.1 eV. The cross near the intensity peak locates the velocity of O_2^+ coming from a unimolecular dissociation of O_2D^+ which is formed via the ideal stripping mechanism. The small circles locate the intensity maxima of the scattered O_2^+.

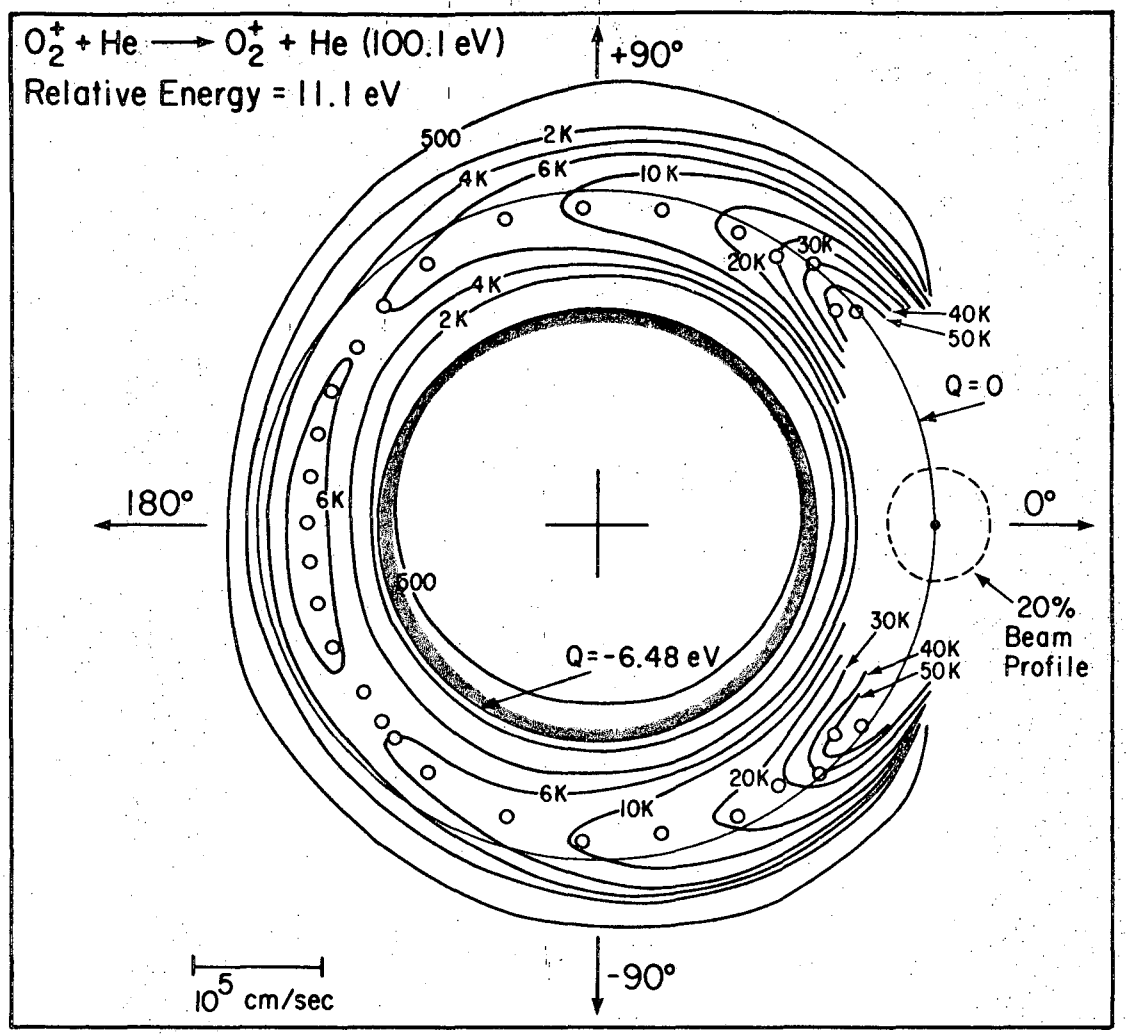

XBL 6912-6696

Fig. 31. An intensity contour map of O_2^+ from O_2^+ + He at 11.1 eV. The small circles locate the intensity maxima of the scattered O_2^+. The circle labeled Q=0 locates the elastic scattering of an infinitely sharp beam from a stationary target.

According to this model the reaction below took place

$$O_2^+ + D_2 \xrightarrow[\text{interaction}]{\text{direct}} O_2D^+ + D \xrightarrow[\text{decay}]{\text{unimolecular}} O_2^+ + D + D \qquad (34)$$

The velocity of O_2^+ coming from this reaction should have nearly the same velocity as O_2D^+. The "X" in the contour map marks the expected position of O_2^+ coming from a unimolecular decay of O_2D^+ following an ideal stripping reaction. While in the N2+(D2,2D)N2+ collision, it was concluded that the intensity peak of N_2^+ was due to a collision induced dissociation of D_2,[9] we are inclined to think that in the present case the O2+(D2,2D)O2+ intensity maximum was due to a unimolecular decay of O_2D^+.

There are two reasons why we believe the O_2^+ case is different from the N_2^+ case. (1) The intensity maximum from N2+(D2,2D)N2+ was sharp and had an angular distribution basically the same as the primary ion beam. In the O_2^+ case, the angular distributions of O_2^+ is reminiscent to that of a stripping reaction. Thus N2+(D2,2D)N2+ and O2+(D2,2D)O2+ do not occur by the same mechanism. (2) Data from OD^+ and L_2^+ seem to complement each other and they may originate from a O_2^+ unimolecular decomposition of O_2D^+. The difficulty of such a model is that the O_2^+ and the OD^+ observed at comparable energies did not have quite the same velocity, with O_2^+ peaking slightly in front of the OD^+. One nice thing about the model is that it does explain the preferentially forward scattered O_2^+.

Similar observations can be made with reactions at 8.3 eV (Figs. 32 and 33). Again the "X" in the $O_2^+ + D_2$ map marks the ideal stripping position and the data agree well with it.

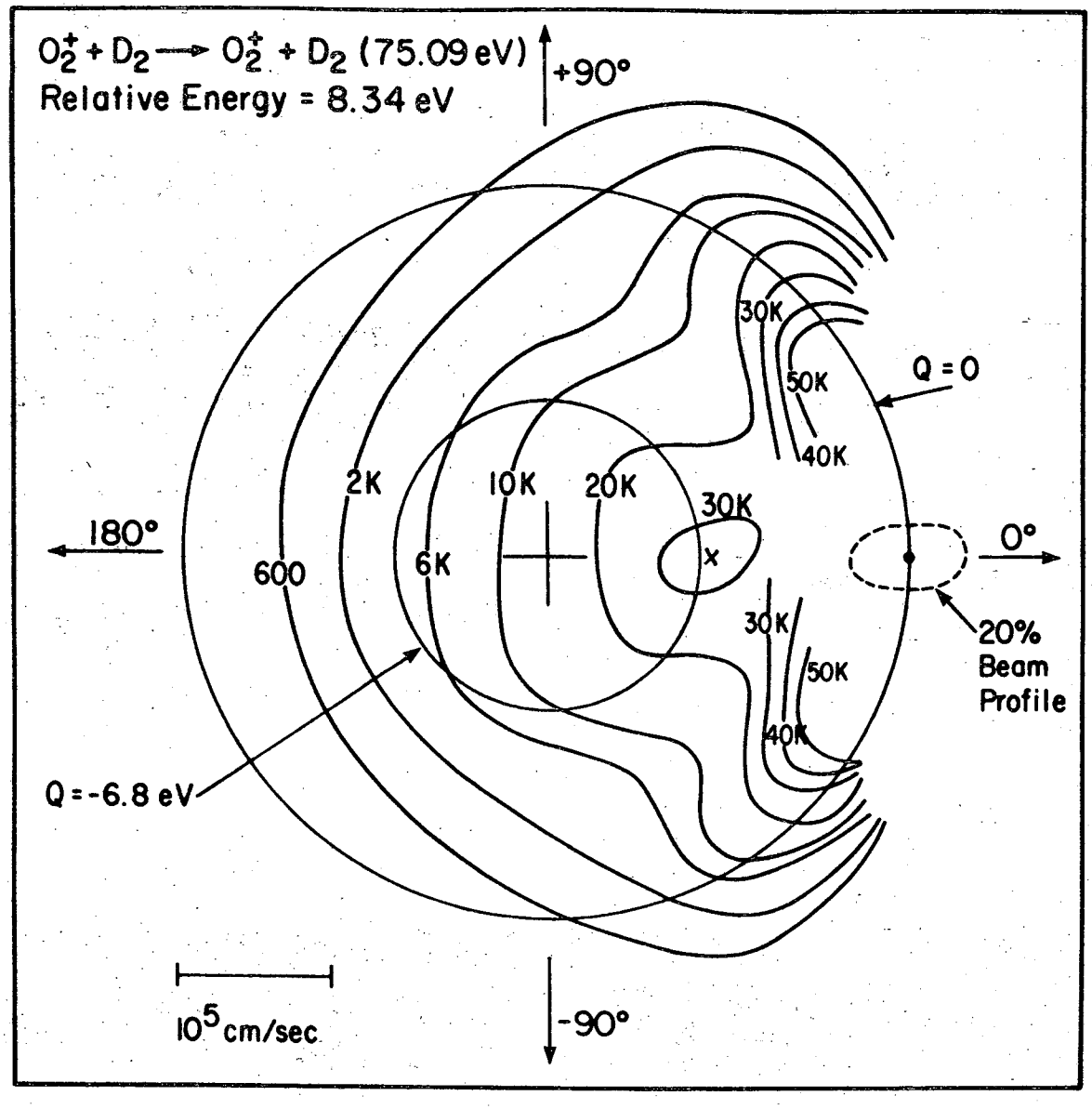

Fig. 32. An intensity contour map of O_2^+ from $O_2^+ + D_2$ at 8.34 eV. The cross near the intensity peak locates the velocity of O_2^+ coming from a unimolecular dissociation of O_2D^+ which is formed via the ideal stripping mechanism.

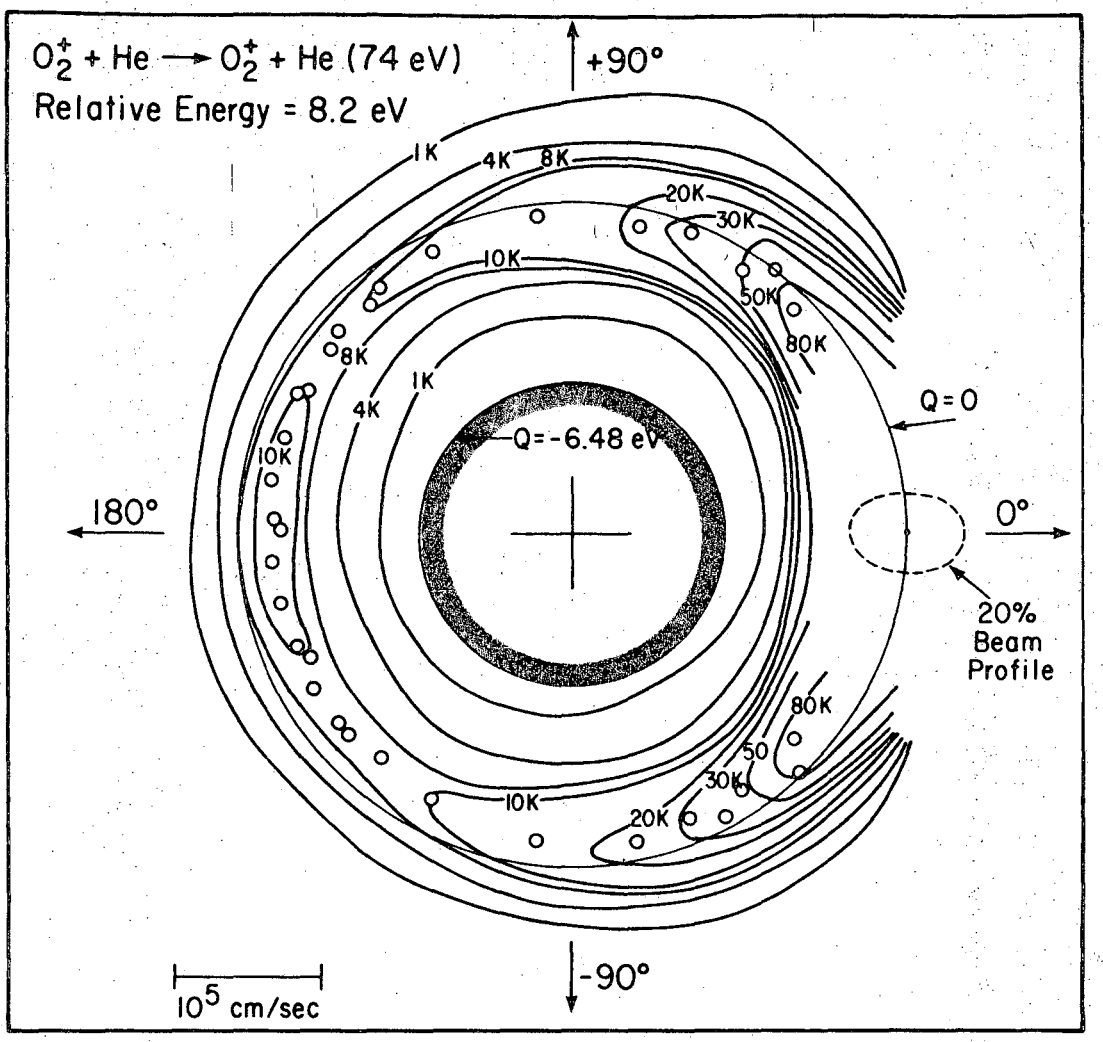

XBL 6912-6697

Fig. 33. An intensity contour map of O_2^+ from O_2^+ + He at 8.2 eV. The small circles locate the intensity maxima of the scattered O_2^+. The circle labeled Q = 0 eV locates the elastic scattering of an infinitely sharp beam from a stationary target.

The reactions at lower energies still retained much of the same features as occurred at higher energies, except the O_2^+ forward peak disappeared; in its place some intensity plateaus were found. This is probably due to energy restrictions. Figures 34 and 35 show the reactions at 5.5 eV. Inside the -4.5 eV circle dissociation of D_2 is energetically possible. The -4.5 eV circle in Fig. 35 does not have any meaing; it was put in for comparison with Fig. 34. The process as explained above still operates here. If the intensities inside the 2 eV circle were lifted from Fig. 19 and added to those in Fig. 35, we would roughly reproduce the scattering pattern in Fig. 34. Of course some of these intensities might come from the unimolecular decay of the complex:

$$D_2O_2^+ \rightarrow O_2^+ + D + D \qquad (35)$$

The arguments given above are speculative at best. Scattering patterns close to that predicted by this model (reaction 34) were indeed observed, and the results in O2+(D2,OD)OD+ and in O2+(D2,2D)O2+ complemented each other. At present we do not have sufficient data to prove or disprove such models. Experiments at higher and lower energies covered in these experiments would definitely help.

It is not surprising to see N2+(D2,2D)N2+ and O2+(D2,2D)O2+ behaving differently, because the chemical interactions involved in these two reactions are quite different. The great mystery would be the Ar+(D2,D2)Ar+.[17] Like O_2^+ and N_2^+, Ar^+ interacts strongly with D_2. Why then did we not see any collision induced dissociation in Ar+(D2,D2)Ar+? Would the difference in the projectile mass make any disparity? Or, did the observations in the Ar+(D2,D2)Ar+ experiments

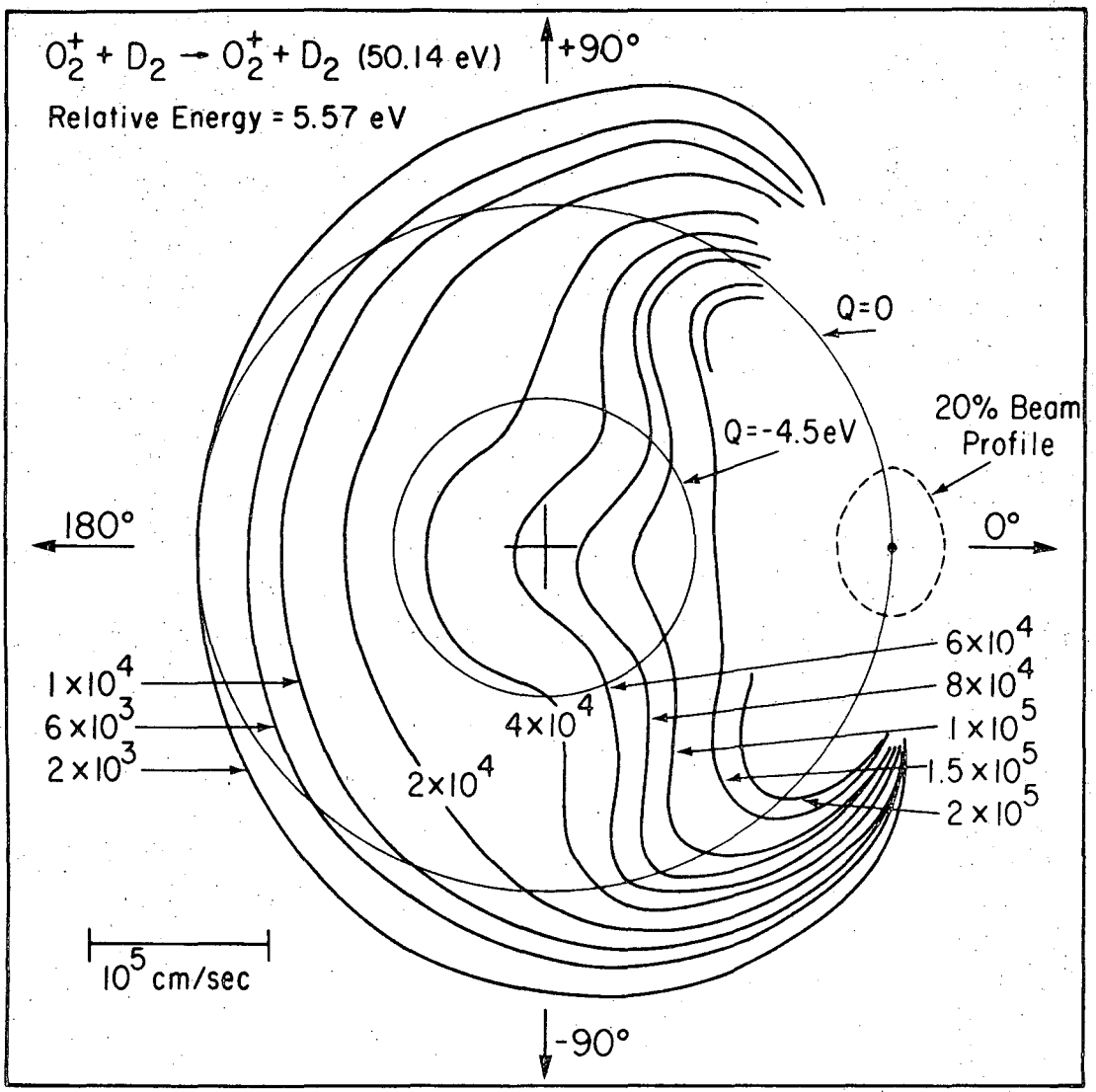

XBL 6912-6692

Fig. 34. An intensity contour map of O_2^+ from $O_2^+ + D_2$ at 5.57 eV.

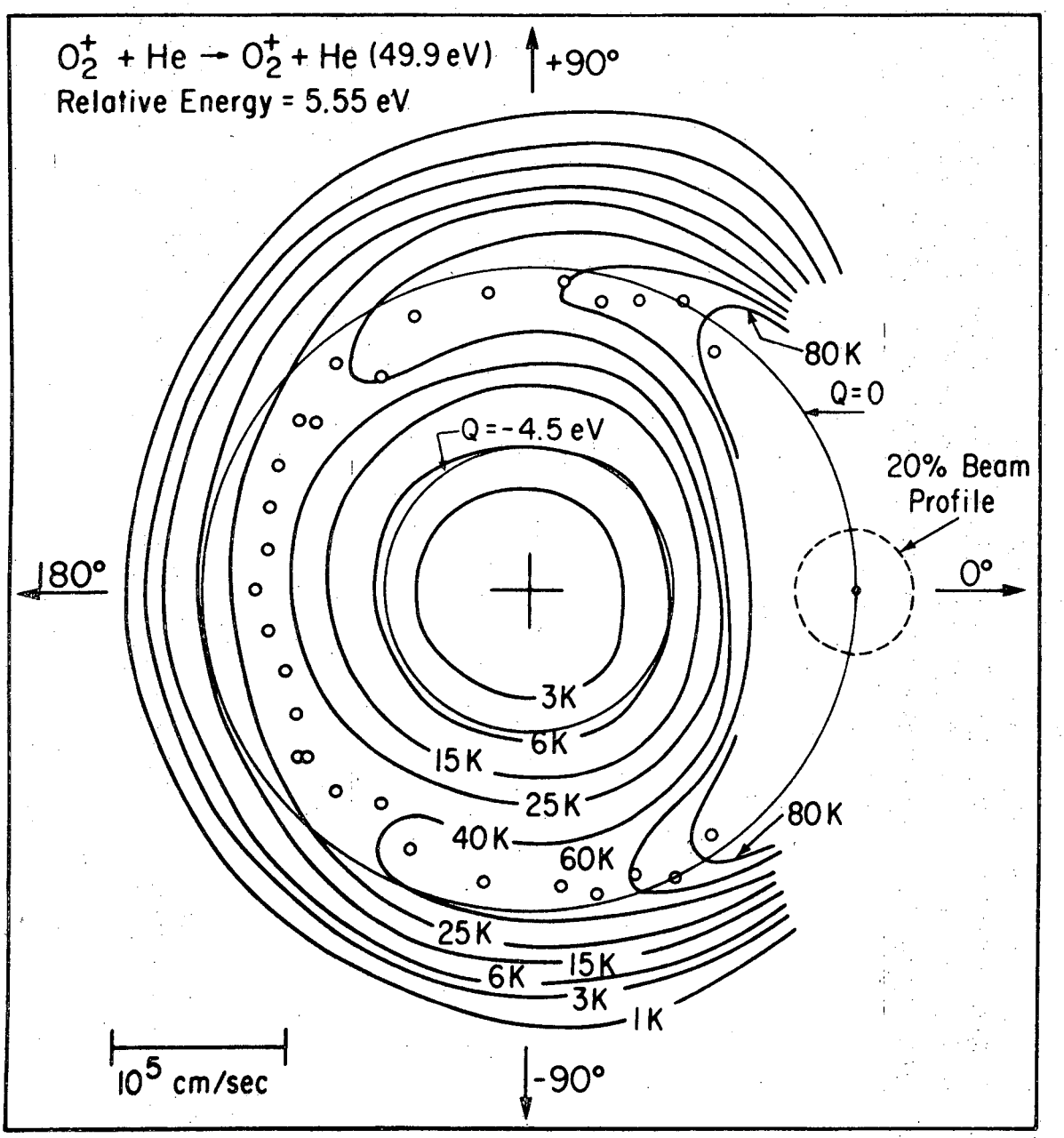

Fig. 35. An intensity contour map of O_2^+ from O_2^+ + He at 5.55 eV. The small circles locate the intensity maxima of the scattered O_2^+. The circle labeled Q = 0 eV locates the elastic scattering of an infinitely sharp beam from a stationary target.

put their weight in favor of the model proposed above? Dittner and Datz[61] have studied the nonreactive collision of K^+ and Na^+ with D_2. No dissociation of D_2 was observed at energies comparable to those studied in $Ar^+(D_2,D_2)Ar^+$. There are many reactions which might shed some light on the mechanism of dissociation of D_2 in reactive systems. $CO^+ + D_2$ is a good case to study. $NO^+ + D_2$ is another. Attempts to observe the formation of NOD^+ from $NO^+ + D_2$ have failed repeatedly in this laboratory.[60] Thus $NO^+ + D_2$ might be a good reaction to test the model experimentally, since in $NO^+ + D_2$ we apparently have a chemically "inert" system. A nonreactive type of dissociation of D_2 can almost be eliminated if we fail to observe the dissociation of D_2 in $NO^+ + D_2$.

F. Isotope Effects

Kinetic isotope effects in ion-molecule reactions have been discussed by many investigators.[62] The reactions between rare gas ions and HD have been particularly well studied.[63] Earlier experiments in mass-spectrometers led to the conclusion that long-lived intermediate complex was formed in these reactions. Later experiments with crossed beams produced no evidence for complex formation down to a CM energy of 0.1 eV.[4] Consequently, the existence of a complex in these reactions are doubtful.

In the study of

$$O_2^+ + HD \rightarrow O_2D^+ + H \qquad (36)$$

$$\rightarrow O_2H^+ + D \qquad (37)$$

we have shown that a complex HDO_2^+ definitely existed for several rotational periods. The substitution of HD in these reactions affects

both the rate and the mechanism of the reactions. The difference in the rate of formation of O_2D^+ and O_2H^+ is not surprising and can be explained in terms of the unimolecular rate theory. The effect of HD on the mechanism of the reaction at high energies is somewhat unexpected. The influence of HD on the mechanism of the reaction shall be discussed first.

1. Influence on the Reaction Mechanism

Figure 36 shows three different velocity spectra of O_2^+ + HD at 2.13 eV, 5.21 eV and 8.57 eV. It should be pointed out that the dimensionless velocity scale should only be used between data of like ions only. For example, the ideal stripping velocity for O_2D^+ is at 0.941 while that for O_2H^+ is at 0.97. The CM velocity is the same for both cases. As the reaction energy is increased, O_2D^+ and O_2H^+ forms via different paths. Let us follow O_2H^+ first. At an energy slightly above the threshold, both ions have peak velocities at the center of mass implying the existence of the complex HDO_2^+. As the reaction energy is increased O_2H^+ starts to peak in front of the center of mass and finally reaches the ideal stripping velocity at 8.57 eV. This aspect of the reaction is completely similar to those in the O2+(D2,D)O2D+. Unlike the formation of O_2D^+ in $O_2^+ + D_2$, very little intensity is observed behind the center of mass. Let us now follow O_2D^+. In Fig. 36(a), O_2D^+ is at the center of mass like O_2H^+. In Fig. 36(b), O_2D^+ is peaking behind the center of mass. However, the peak is not as prominent as that of the O_2H^+. In Fig. 36(c), we can discern two well-defined peaks, one peaking forward the other backward to the center of mass, with the backward peak intensity 1-1/2 times that

Fig. 36. Velocity spectra of O_2D^+ and O_2H^+ from O_2^+ + HD.

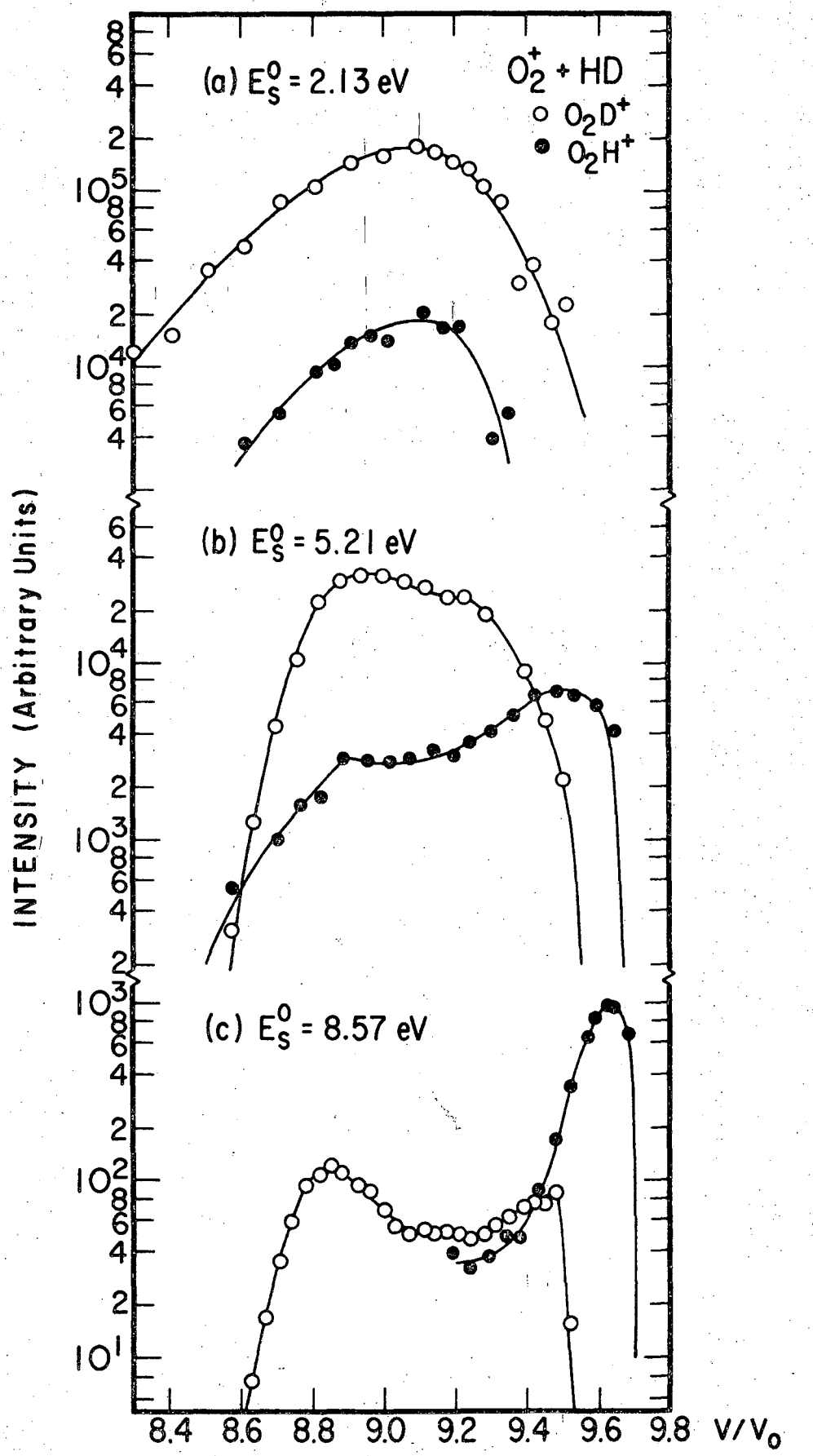
(a) E_s^0 = 2.13 eV
O_2^+ + HD
O_2D^+
O_2H^+
(b) E_s^0 = 5.21 eV
(c) E_s^0 = 8.57 eV
INTENSITY (Arbitrary Units)
8.4 8.6 8.8 9.0 9.2 9.4 9.6 9.8 V/V$_0$

Fig. 36

of the forward. The products formed in these isotopic reactions at high energies are: O_2D^+ predominently backward and O_2H^+ predominently forward. The behavior of O_2H^+ at higher energies can easily be explained in terms of the stripping process which is not surprising since we found similar effects with O2+(D2,D)O2D+. Simple calculation shows that at higher energies O_2D^+ could be formed by the following process: (1) O_2^+ collides completely inelastically with the D end of HD, (2) the resulting O_2D^+ molecule collides elastically or inelastically with the H atom, (3) as a result of the collision H recoils forward while O_2D^+ bounces backward. For an ideal process $V/V_0 = 0.81$, as calculated in Section II. The charge is favored to stay on O_2D^+ since it has a lower ionization potential than the H atom. While these simple models do explain quantitatively the behavior of the reactions at higher energies but they failed to explain why one is favored over the other.

There is one simple geometric explanation for all these. If we take the stand that the HD molecule has its center of mass shifted toward the D atom, in rotation, H will be forming an outer shell covering the D atom. Since stripping processes take place at large distances, O_2^+ will be seeing the H atom most of the time and the formation of O_2H^+ is favored. At higher energies, the molecule HD will appear "frozen" in space to the incoming O_2^+ and both O_2D^+ and O_2H^+ will be formed at the same rate. Since the stability of O_2D^+ and O_2H^+ at higher energies is determined by the amount of internal excitation, O_2H^+ is again favored. For the back scattered products, the rotation of the HD molecule gives the D atom a greater density at

the core, hence the formation of $O_2D^+(180°)$ is favored. Furthermore, inelastic collision between O_2H^+ and D, or O_2D^+ and H will transfer more energy to the molecule in the former case.[64] This is the reason why we did not see too much O_2H^+ scattered to 180° at higher energies. Similar isotope effects for the 180° peak were also observed in N_2^+ + HD.[65] The velocity spectra data are summarized in Table VIII.

2. Influence on the Reaction Rate

In terms of the Lindemann mechanism,[14] reactions (36) and (37) can be written as

$$O_2^+ + HD \rightleftarrows [HDO_2^+]^* \tag{38}$$

$$[HDO_2^+]^* \xrightarrow{k_{a1}} [HDO_2^+]^\dagger \rightarrow O_2H^+ \tag{39}$$

$$[HDO_2^+]^* \xrightarrow{k_{a2}} [HDO_2^+]^\dagger \rightarrow O_2D^+ \tag{40}$$

where the * indicates that the molecule has an internal energy E^* equal to or greater than the critical energy for dissociation (E_c), † denotes an activated complex, and k_{a1}, k_{a2} are the first order rate constants for the decomposition of an excited HDO_2^+ into the products. In the present experiments, only the forward reaction in Equation (38) was investigated.

The k_a involved has been the subject of intensive studies in the theory of unimolecular rate theory. Using a quantum statistical model: Rice, Ramsperger, Kassel and Marcus developed the so called RRKM theory of unimolecular decomposition.[66,67] In this theory, k_a in its simplified form, in which rotation is inactive, is

$$k_a = \frac{Q_r^\dagger}{Q_r} \left(\frac{E^\dagger + E_z^\dagger}{E^* + E_z^*} \right)^{s-1} \prod_{i=1}^{s} \nu_i^* / \prod_{i=1}^{s-1} \nu_i^\dagger \qquad (41)$$

$$= \nu \left(\frac{E^\dagger + E_z^\dagger}{E^* + E_z^*} \right)^{s-1} \qquad (42)$$

where $Q_r^\dagger$ and Q_r are the rotational partition functions for the activated complex and the unenergized molecule respectively, $E^\dagger = E^* - E_c$, E_z and $E_z^\dagger$ are the zero point energies of the molecule and the activated complex $[HDO_2^+]^\dagger$. The first product in equation (41) is of the fundamental vibrational frequencies (ν_i) of the unenergized HDO_2^+ and the other is of the frequencies of the activated complex. The total number of vibrational modes of the molecule is s.

By semi-empirical reasoning, Rabinovitch and Diesen[67] modified the semiclassical energy level density expression of Equation (41) for s vibrational modes,

$$(E^* + E_z^*)^{s-1} / \Gamma(s) \prod_{i=1}^{s} h\nu_i \qquad (43)$$

by the inclusion of an empirical correction factor "a". It gives

$$(E^* + a\, E_z^*)^{s-1} / \Gamma(s) \prod_{i=1}^{s} h\nu_i \qquad (44)$$

Substituting (44) into (42) we obtained the expression

$$k_a = \nu \left[\frac{E^* + aE_z - E_c}{E^* + aE_z} \right]^{s-1} \qquad (45)$$

Slater[14] using a dynamical model derived an equivalent expression for k_a

$$k_a = \langle \nu \rangle \left[\frac{E^* - E_c}{E^*} \right]^{n-1} \qquad (46)$$

where $\langle \nu \rangle$ is the weighted mean frequency of the molecule, and n is the number of normal coordinates that contribute to the reaction coordinate. Comparing Equations (46) and (45) one notes that $\langle \nu \rangle$ and ν are similar. Monte Carlo calculations for simple molecules by Bunker[68] showed that these two terms are within a factor of two within one another. Since $\langle \nu \rangle$ of the Slater formulation is much easier to calculate, we substitute $\langle \nu \rangle$ into equation (45). With this simplification, one is left with

$$k_a \approx \langle \nu \rangle \left[\frac{E^* + aE_z - E_c}{E^* + aE_z} \right]^{s-1} \tag{47}$$

In the decomposition of HDO_2^+, E_c of reaction (40) is greater than E_c of reaction (39). An examination of equation (47) gives $k_{a2}/k_{a1} > 1$. Actually, the k_{a2}/k_{a1} ratio is also compounded by the energy level densities of the activated complex which again favor the product O_2D^+ as can be seen in equation (41).

Now the collision rate constant k is given by

$$k_{O_2D^+} = n_1 n_2 \int \sigma_{O_2D^+} \, gf(g)dg \tag{48}$$

where n_1, n_2 are the density of the colliding particles O_2^+ and HD, $\sigma_{O_2D^+}$ is the total reaction cross-section leading to O_2D^+, g is the relative velocity vector and f(g) is a distribution function of the velocity vector. A similar equation can be written for the formation of O_2H^+. Comparing equation (36) and (35), we see that

$$k_{a2}/k_{a1} \propto \frac{\sigma_{O_2D^+}}{\sigma_{O_2H^+}} > 1 \tag{49}$$

At higher reaction energies, direct interaction took place and the isotope ratio would be reversed as predicted by the ideal stripping model. Table VIII presents the data obtained in the isotopic studies of these reactions. In these investigations total cross-sections were not measured; they cannot be determined conveniently in our apparatus. Instead, differential cross-sections I(X) were calculated according to equation (14) where $I(X) = I(0^\circ) + I(180^\circ)$. At low energies, the ratios of I(X) are good approximations to the ratios of the total reactive cross-section. In the region of the energy where a complex is expected, $I(X)_{O2D+}/I(X)_{O2H+}$ gradually rises to a maximum value of 4; then direct reaction becomes more important and the ratio drops to 0.121 at 100 eV(lab). One should not take these ratios too seriously, but they do give qualitative values as expected from a statistical complex. We should further point out that the isotope ratios as calculated above could be meaningless at high energies, since the mechanism of formation of O_2H^+ and O_2D^+ are quite different.

G. Lifetime of the Complex

Attempts were made to detect the complex $H_2O_2^+$ directly at threshold energies. All efforts failed, indicating that the $H_2O_2^+$ lived less than 10^{-5} seconds—the time an ion takes to get from the reaction cell to the detector. We cannot rule out the possibility of finding $H_2O_2^+$ with a lifetime longer than 10^{-5} seconds. Norton[69] observed a mass peak 34 when a mixture of O_2 and H_2 were introduced into a Nier 60° type of mass spectrometer. Of course the complex could be stabilized by collisions in the mass spectrometer.

Table VIII

Isotope effects

Exp.	E_0	V_0	V_H [a]	V_H/V_0	Q_H	$I_{(x)_H}$ [c]	V_{CM}	V_D [b]	V_D/V_0	Q_D	$I_{(x)_D}$ [c]	$I_{(x)_D}/I_{(x)_H}$	E_S^0
440 441	24.82	12.24	11.18	0.913	-2.13	1.145×10^3	11.19	11.13	0.909	-2.11	2.49×10^4	2.17	2.13
513 514	37.18	14.98	13.84	0.923	-3.00	3.23×10^2	13.70	13.54	0.903	-3.04	8.88×10^2	2.75	3.19
509 510	50.00	17.38	16.31	0.938	-3.74	2.012×10^3	15.89	15.86	0.912	-4.28	8.271×10^3	4.11	4.29
516 517	60.80	19.16	18.17	0.948	-3.95	3.264×10^3	17.52	17.15	0.895	-4.30	6.626×10^3	2.03	5.21
518 519	74.66	21.23	20.34	0.958	-3.81	2.188×10^3	19.41	18.91	0.890	-4.80	2.16×10^3	0.99	6.40
522 523	90.27	23.35	22.46	0.961	-4.03	1.521×10^3	21.35	20.70	0.886	-5.23	5.24×10^2	0.34	7.74
546 547	100.02	24.57	23.66	0.962	-4.34	6.05×10^2	22.47	21.77	0.886	-5.58	7.348×10^1	0.121	8.57
543	74.98	21.28	-	-	-	-	19.45	18.95	0.890	-4.86	-	-	6.43
550	139.89	29.06	-	-	-	-	26.57	25.69	0.884	-7.21	-	-	11.99

All energies have units of eV

All velocities have units of 10^5 cm/sec

[a] H denotes O_2H^+ [b] D denotes O_2D^+ [c] Arbitrary units

The lifetime of the complex (τ) at different energies can roughly be estimated if all the terms in k_a are known

$$\tau = \frac{1}{k_a} \approx \langle \nu \rangle \left[\frac{E^* + aE_z}{E^* + aE_z - E_c} \right]^{s-1} \qquad (50)$$

Since E^* is specified in the experiment and E_c can be calculated accurately from the known quantities listed in Table V, the problem now is in the evaluation of $\langle \nu \rangle$ and aE_z. Both of these terms require knowledge of the fundamental frequencies of $D_2O_2^+$.

No spectroscopic data is available on $D_2O_2^+$. However, a good estimation can be had if ν_1, ν_2, ν_4, ν_5, and ν_6 could be taken the same as a normal D_2O_2 [70,71] and ν_3 is set equal to ν_2 of HNO[72] since HNO is isoelectronic with HO_2^+. The moment of inertia I_B, around the C_2 axis of D_2O_2, was measured by microwave techniques.[73] These molecular constants are tabulated in Table IX.

With the knowledge of ν_i, $\langle \nu \rangle$ was calculated as the root mean square of ν_i and the zero point energy E_z was also calculated. The "a" factor was evaluated by the method outlined by Whitten and Rabinovitch.[74] In general for this reaction the "a" factor is slightly less than 1 at the threshold energy; for example, a = 0.98 for reaction (20). "a" can be set equal to 1 if $E \geq 10\ E_z$ without causing much error. The constants required to calculate "a" are also tabulated in Table IX.

In calculating the lifetime of a complex, it is convenient to express τ in terms of molecular rotations (τ_{rot}). The rotational frequency (ν_{rot}) of a complex can be estimated by

Table IX

Molecular constants

	Dimensions	$H_2O_2^+$	$D_2O_2^+$
ν_1	cm^{-1}	3610	2670
ν_2	cm^{-1}	1315	1042
ν_3	cm^{-1}	1562	1562
ν_4	cm^{-1}	170	131
ν_5	cm^{-1}	3614	2680
ν_6	cm^{-1}	1266	947
I_A	$g\ cm^2$	2.96×10^{-40}	5.6×10^{-40}
$I_B \approx I_C$	$g\ cm^2$	34×10^{-40}	$\sim 34\times10^{-40}$
E_z	eV	0.673	0.56
V		1.5398	1.3791
S		6	6
β		1.2832	1.1493
$\langle\nu\rangle^{-1}$	sec	1.485×10^{-14}	1.886×10^{-14}
$\nu_{rot}\ I_B$	rot/sec	$0.26\times10^{13}\times g$	$0.49\times10^{13}\times g$

ν_1 = symmetric vibrations of stretching of O–H

ν_2 = symmetric vibrations of bending

ν_3 = vibrations of O–O stretching

ν_4 = torsional vibrational frequency

ν_5 = antisymmetric vibrations of O–D stretching

ν_6 = antisymmetric vibrations of bending

$$I\,\nu_{rot} = \mu b g/2\pi \qquad (51)$$

where μ is the reduced mass and b is an impact parameter. However, the gas kinetic cross-section σ(gas) is defined as

$$\sigma\,(\text{gas}) = \pi\, b^2 \qquad (52)$$

Ordinary σ(gas) varies from 1 Å^2 to 10 Å^2, so b is not too sensitive to the variations in σ(gas). We arbitrarily set b equal to 10^{-8} cm. With the measured moments of inertia I_B and I_A, the rotational frequencies of the complexes can be estimated by equation (51).

For $D_2O_2^+$

$$\nu_{rot}\,(I_B) \approx 0.49 \times 10^{13} \times g \text{ rotations/sec}$$

$$\nu_{rot}\,(I_A) \approx 0.30 \times 10^{14} \times g \text{ rotations/sec}$$

For $H_2O_2^+$

$$\nu_{rot}\,(I_B) \approx 0.26 \times 10^{13} \times g \text{ rotations/sec}$$

$$\nu_{rot}\,(I_A) \approx 0.30 \times 10^{14} \times g \text{ rotations/sec}$$

where g is the relative velocity and it has a unit of 10^6 cm/sec. The lifetime τ of $D_2O_2^+$ and $H_2O_2^+$ with respect to the total reaction energy E^* is tabulated in Table X. E^* is defined as

$$E^* = E_s^0 + E_{vib} \qquad (53)$$

The vibrational energy of O_2^+ (E_{vib}) was estimated earlier to be 0.6 eV to 0.7 eV. Here we took E_{vib} = 0.6 eV. Of course any meaningful comparison between the calculated τ and the experimental data depends on the accuracy of the numerical results used in the computation of τ. We believe that the τ tabulated in Table X were underestimated.

Table X
Calculated lifetime of the complex

E_0 (eV)	V_0 $\times 10^{-5}$ cm/sec	E_S^0 (eV)	E^* (eV)	τ (sec)	τ rotations
For $D_2O_2^+$					
16.2	8.07	1.2	1.8	1.27×10^{-9}	5.02×10^{3}
34.75	14.5	3.86	4.5	1.48×10^{-12}	10.5
42.13	15.95	4.68	5.3	8.49×10^{-13}	6.6
49.2	17.24	5.47	6.1	5.31×10^{-13}	4.5
61.14	19.21	6.79	7.4	3.06×10^{-13}	3
75.20	21.29	8.36	9.0	1.90×10^{-13}	2
For $H_2O_2^+$					
20.67	11.17	1.22	1.82	4.41×10^{-10}	1.28×10^{3}
50.0	17.4	2.94	3.54	2.91×10^{-12}	13
65.89	19.94	3.88	4.48	1.05×10^{-12}	5

However, some qualitative statements can still be made even though the above calculations were an order of magnitude off from the actual value.

Comparison between the experimental data and τ can be made conveniently at E^* = 1.8 eV, 4.5 eV and 9.0 eV. E^* = 1.8 eV is the thermodynamic threshold for the reaction O2+(D2,D)O2D+; the lifetime of $D_2O_2^+$ is fairly long but not long enough for a direct detection by our apparatus. Examination of equation (50) tells us that we might have $\tau = \infty$ at a reaction energy of $E^* = 1.8 - E_z$ eV. Such a measurement is a direct proof of the validity of the statistical model at an energy close to the threshold. At E^* = 4.5 eV and above, the reaction mechanism changes to a more direct type of interaction. Contrary to the ordinary definition of a direct interaction, the complex still lives about 10 rotations at this energy range. At E^* = 9.0 eV, the experimental data shows that O_2D^+ has a velocity close to that of an ideal stripping process. However, the calculated τ is about two rotations, a time maybe long enough for the complex to forget its initial directions. If the common belief that direct interactions took place in less than one rotational period were correct, the present experiments and computations hinted that statistical models may not be applied to situations where the lifetime of the complex is shorter than, say, 10 rotational periods. A more accurate calculation of τ is required to examine this point critically.

In summary, the lifetime of the complex $D_2O_2^+$ at various reaction energies was calculated. As expected the lifetime of $D_2O_2^+$ at energies

closed to the reaction threshold was quite long. Difficulties in the comparison between the experimental data and the computed value arise in the higher energy regime. At high reaction energies and when the lifetime of the complex is short, the choice of the molecular constants in these calculations becomes more critical. In view of the lack of experimental data in the molecular constants of $D_2O_2^+$, care should be taken not to over interpret the calculated lifetime at energies above 4.5 eV. Moreover, the configuration of the complex at 4.5 eV and above may not be the same as an ordinary $D_2O_2^+$ as suggested in Section H below. Thus the computation at 4.5 eV and above could be off by several orders of magnitude. We should also keep in mind that the unimolecular rate theory may not apply to small molecules like $D_2O_2^+$ as successfully as to large molecules.

H. Mass Spectrum

We have shown that a complex was formed in the reaction $O_2^+ + H_2$. Earlier Field, Franklin, and Lampe[75] found that if a complex were formed in an ion-molecule reaction, the decomposition pattern of this complex could be similar to the mass-spectrum of a molecule which had the same composition. Thus a comparison between the mass-spectra of $H_2O_2^+$ and $O_2^+ + H_2$ could be both interesting and instructive. Such a comparison is done in Table XI. To facilitate comparison, the intensity of O_2H^+ was normalized to 1. All the other intensities were calculated relative to that of O_2H^+. Of these data, it is felt that the work of Hudson and Foner,[76] and Kerwin and Cottin[77] to be most reliable. Data from $H_2O_2^+$ all exhibit the same general results, that is the intensity

Table XI

Mass Spectra of $H_2O_2^+$ Intensity

Products	Cottin and Kerwin 100 eV e^-	Foner and Hudson 50 eV e^-	Robertson[78] 40 eV e^-	Gruffy and Lindeman[79] 70 eV e^-	This work 50 eV O_2^+
O^+	12	0.05	< 0.2	0.23	0
OH^+	37.5	1.32	20	2.3	0.09
H_2O^+	122	3.3	(10^3)	(15)	0.08
O_2^+	12.5	0.4	(15)	(7.6)	--
O_2H^+	1	1	1	1.	1
$H_2O_2^+$	1.5	22.0	10	11.5	0

( ) Data very uncertain

of OH^+ and H_2O^+ are larger than that of O_2H^+. Our data is exactly opposite; the O_2H^+ intensity was 10 times those of OH^+ and H_2O^+. This result is rather puzzling. It was calculated earlier that the $(H_2O_2^+)^*$ had a lifetime of about 10 rotations, at a reaction energy of 3.54 eV. Under such conditions the $(H_2O_2^+)$ may not have enough time to become equilibrated and behave more like a $H_2O_2^+$ and a mass-spectrum like $H_2O_2^+$ is not expected. It is tempting to conclude that our intermediate did not have a configuration like an ordinary $H_2O_2^+$, at that particular energy.

---

*$(H_2O_2^+)$ is the complex from $O_2^+ + H_2$.

VI. SUMMARY AND PERSPECTIVE

The dynamics of N+(H2,H)NH+ has been studied in detail from 20 eV to 70 eV(lab); in this energy range the reaction occurs mainly by a direct mechanism. Some of the electronic states of the products could be identified due to the restrictions of the Q value limits. However, the more interesting energy range 0 eV to 20 eV could not be reached by the present experimental set up. Hence the existence of a reaction complex at low energies is still unsolved. Naturally, future investigations should concentrate on low energy experiments, on the threshold behavior of the reaction, and on the angular distributions of the products. Because of the simplicity of the reaction, it should be a very attractive system for theoretical computations. The initial quantum states of the reactants could be specified unambiguously and the final quantum states (vibrational and electronic) of the products, particularly those formed at low reaction energies, could also be identified by virtue of energy conservation arguments. Thus the data generated in the present and future experiments of N+(H2,H)NH+ should provide a rigid test for any theoretical calculations.

The mechanism for the conversion of the translational energy into electronic excitation is still not well understood, though a mechanism was proposed to account for the observations. The difficulties in the interpretation was compounded by the uncertainty in the initial states of the primary ion. Generation of the ground electronic state of atomic ions must be further developed. The translational energy spectrum of O^+, C^+ and F^+ on He should be more revealing than N^+ studied here, because the first few electronic energy level spacings of these

ions are separated further apart than those in N^+. Thus the identification of the states of the ions after a collision with He could be made with less ambiguity. Again such excitation process should be within reach by theoretical investigations and the data obtained here serve to be a guide and a test for any computational models. The non-reactive N^+ studied here are by no means complete; the uncertainty in the assignment of the electronic states is still waiting to be confirmed.

In the O_2^+ experiments, we have made a rather extensive study on the major features of the reaction. From the angular measurements (contour maps) and the velocity spectra, it was observed that five different products O_2H^+, H_2O^+, OH^+, O^+, and O_2^+ came out from the reaction $O_2^+ + H_2$. At lower energies, the contour maps and the velocity spectra led to the conclusion that an intermediate complex was formed in these reactions. However, each channel of reaction gives a different insight into the details of the reaction mechanism and dynamics.

The formation of O_2H^+ has the biggest cross-section among the products O_2H^+, OH^+, H_2O^+, and O^+. About one half of the efforts in these experiments were concentrated on O_2H^+. This channel of the reaction gave a rather detailed picture on the partition of the total reaction energy into the internal excitation and the translational motions of the products. The reaction mechanism involved in this channel is as follows: at low energies a reaction complex was formed and the O_2H^+ came from the unimolecular decay of $H_2O_2^+$, while direct reactions took place at higher energies. This is the first case where a clear transition from complex to direct reactions is observed. It

would be interesting to see if such transitions could be detected in the energy dependence of the total reaction cross-sections.

The formation of OH^+ was similar to O_2H^+ at low energies. At high energies the formation of OH^+ seemed to proceed via a two step process: first O_2H^+ was formed in a direct reaction, and then OH^+ came from the unimolecular decomposition of O_2H^+. Recent experiments[80] on

$$O_2^+ + C_2D_2 \rightarrow OD^+ + C_2D + O \qquad (54)$$

gave further support of such mechanism.

Unlike O_2H^+ and OH^+, H_2O^+ came only from a reaction complex. Its range of reaction energy was quite narrow compared to those of O_2H^+ and OH^+. From the investigation of H_2O^+, a suggestion was made that the reaction $O_2^+ + H_2$ had a substantial activation barrier. Such a proposal is best verified by a threshold measurement. The threshold behavior of the different reaction channels plays a very important role in the understanding of $O_2^+ + H_2$. Unfortunately, at present we could only determine the threshold for the formation of O^+.

It is surprising to find that the majority of O^+ formed via a direct process--that of a stripping. The formation of O^+ is similar to the O^+ from $O_2^+ + He$, indicating that the mechanism involved was some type of dissociation induced by collision.

Using the unimolecular rate theory, the lifetime of $H_2O_2^+$ at different reaction energies was calculated. Such computations did not agree with the experimental data at high energies, and when the lifetime of the complex is short. The isotope effects, at low energies, for the formation of O_2H^+ and O_2D^+ from $O_2^+ + HD$ came out as expected from the unimolecular decay of a complex. Careful measurements of

the total cross-sections for the formation of O_2D^+ and O_2H^+ should offer a most stringent test for the unimolecular rate theory. Surprisingly, isotopic substitution also affected the mechanism of reaction at high energies. The reaction mechanisms were identified, but the intrinsic difference between $O_2^+ + H_2$ and $O_2^+ + HD$ remains unclear.

ACKNOWLEDGEMENTS

I should like to take this opportunity to express my gratitude to Prof. Bruce Mahan for his patient guidance and discussions throughout these projects. The four years in his laboratory are the most enjoyable period of my educational career.

A project of this nature cannot be completed alone. Sincere appreciation is due to: Prof. Y. T. Lee and Dr. Ron Gentry for their most important contribution toward the design of the apparatus; Prof. E. A. Gislason who cooperated with the author with most of these experiments. It was a team enjoyed by both of us; Mr. Arthur Werner for assistance in the O_2^+ experiments; and Mr. Mervyn Chiang for constructing the microwave discharge source and for the assistance in some of the experiments which lasted into the wee hours in the morning.

Special thanks are extended to Shirley Ashley who typed the thesis and Nancy Monroe who did the drawings.

Finally, the generous financial support received from the Department of Chemistry and the Inorganic Materials Research Division are gratefully acknowledged.

This work was performed under the auspices of the U. S. Atomic Energy Commission.

REFERENCES

1. F. W. Lampe, J. L. Franklin and F. H. Field, Prog. Reaction Kinetics 1, 69 (1961).
2. L. Friedman, Ann. Rev. Phys. Chem. 19, 273 (1968).
3. B. R. Turner, M. A. Fineman, and R. F. Stebbings, J. Chem. Phys. 42, 4088 (1965).
4. Z. Herman, J. Kerstetter, T. Rose, and R. Wolfgang, Disc. Faraday Soc. 44, 123 (1967); J. Chem. Phys. 46, 2844 (1967).
5. C. F. Giese and W. B. Maier II, J. Chem. Phys. 39, 197 (1963); J. Chem. Phys. 39, 739 (1963).
6. A. Henglein, Adv. Chem. Ser. 58, 63 (1966).
7. D. C. Lorents and W. Aberth, Phys. Rev. 144, 109 (1966).
8. R. L. Champion, L. D. Doverspike, and T. L. Bailey, J. Chem. Phys. 45, 4377 (1966).
9. W. R. Gentry, E. A. Gislason, B. H. Mahan, and Chi-wing Tsao, J. Chem. Phys. 49, 3058 (1968).
10. M. Chiang, E. A. Gislason, B. H. Mahan, C. W. Tsao, and A. S. Werner, J. Chem. Phys. (to be published 1970).
11. E. A. Gislason, Bruce H. Mahan, Chi-wing Tsao, and A. S. Werner, J. Chem. Phys. 50, 142 (1969).
12. A. Ding, A. Henglein, D. Hyatt and K. Lacmann, Z. Naturforsch 23, 2084 (1968).
13. G. Gioumousis and D. P. Stevenson, J. Chem. Phys. 29, 294 (1958).
14. H. S. Johnston, "Gas Phase Reaction Rate Theory" The Ronald Press, N. Y. (1966).

15. (a) W. B. Miller, S. A. Safron and D. R. Herschbach, Disc. Faraday Soc. 44, 108 (1967). (b) S. A. Safron, Ph.D. thesis, Harvard University (1969).

16. R. Colins and A. E. Douglas, Can. J. Phys. 46, 61 (1968).

17. G. Herzberg, "Spectra of Diatomic Molecules" D. Van Nostrand Co., Inc., Princeton, N. J. (1967).

18. See for example, G. Friedlander, J. W. Kennedy, J. M. Miller, "Nuclear and Radiochemistry" 2nd ed. John Wiley and Sons, Inc., New York (1964).

19. See for example, D. R. Herschbach, Disc. Faraday Soc. 33, 149 (1962).

20. See for example, J. B. Marion "Classical Dynamics of Particles and Systems", Academic Press, N. Y. (1965).

21. I. Halpern and V. M. Strutinski, Paper P/1513, Proc. Intern. Conf. Peaceful Uses Atomic Energy, 2nd Conf. (Geneva 1958).

22. W. R. Gentry, University of California Lawrence Radiation Lab. Rept. UCRL-17691, (1967).

23. C. E. Carlson and G. D. Magnuson, Rev. Sci. Instr. 33, 905 (1962).

24. F. C. Fehsenfeld, K. M. Evenson, and H. P. Broida, Rev. Sci. Instr. 36, 294 (1965).

25. M. Chiang, private communications.

26. W. McGowan and L. Kerwin, Proc. Phys. Soc. 82, 357 (1963).

27. D. K. Böhme and J. M. Goodings, J. Appl. Phys. 37, 4261 (1966).

28. F. H. Dorman and J. D. Morrison, J. Chem. Phys. 35, 575 (1961).

29. B. R. Turner, J. A. Rutherford, and D. M. J. Compton, J. Chem. Phys. 48, 1602 (1968).

30. F. C. Fehsenfeld, A. L. Schmeltekopf and E. E. Ferguson, J. Chem. Phys. 46, 2802 (1967).

31. A. G. Gaydon, "Dissociation Energies and Spectra of Diatomic Molecules" 3rd ed. Chapman and Hall (1968).

32. G. Herzberg "Atomic Spectra and Atomic Structure" Dover publication N. Y. (1944).

33. M. W. Feast, J. Astrophys. 114, 344 (1957).

34. "Ionization Potentials, Appearance Potentials and Heats of Formation of Gaseous Positive Ions" NSRDS-NBS 26 (1969).

35. W. C. Price, T. R. Passmore, and D. M. Roessler, Disc. Faraday Soc. 35, 201 (1963).

36. G. Herzberg "Molecular Spectra and Molecular Structure III Electronic Spectra and Electronic Structure of Polyatomic Molecules" D. Van Nostrand Co., Inc., N. J. (1966).

37. G. Herzberg and J. W. C. Johns, Proc. Roy. Soc. A 295, 107 (1966).

38. W. Aberth and D. C. Lorents, Phys. Rev. 182, 162 (1969).

39. B. H. Mahan, Acc. Chem. Res. 1, 217 (1968).

40. C. E. Moore, "Atomic Energy Levels as derived from the Analysis of Optical Spectra" NBS Circular 467 Vol I (1949).

41. P. M. Hierl and J. L. Franklin, J. Chem. Phys. 47, 3154 (1967).

42. W. B. Maier II, J. Chem. Phys. 46, 4991 (1967).

43. C. F. Giese, Adv. Chem. Ser. 58, 20 (1966).

44. (a) D. O. Schissler and D. P. Stevenson, J. Chem. Phys. 24, 926 (1956). (b) D. P. Stevenson and D. O. Schissler, J. Chem. Phys. 29, 282 (1958).

45. T. F. Moran and L. Friedman, J. Chem. Phys. 42, 239 (1965).

46. K. M. Refaey and W. A. Chupka, J. Chem. Phys. 43, 2544 (1965).

47. V. I. Vedeneyev, L. V. Gurvich, V. N. Kondratyev, V. A. Medvedev and Ye. L. Frankevich, "Bond Energies, Ionization Potentials and Electron Affinities" St. Martin's Press, New York (1966).

48. See for example, R. I. Reed "Ion Production by Electron Impact" Academic Press, N. Y. (1962).

49. G. Herzberg, "Molecular Spectra and Molecular Structure II Infrared and Raman Spectra of Polyatomic Molecules" D. Van Nostrand Inc. Princeton, N. J. (1951).

50. (a) D. R. Herschbach, Adv. Chem. Phys. 10, 319 (1966).
(b) R. B. Bernstein and J. T. Muckerman, Adv. Chem. Phys. 12 389 (1967).

51. (a) D. O. Ham, J. L. Kinsey, and F. S. Klein, Disc. Faraday Soc., 44, 174 (1967). (b) J. Chem. Phys. 48, 929 (1968).

52. L. D. Doverspike and R. L. Champion, J. Chem. Phys. 46, 4718 (1967).

53. C. W. Tsao and B. H. Mahan, unpublished results, this Laboratory.

54. Z. Herman, A. Lee, and R. Wolfgang, J. Chem. Phys. 51, 452 (1969).

55. E. A. Gislason, B. H. Mahan, C. W. Tsao, and A. S. Werner, J. Chem. Phys. 50, 5418 (1969).

56. A. Ding and A. Henglein, Ber. Brnsenges. Phys. Chem., in press.

57. Section IV, this thesis.

58. T. F. Moran and J. R. Roberts, J. Chem. Phys. 49, 3411 (1968).

59. (a) M. H. Cheng, M. Chiang, E. A. Gislason, B. H. Mahan, C. W. Tsao, and A. S. Werner, J. Chem. Phys. (to be published).
(b) M. H. Cheng, Ph. D. thesis, Univ. of Calif., Berkeley (1969).

60. M. H. Cheng and M. Chiang, unpublished data, this Laboratory.

61. P. F. Dittner and S. Datz, J. Chem. Phys. 49, 1969 (1968).

62. See for example, "Ion Molecule Reactions in the Gas Phase" R. F. Gould, Ed. ACS publication (1966).

63. F. S. Klein and L. Friedman, J. Chem. Phys. 41, 1789 (1964).

64. (a) J. D. Kelley and M. Wolfsberg, J. Chem. Phys. 44, 324 (1966). (b) M. H. Cheng, Ph. D. thesis, Univ. of Calif. (1969).

65. Ron Gentry, Ph. D. thesis, Univ. of Calif., Berkeley (1967).

66. Don L. Bunker "Theory of Elementary Gas Reaction Rates" Pergamon Press, N. Y. (1966).

67. B. S. Rabinovitch and R. W. Diesen, J. Chem. Phys. 30, 735 (1959).

68. Don L. Bunker, J. Chem. Phys. 40, 1946 (1964).

69. F. J. Norton, Nat'l. Bur. Stand. Circular No. 522, 201 (1953).

70. See for example (a) N. T. Storchai and V. P. Morozov, Dopov. Akad. Nauk, Ukr RSR 1966 1596-9. (b) P. A. Giguere and O. Bain, J. Phys. Chem. 56, 340 (1952).

71. R. H. Hunt and R. A. Leacock, J. Chem. Phys. 45, 3141 (1966).

72. J. L. Bancroft, J. M. Hollas, and D. A. Ramsay, Can. J. Phys. 40, 322 (1962).

73. J. T. Massey and D. R. Bianco, J. Chem. Phys. 22, 442 (1954).

74. G. Z. Whitten and B. S. Rabinovitch, J. Chem. Phys. 38, 2466 (1963).

75. F. H. Field, J. L. Franklin, and F. W. Lampe, J. Am. Chem. Soc., 79, 2419 (1957); 79, 2665 (1957).

76. S. N. Foner and R. L. Hudson, J. Chem. Phys. 36, 2676 (1962).

77. Larkin Kerwin and M. Cottin, Can. J. Phys. 36, 184 (1962).

78. A. J. B. Robertson, Trans. Faraday Soc. 48, 228 (1952).

79. L. P. Lindeman and J. C. Guffy, J. Chem. Phys. 29, 246 (1958).

80. M. Chiang, C. Maltz, unpublished data, this laboratory.

TECHNICAL INFORMATION DIVISION
LAWRENCE RADIATION LABORATORY
UNIVERSITY OF CALIFORNIA
BERKELEY, CALIFORNIA 94720